HOMOGENIZATION OF BWR ASSEMBLIES
BY RESPONSE MATRIX METHODS

by

Alexander Y. C. Cheng

B. S., National Tsing-Hua University, R. O. C.
(1975)

SUBMITTED TO THE
DEPARTMENT OF NUCLEAR ENGINEERING
IN PARTIAL FULFULLMENT OF THE
REQUIREMENTS FOR THE
DEGREE OF

DOCTOR OF PHILOSOPHY

at the

MASSACHUSETTS INSTITUTE OF TECHNOLOGY

May 1981

Signature of Author_____,_____
Department of Nuclear Engineering
May 13, 1981

Certified by_____
Allan F. Henry
Thesis Supervisor

Accepted by_____
Allan F. Henry
Chairman, Departmental Graduate Committee

HOMOGENIZATION OF BWR ASSEMBLIES

BY RESPONSE MATRIX METHODS

by

Alexander Y. C. Cheng

ABSTRACT

The objective of this research is to develop accurate
and efficient methods for generating equivalence theory
parameters for coarse mesh analysis of light water reactors.
Equivalence theory is an exact homogenization scheme developed
by K. Koebke and K. Smith. Methods for computing approxi-
mate equivalence parameters are reviewed and they show that
an efficient method to solve local fixed-source problems is
needed.

In order to fulfill this need response matrix methods
using conventional partial current response matrices for
solving fixed-source problems are first investigated.
Analysis of a rather idealized BWR benchmark problem shows
that because of the spatial approximation made for the in-
coming partial currents used in generating partial current
response matrices, the accuracies of the estimated equiva-
lence parameters are poor and thus the resultant power dis-
tributions are greatly in error.

Response matrix methods using net current response
matrices are then introduced. Analysis of several BWR bench-
mark problems demonstrates that use of net current response
matrices leads to homogenized power distributions with maxi-
mum errors in assembly powers of approximately 1-3%. For
practical cases, these errors are about one-third of those
obtained using more conventional methods to estimate equiva-
lence parameters.

The computational efficiency of solving reactor problems
using such global-local iteration scheme is shown to be one
to two orders of magnitude greater than that of solving the
entire reactor heterogeneously.

Thesis Supervisor: Allan F. Henry
Title: Professor of Nuclear Engineering

TABLE OF CONTENTS

ACKNOWLEDGEMENTS

I wish to thank my thesis supervisor, Professor Allan F. Henry, for all his invaluable guidance and support during the course of this investigation. His willingness to teach, argue, listen and learn has made my association with him an extremely rewarding experience.

Thanks are also due to Professor David D. Lanning, who served as reader for this thesis.

I am also indebted to my office mates, Greg Greenman, Kord Smith, Jean Koclas, Rich Loretz, Chris Hoxie, and Hussein Khalil, for the opportunity to work, study, and learn with them. I especially would like to thank Kord and Chris for providing me with ample assistance and friendship.

I also wish to thank Ms. Clare Egan and Mr. Jon Runge for their assistance in the preparation of this document.

Never will I find the combination of words to express the deep feelings of love and gratitude to the members of my family. Their support and encouragement are essential ingredients for me to fulfill the requirements of the M.I.T. experience.

BIOGRAPHICAL NOTE

Alexander Y. C. Cheng was born on November 25, 1953 in Taipei, Republic of China. He grew up along with his brothers, Caesar, Tracy, MacMillan, and his sister, Wendy.

The author enrolled at National Tsing-Hua University (R.O.C.) in September 1971 and graduated with a B.S. degree in 1975. After serving two years in the Army, he entered the Graduate School of National Tsing-Hua University in September 1977.

In September 1978, the author entered the Massachusetts Institute of Technology as a graduate student in the Department of Nuclear Engineering.

In July 1979, the author married I-Hwa Lei and they had a girl, Wan-Lae, in February 1981.

The author received the Ph.D. degree in Nuclear Engineering in June 1981.

LIST OF FIGURES

LIST OF TABLES

CHAPTER ONE

INTRODUCTION

1.1 OVERVIEW AND MOTIVATION FOR SPATIAL HOMOGENIZATION

The design and analysis of modern light water reactors require an extensive knowledge of spatial power distributions, control rod worths and neutron absorption rates. Determination of these quantities requires a knowledge of the neutron density in phase space (position, direction, and energy). Two of the most accurate methods used today to determine these quantities are the Monte Carlo method and the discrete ordinates method. [1,11,12] They both have the advantage of explicitly accounting for the transport phenomena in a reactor. Unfortunately, explicit transport theory modeling of the heterogeneities (such as control rods, burnable poisons, water rods, etc.) that exist in a reactor results in a problem of such magnitude as to be incredibly expensive for even the most advanced computers.

Therefore, in order to reduce cost, approximations to the transport equation are used. The most commonly employed method is to reduce the size of the problem by using the diffusion approximation which explicitly assumes that the angular distribution of neutrons be at most linearly anisotropic. [1] Although the actual angular distributions near regions of high neutron absorption (such as control rods or burnable poison pins) or near highly scattering regions with

little absorption (such as water rods or reflectors) are not accurately represented by the diffusion theory approximation, the quantities of interest (power distributions, control rod worths, etc.) can be predicted quite accurately by the diffusion theory model provided "equivalent" homogenized cross sections and diffusion constants can be determined.

The determination of these equivalent diffusion theory parameters for each localized heterogeneous region (fuel pins, control rods, etc.) constitute the first distinct level of homogenization. With this stage of homogenization carried out, solving the resulting diffusion theory equations may remain costly simply because there exists a very large number (several hundred thousand) of spatial regions in a reactor core. Moreover, the design and analysis of a reactor requires many core calculations (e.g. the power distribution at the beginning of each depletion time step and during thermal-hydraulic feedback analysis, transient analysis, etc.) Thus there is strong economic incentive to use a large "node" (an assembly or a cluster of assemblies) as the homogenized region. If equivalent homogenized parameters for such large nodes (usually spatially constant within each node) can be determined, the core calculation can be reduced to a problem involving only several hundred homogeneous regions in each axial plane of the reactor core. Once this second stage of homogenization has been reached, the resulting equations can be solved by nodal or finite element methods.[2,14,15,16]

These methods are computationally very efficient because large mesh spacings can be employed.

Techniques by which the equivalent homogenized parameters need for this second stage of homogenization can be obtained efficiently are the subject of this thesis.

1.2 HOMOGENIZED PARAMETERS BASED ON DIFFUSION THEORY

1.2.1 THE NONEXISTENCE OF EXACT HOMOGENIZED PARAMETERS FOR DIFFUSION THEORY

In order to solve reactor problems with homogenization, certain information which is available if the reactor is analyzed without homogenization must be sacrificed. However, certain quantities which are the characteristics of the reactor need to be preserved. These quantities are the reactor eigenvalue, the nodal reaction rates in each energy group, the nodal power densities, and the group currents on all the surfaces of each node.

In order to demonstrate the difficulties associated with homogenization based on diffusion theory, the exact values (as functions of space, direction, and energy) of all reactor quantities will be assumed known. Accordingly the following quantities are also known:

$\phi_g(\underline{r}) \equiv$ scalar neutron flux in group g (cm^{-2} sec^{-1})

$J_g^u(\underline{r}) \equiv$ net neutron current in direction u (u=x,y,z) and group g (cm^{-2} sec^{-1})

$\Sigma_{tg}(\underline{r}) \equiv$ macroscopic total cross section for group g (cm^{-1})

$\Sigma_{gg'}(\underline{r}) \equiv$ macroscopic transfer cross section from group

g' to group g (cm^{-1})

$\chi_g(\underline{r}) \equiv$ fission neutron spectrum contribution to

group g

$\nu\Sigma_{fg}(\underline{r}) \equiv$ macroscopic fission cross section for group g

times the mean number of neutron emitted per

fission (cm^{-1})

$\lambda \equiv$ reactor eigenvalue (k_{eff})

If the corresponding quantities for the homogenized diffusion

theory problem are denoted by addition of a circumflex, the

homogenized parameters should be determined such that all

group reaction rates, all group surface currents, and reactor

eigenvalue are preserved, i.e. the following equalities

should hold:

$$\int_{V_i} d\underline{r}\ \hat{\Sigma}_{\alpha_g}(\underline{r})\ \hat{\phi}_g(\underline{r}) = \int_{V_i} d\underline{r}\ \Sigma_{\alpha_g}(\underline{r})\ \phi_g(\underline{r})$$

$$-\int_{S_i^k} dS\ \hat{D}_g(\underline{V})\ \frac{\partial}{\partial u}\ \hat{\phi}_g(\underline{r}) = \int_{S_i^k} dS\ J_g^u(\underline{r})\quad ,$$

$$\hat{\lambda} = \lambda\ ;\qquad\qquad g = 1,2,\ldots,G,$$
$$\alpha = t,f,g',\ \text{etc.},$$
$$k = 1,2,\ldots,K,$$
$$u = x,y,z \qquad\qquad (1.1)$$

where

G ≡ the total number of neutron energy groups,

K ≡ the number of surfaces for each homogenized region,

V_i ≡ the volume of the ith homogenized region,

S_i^k ≡ the kth surface of the ith homogenized region.

If all homogenized parameters are assumed to be spatially constant within each node, the exact homogenized parameters will then be defined by

$$\hat{\Sigma}_{\alpha_g}^{(i)} \equiv \frac{\int_{V_i} d\underline{r}\ \Sigma_{\alpha_g}(\underline{r})\phi_g(\underline{r})}{\int_{V_i} d\underline{r}\ \hat{\phi}_g(\underline{r})} \qquad , \qquad (1.2a)$$

$$\hat{D}_g^{(i)} \equiv \frac{\int_{S_i^k} dS\ J_g^u(\underline{r})}{\int_{S_i^k} dS\ \frac{\partial}{\partial u}\hat{\phi}_g(\underline{r})} \qquad . \qquad (1.2b)$$

Examination of (1.2) shows that in addition to a priori knowledge of integrated reaction rates and net surface currents for each node information concerning the homogenized flux distribution must also be available in order to determine the exact homogenized parameters. Since the homogenized fluxes depend strongly on the homogenized parameters, a

nonlinearity is introduced in the determination of the homogenized parameters. Moreover, Equation (1.2b) in general defines different values of $\hat{D}_g^{(i)}$ for different surfaces of node i and thus contradicts the assumption that all of the homogenized parameters are spatially constant within each node.

It thus seems clear that except for very special cases it is impossible to define spatially constant exact homogenized parameters for diffusion theory.

1.2.2 CONVENTIONAL HOMOGENIZED PARAMETERS

To circumvent the theoretical pitfalls mentioned in the preceding section, homogenized parameters for diffusion theory are conventionally defined by relaxing the conditions imposed by (1.1). Traditionally, the homogenized diffusion constant is approximated as

$$\hat{D}_g^{(i)} \equiv \left[\frac{\int_{V_i} d\underline{r}\ D_g^{-1}(\underline{r})\ \phi_g(\underline{r})}{\int_{V_i} d\underline{r}\ \hat{\phi}_g(\underline{r})} \right]^{-1} . \tag{1.3}$$

The justification for this approximation is that $D_g^{-1}(\underline{r})$ is proportional to the macroscopic transport cross section[1], and it is desired to preserve the neutron transport rate. However, the transport cross section is a function of the net current and thus weighting it by the flux does not preserve the transport rate.

In order to determine the numerator of (1.2a) and
(1.3), the distribution of the heterogeneous flux is needed.
Since in practice the exact solution of the heterogeneous
problem is never known, the integrated reaction rates are
approximated by those obtained from an $\underline{n} \cdot \underline{J}_g = 0$ assembly
calculation for each distinct type of fuel assembly. These
assembly calculations can be performed by any method avail-
able (Monte Carlo method, integral transport method, etc.).
The assumption that the integrated reaction rates can be
obtained from such assembly calculations is usually rational-
ized by noting that most assemblies in a reactor are sur-
rounded by other assemblies of a similar composition. Also,
global flux shapes usually have only a small curvature across
each assembly and thus the surface currents are small in
magnitude.

The next approximation which is generally made, to
determine the denominators of (1.2a) and (1.3) is that the
node-integrated homogenized flux is equal to the node-
integrated heterogeneous flux obtained from the assembly
calculation, i.e.:

$$\int_{V_i} d\underline{r} \; \hat{\phi}_g(\underline{r}) \;\; = \;\; \int_{V_i} d\underline{r} \; \phi_g^A(\underline{r})$$

where $\phi_g^A(\underline{r})$ is the group heterogeneous flux obtained from
the $\underline{n} \cdot \underline{J}_g = 0$ assembly calculation. This approximation is
never strictly valid since none of the homogeneous regions

in realistic reactors satisfies the zero net current con-
dition.

The homogenized parameters determined by making the
previous three approximations are generally referred to as
flux-weighted constants (FWC). The procedure is widely used
in modern LWR analysis although significant deficiencies
and limitations exist for this method. For example, the
solution of the global homogenized problem defined by FWC
preserves none of the quantities of (1.1). Moreover, although
the aforementioned assumptions are plausible, there exists
many assemblies in a reactor for which they are quite in-
valid, and consequently their use results in large errors in
predicted power densities. Specifically in BWR analysis, the
flux-weighted two-group constants tend to overpredict sig-
nificantly the thermal neutron currents between assemblies.[3]
As a result, the predicted assembly power densities may be
in error by as much as 20% [6] in extreme cases.

1.3 EXACT HOMOGENIZED PARAMETERS

Many prescriptions for eliminating the inaccuracies
which result from the use of flux-weighted parameters have
been developed. [18,19,20,21] As with the flux-weighted con-
stants, many of these have questionable theoretical founda-
tions and consequently their adoption is justified primarily
by empirical demonstrations of their accuracy. These methods
will not be described here. There are, however, homogeniza-
tion methods which are capable of reproducing rigorously all

of the desired quantities of (1.1). One particularly attrac-
tive method is due to Koebke [22] and has been modified and
implemented by Smith.[3] It will be called equivalence theory.
In this theory, instead of relaxing the conditions imposed
by (1.1) as in the flux-weighted constants, extra degrees
of freedom are added to the homogenized parameters by intro-
ducing new parameters which will be called the discontinuity
factors.

With the introduction of discontinuity factors, it can
be shown that exact homogenized parameters can be obtained
to match any reference solution (obtained by Monte Carlo
method, transport theory, multigroup diffusion theory, etc.).
Also it can be shown that the homogenized problem can be
solved by any approximate method with the reference solution
still preserved. This aspect of equivalence theory is unique
in that one is not attempting to find homogenized parameters
which reproduce the exact reactor solution when the homogen-
ized group-diffusion equations for the reactor are solved
exactly, but rather, one defines homogenized parameters which
reproduce the exact reactor solution even though the homogen-
ized reactor equations are solved approximately.

A detailed discussion of the equivalence theory will
be presented in Chapter 2.

1.4   BENCHMARK PROBLEMS

In this thesis, three BWR benchmark problems are chosen to test the accuracy and efficiency of the homogenization methods to be developed. Because the flux distribution is rather smooth in the axial direction, our principal concern is with homogenization in the radial plane. Thus all three benchmark problems represent two dimensional reactor cores.

1.4.1   THE CISE BWR BENCHMARK PROBLEM

The CISE BWR benchmark problem [3,17] is an idealized model of a two dimensional BWR. Its core consists of 208 fuel assemblies with widths of 15 cm surrounded radially by a 15 cm water reflector. The fuel in each assembly is modeled as homogeneous, but all control blades and water gaps are explicitly modeled. The major simplifications in this problem are that the actual fuel heterogeneities (enrichment zones, burnable poison rods, and water rods) are represented homogeneously. Nevertheless, the problem serves as a significant test of any homogenization scheme. A detailed description of this problem is given in Appendix A.1.

The reference solution for the CISE BWR benchmark problem was obtained by Smith [3] from a nodal code QUANDRY. [2] A short description of that code is given in Section 2.3. To get the reference solution, 64 mesh points per assembly (11 in each quarter of a control rod, 25 in the fuel region, and 28 in the gap regions) were used.

1.4.2 THE HAFAS BWR BENCHMARK PROBLEM

The HAFAS (Heterogeneously Arranged Fuel Assembly)
BWR benchmark problem[3] is a two dimensional BWR which is
much more complicated than the CISE BWR benchmark. Its
core consists of 308 fuel assemblies with widths of 15.31 cm,
surrounded by a 15.31 cm thick water reflector. The radial
enrichment zones in each assembly are modelled such that
the fuel enrichment is constant within four fuel pin clus-
ters, and the fuel zone is then represented by sixteen
distinct regions. The radial enrichment is modelled by fuel
pins having three different fuel enrichments. Water gaps
between fuel assemblies are modelled explicitly as "wide"
and "narrow" gaps. Moreover, the central assemblies are
modelled as partially voided (40% or 70%). A complete
description of the problem is given in Appendix A.2.

The reference solution for this problem is a QUANDRY
solution involving 49 mesh points per assembly (16 in the
fuel region, 9 in each quarter of a control blade, and 24
in the gap regions).

1.4.3 THE LSHBWR BENCHMARK PROBLEM

The LSHBWR (Loretz-Smith-Henry) benchmark problem[6] is
a detailed, two dimensional model of a BWR core composed of
fuel assemblies characteristic of the Vermont Yankee Reactor.
The core consists of 160 fuel assemblies with width of
15.31 cm, and is surrounded by a 30.62 cm water reflector.
In each assembly, the wide and narrow gaps, water holes,
gadolinium rods, control blades, and fuel pins are explicitly

modelled and the zones of enrichment within the fuel regions
are included. In addition, the central assemblies are
modelled as partially voided (40% or 70%). The only non-
explicit modeling is for the can material surrounding the
fuel regions. However, its presence is accounted for in
the heterogeneous diffusion theory parameters. A complete
description of this problem is given in Appendix A.3.

The reference solution for this problem is a QUANDRY
solution involving 169 mesh points in each fuel assembly.

1.5 OBJECTIVES AND SUMMARY

The objective of this thesis is to develop accurate,
efficient methods to estimate homogenized parameters for
coarse mesh analysis of boiling water reactors (BWR's).
In Chapter 2, homogenized parameters based on equivalence
theory and previous work [3,6,22] will be reviewed. In
Chapter 3, several methods based on partial current response
matrix techniques are introduced. Results show that they
are not acceptable. Alternative methods, which are based
on net current response matrix techniques, are developed in
Chapter 4 and their accuracy is established by application
to all three benchmark problems. Finally, a summary of this
investigation and recommendations for future research are
given in Chapter 5.

CHAPTER TWO

HOMOGENIZED PARAMETERS BASED ON EQUIVALENCE THEORY

2.1 INTRODUCTION

In Capter 1, it was shown that exact homogenized para-
meters in general do not exist for a diffusion theory model
because of the lack of flexibility of the equations embodying
that model. In addition, it was pointed out that conventional
flux weighted constants do not preserve any of the integral
quantities of interest (eigenvalue, nodal reaction rates,
and nodal surface currents). However, exact homogenized
parameters based on an extension of the diffusion theory
model which we shall call "equivalence theory" do exist.

In this chapter, first "equivalence theory" will be
presented. A simple method to estimate the resultant "equi-
valence theory" homogenized parameters and some possible
improvements will then be discussed.

2.1.1. NOTATION

Throughout this investigation, all problems are treated
in three-dimensional Cartesian geometry. In addition to
using x, y, and z to represent the coordinate directions,
a more general notation (u, v, w) for the coordinate direc-
tions are used as generalized coordinate subscripts. The
spatial domain of all problems are subdivided into a regular
array of right rectangular parallelopipeds (nodes) with grid
indices defined by u_ℓ, v_m, w_n where

$$\ell, m, n \equiv \begin{cases} i = 1, 2, \ldots, I+1; \ u, v, w=x \\ j = 1, 2, \ldots, J+1; \ u, v, w=y \\ k = 1, 2, \ldots, K+1; \ u, v, w=z. \end{cases}$$

As an example of future use of this generalized coordinate notation, the net currents on the faces of node (i, j, k) as a function of the two transverse directions are expressed as

$$\hat{J}^u_{g_{i,j,k}}(v,w) = - \hat{D}_{g_{i,j,k}} \frac{\partial}{\partial u} \hat{\phi}_g(u_\ell, v, w); \quad \begin{matrix} u=x,y,z \\ v \neq u \\ w \neq u \neq v \end{matrix}.$$

This single equation actually expresses three equations:

(1) The x-directed net current on the $x = x_i$ face, as a function of y and z (u=x, v=y, w=z)

(2) The y-directed net current on the $y=y_j$ face, as a function of x and z (u=y, v=x, w=z)

(3) The z-directed net current on the $z=z_k$ face, as a function of x and y (u=z, v=x, w=y)

The node (i,j,k) is defined by

$$x \ \epsilon \ [x_i, \ x_{i+1}]$$
$$y \ \epsilon \ [y_j, \ y_{j+1}]$$
$$z \ \epsilon \ [z_k, \ z_{k+1}].$$

The nodal widths are then defined as

$$h^u_\ell \equiv u_{\ell+1} - u_\ell; \quad u = x, y, z$$

and the nodal volume is

$$v_{i,j,k} \equiv h^x_i \ h^y_j \ h^z_k.$$

The nodal surfaces of node (ℓ,m,n) will be represented by u+

and u- where

$u+ \equiv$ surface $(u_{\ell+1}, v, w)$ of node (ℓ, m, n),

$u- \equiv$ surface (u_ℓ, v, w) of node (ℓ, m, n); $u = x, y, z$.

The external boundaries of the spatial domain and its outward normals will be denoted by Γ and u_Γ, respectively.

2.2. EQUIVALENCE THEORY

By integrating the Boltzmann transport equation for a critical reactor over all directions, $\vec{\Omega}$, of neutron travel and over an energy range ΔE_n; $n = 1, 2, \ldots N$, we obtain a set of formally exact equations[1]

$$\nabla \cdot \underline{J}_n(\underline{r}) + \Sigma_{t_n}(\underline{r}) \phi_n(\underline{r}) = \sum_{n'=1}^{N} [\Sigma_{nn'}(\underline{r}) + \frac{1}{\lambda} M_{nn'}(\underline{r})] \phi_{n'}(\underline{r}) \quad (2.1)$$

where

$$\phi_n(\underline{r}) \equiv \int d\Omega \int_{\Delta E_n} dE \ \psi(\underline{r}, \underline{\Omega}, E) \equiv \int_{\Delta E_n} dE \ \phi(\underline{r}, E) \quad ,$$

$$\underline{J}_n(\underline{r}) \equiv \int d\Omega \int_{\Delta E_n} dE \ \underline{\Omega} \ \psi(\underline{r}, \underline{\Omega}, E) \equiv \int_{\Delta E_n} dE \ \underline{J}(\underline{r}, E) \quad ,$$

$$\Sigma_{t_n}(\underline{r}) \equiv \frac{\int_{\Delta E_n} dE \ \Sigma_t(\underline{r}, E) \ \phi(\underline{r}, E)}{\phi_n(\underline{r})} \quad , \qquad (2.2)$$

$$\Sigma_{nn'}(\underline{r}) \equiv \frac{\int_{\Delta E_n} dE \int_{\Delta E_{n'}} dE' \ \Sigma_{so}(\underline{r}, E' \to E) \ \phi(\underline{r}, E')}{\phi_{n'}(\underline{r})}$$

$$M_{nn'}(\underline{r}) \equiv \frac{\int_{\Delta E_n} dE \int_{\Delta E_{n'}} dE' \ M(\underline{r}, E' \to E) \ \phi(\underline{r}, E')}{\phi_{n'}(\underline{r})}$$

$$\equiv \frac{\int_{\Delta E_n} dE \int_{\Delta E_{n'}} dE' \sum_s f^S(E) \nu^S \Sigma_f^S(\underline{r},E') \phi(\underline{r},E')}{\phi_{n'}(\underline{r})}$$

$$\equiv \sum_s \chi_n^S \nu^S \Sigma_{f_{n'}}^S(\underline{r}) \quad ,$$

$$\lambda \equiv \text{reactor eigenvalue.}$$

In these definitions

$$\chi_n^S \equiv \int_{\Delta E_n} dE \ f^S(E) \quad ,$$

$$\nu^S \Sigma_{f_n}^S(\underline{r}) \equiv \frac{\int_{\Delta E_n} dE \ \nu^S \Sigma_f^S(\underline{r},E) \ \phi(\underline{r},E)}{\phi_n(\underline{r})} \quad ,$$

$$\psi(\underline{r},\underline{\Omega},E) \equiv \text{directional flux density,}$$

$$\Sigma_{so}(\underline{r},E' \rightarrow E) \equiv \int_{-1}^{1} \frac{d\mu_o}{2} \Sigma_s(\underline{r},E' \rightarrow E, \mu_o) \quad ,$$

$$f^S(E) \equiv \text{fission spectrum for isotope s,}$$

and the cross section notation is standard.

The problem of finding $\Sigma_{t_n}(\underline{r})$, $\Sigma_{nn'}(\underline{r})$, and $M_{nn'}(\underline{r})$ is not trivial. The usual approach is to assume that the flux is separable in space and energy within each group and composition. The energy distribution of the flux is then determined either by a spectrum calculation or by an arbitrarily chosen shape.[1] This problem will not be discussed further, and it is assumed that we have the required cross sections.

In order to solve (2.1) more efficiently, we will do spatial as well as energy homogenization to reduce the number of unknowns in the homogenized problem to be developed. In-

tegration of (2.1) over volume $V_{i,j,k}$ and summation over n for the $\Delta E_n \subseteq \Delta E_g$; $g = 1,2,\ldots G$, gives

$$h_j^y h_k^z (J_{g_{i+1,j,k}}^x - J_{g_{i,j,k}}^x) + h_i^x h_k^z (J_{g_{i,j+1,k}}^y - J_{g_{i,j,k}}^y)$$

$$+ h_i^x h_j^y (J_{g_{i,j,k+1}}^z - J_{g_{i,j,k}}^z) + V_{i,j,k} \overline{\Sigma}_{t_{g_{i,j,k}}} \overline{\phi}_{g_{i,j,k}}$$

$$= \sum_{g'=1}^{G} V_{i,j,k} (\overline{\Sigma}_{gg'_{i,j,k}} + \frac{1}{\lambda} \overline{M}_{gg'_{i,j,k}}) \overline{\phi}_{g'_{i,j,k}} \; ;$$

$$\begin{aligned} i &= 1,2,\ldots I, \\ j &= 1,2,\ldots J, \\ k &= 1,2,\ldots K \end{aligned} \qquad (2.3)$$

where

$$\overline{\phi}_{g_{i,j,k}} \equiv \frac{\sum\limits_{n \subseteq g} \int_{V_{i,j,k}} d\underline{r} \; \phi_n(\underline{r})}{V_{i,j,k}} \quad,$$

$$\overline{\Sigma}_{t_{g_{i,j,k}}} \equiv \frac{\sum\limits_{n \subseteq g} \int_{V_{i,j,k}} d\underline{r} \; \Sigma_{t_n}(\underline{r}) \; \phi_n(\underline{r})}{\overline{\phi}_{g_{i,j,k}} V_{i,j,k}}$$

$$\overline{\Sigma}_{gg'_{i,j,k}} \equiv \frac{\sum\limits_{n' \subseteq g'} \sum\limits_{n \subseteq g} \int_{V_{i,j,k}} d\underline{r} \; \Sigma_{nn'}(\underline{r}) \; \phi_{n'}(\underline{r})}{\overline{\phi}_{g'_{i,j,k}} V_{i,j,k}} \qquad (2.4)$$

$$\overline{M}_{gg'_{i,j,k}} \equiv \frac{\sum\limits_{n' \subseteq g'} \sum\limits_{n \subseteq g} \int_{V_{i,j,k}} d\underline{r} \; M_{nn'}(\underline{r}) \; \phi_{n'}(\underline{r})}{\overline{\phi}_{g'_{i,j,k}} V_{i,j,k}}$$

$$J^u_{g_{i,j,k}} \equiv \frac{\sum\limits_{n \in g} \int_{V_m}^{V_{m+1}} dV \int_{W_n}^{W_{n+1}} dW \; J_n(u_\ell, v, w)}{h^v_m \, h^w_n} \; ;$$

$$u = x, y, z; \quad v \neq u; \quad w \neq u \neq v.$$

Now we define a new mathematical problem for which the defining domain has the same geometry as the real problem but has constant cross sections in each energy range ΔE_g and volume $V_{i,j,k}$. Its governing equation is

$$\nabla \cdot \hat{\underline{J}}_g(\underline{r}) + \hat{\Sigma}_{t_g} \hat{\phi}_g(\underline{r}) = \sum_{g'=1}^{G} [\hat{\Sigma}_{gg'} + \frac{1}{\lambda} \hat{M}_{gg'}] \hat{\phi}_{g'}(\underline{r}) \qquad (2.5)$$

$$g = 1, 2, \ldots G$$

where $\underline{n} \cdot \hat{\underline{J}}_g(\underline{r})$ is continuous across any surface perpendicular to $\underline{n}$. Integration over $V_{i,j,k}$ yields

$$h^y_j h^z_k (\hat{J}^x_{g_{i+1,j,k}} - \hat{J}^x_{g_{i,j,k}}) + h^x_i h^z_k (\hat{J}^y_{g_{i,j+1,k}} - \hat{J}^y_{g_{i,j,k}})$$

$$+ h^x_i h^y_j (\hat{J}^z_{g_{i,j,k+1}} - \hat{J}^z_{g_{i,j,k}}) + V_{i,j,k} \hat{\Sigma}_{t_{g_{i,j,k}}} \hat{\bar{\phi}}_{g_{i,j,k}}$$

$$= \sum_{g'=1}^{G} V_{i,j,k} (\hat{\Sigma}_{gg'_{i,j,k}} + \frac{1}{\lambda} \hat{M}_{gg'_{i,j,k}}) \hat{\bar{\phi}}_{g'_{i,j,k}} \qquad (2.6)$$

$$i = 1, 2, \ldots I; \quad j = 1, 2, \ldots J; \quad k = 1, 2, \ldots K$$

where

$$\hat{\bar{\phi}}_{g_{i,j,k}} \equiv \frac{\int_{V_{i,j,k}} d\underline{r} \; \hat{\phi}_g(\underline{r})}{V_{i,j,k}} \qquad (2.7)$$

Comparison with (2.3) shows that if we define "homogenized

cross sections" as

$$\hat{\Sigma}_{t_{g_{i,j,k}}} = \overline{\Sigma}_{t_{g_{i,j,k}}}$$

$$\hat{\Sigma}_{gg'_{i,j,k}} = \overline{\Sigma}_{gg'_{i,j,k}} \qquad (2.8)$$

$$\hat{M}_{gg'_{i,j,k}} = \overline{M}_{gg'_{i,j,k}}$$

and demand that

$$\hat{J}^u_{g_{i,j,k}} = J^u_{g_{i,j,k}} \quad ; \quad u = x, \ y, \ z \qquad (2.9)$$

then

$$\hat{\overline{\phi}}_{g_{i,j,k}} = \overline{\phi}_{g_{i,j,k}} \qquad , \qquad (2.10)$$

$$\hat{\lambda} = \lambda \quad . \qquad (2.11)$$

To maintain continuity with conventional solution techniques, it is necessary to postulate a relation (model) between homogenized surface-averaged currents, homogenized surface-averaged fluxes and homogenized volume-averaged fluxes. In addition, a relation between homogenized surface-averaged fluxes of neighboring nodes which share a common surface is needed to couple equation (2.6) to other nodes. Since this new homogenized problem is a mathematical problem, there is no reason that homogenized surface-averaged fluxes should be continuous across nodal surfaces. However, we know that in the original physical problem, the one dimensional heterogeneous flux

$$\phi^u_{g_{\ell,m,n}}(u) \equiv \frac{\displaystyle\sum_{n \in g} \int_{V_m}^{V_{m+1}} dV \int_{W_n}^{W_{n+1}} dW \ \phi_n(u,v,w)}{h^V_m \ h^W_n} \qquad (2.12)$$

is a physical quantity so that it is continuous across any nodal surface. On boundaries it is given by

$$\phi_g^{u_\Gamma}(\Gamma) = \alpha_g^{u_\Gamma}(\Gamma) \ J_g^{u_\Gamma}(\Gamma) \qquad (2.13)$$

where Γ is the reactor boundary with u_Γ as its outward normal and $\alpha_g^{u_\Gamma}(\Gamma)$ is u_Γ-direction group g albedo on Γ. If we define "discontinuity factors"

$$f_{g_{\ell,m,n}}^{u-} = \frac{\phi_{g_{\ell,m,n}}^{u}(u_\ell)}{\hat{\phi}_{g_{\ell,m,n}}^{u}(u_\ell)}$$

$$\qquad (2.14)$$

$$f_{g_{\ell,m,n}}^{u+} = \frac{\phi_{g_{\ell,m,n}}^{u}(u_{\ell+1})}{\hat{\phi}_{g_{\ell,m,n}}^{u}(u_{\ell+1})}$$

then we obtain

$$f_{g_{\ell-1,m,n}}^{u+} \ \hat{\phi}_{g_{\ell-1,m,n}}^{u}(u_\ell) = f_{g_{\ell,m,n}}^{u-} \ \hat{\phi}_{g_{\ell,m,n}}^{u}(u_\ell) \qquad (2.15)$$

on internal surfaces and

$$\hat{\phi}_g^{u_\Gamma}(\Gamma) = \hat{\alpha}_g^{u_\Gamma}(\Gamma) \ \hat{J}_g^{u_\Gamma}(\Gamma) = \frac{\alpha_g^{u_\Gamma}(\Gamma)}{f_g^{u_\Gamma-}(\Gamma)} \ \hat{J}_g^{u_\Gamma}(\Gamma) \qquad (2.16)$$

on boundaries of the defining domain. In (2.16), $f_g^{u_\Gamma-}(\Gamma)$ is the discontinuity factor associated with the interior side of Γ in the direction of u and group g. Using these relations along with the chosen model, (2.6) can be solved and it will reproduce any solution of (2.1) (obtained by Monte-Carlo method, transport theory, multi-group diffusion theory, etc.)

as long as that solution has been used to generate the homogenized cross sections $\hat{\Sigma}_{t_{g_{i,j,k}}}$, $\hat{\Sigma}_{gg'_{i,j,k}}$, $M_{gg'_{i,j,k}}$, and the discontinuity factors $f^{u\pm}_{g_{\ell,m,n}}$. These homogenized cross sections and discontinuity factors will be called "equivalence parameters". All of them are needed to define fully the new homogenized mathematical problem. Another implication of equivalence theory is that exact homogenized parameters can be defined for any model. Different models will yield different values for discontinuity factors, but the equivalence parameters will make all quantities of interest be preserved when the global homogenized problem is solved. An important point to note is that it is crucial that the identical model be used in determination of discontinuity factors and in solving the homogenized mathematical problem.

We have pointed out that an exact homogenization over both volume and energy can reporduce any reference solution. In this thesis, however, only volume homogenization will be investigated (i.e.; N=G) and two group fine mesh solutions of the diffusion equation will be taken as references. Before discussing how to estimate equivalence parameters under these restrictions we shall first review the nodal model used in the code "QUANDRY".

2.3 THE QUANDRY MODEL

QUANDRY is a coarse mesh nodal code initially developed to solve two group diffusion equations.[2] Kord Smith has

extended it to solve equivalence equations.[3] In QUANDRY the discontinuity factors $f^{u\pm}_{g_{\ell,m,n}}$ are determined from one-dimensional homogenized flux equations obtained by integrating (2.5) over the transverse directions. The homogenized surface-averaged fluxes $\hat{\phi}^u_{g_{\ell,m,n}}(u_{\ell+1})$ and $\hat{\phi}^u_{g_{\ell,m,n}}(u_\ell)$ can be obtained from an analytical solution of these equations. With the definitions

$$\hat{J}^u_{g_{i,j,k}}(\underline{r}) = -\hat{D}_{g_{i,j,k}} \frac{\partial \hat{\phi}_{g_{i,j,k}}(\underline{r})}{\partial u} \quad ; \tag{2.17}$$

$$\underline{r} \in V_{i,j,k}; \quad u = x,\ y,\ z;\ g = 1,\ 2,\ldots G,$$

and

$$\hat{D}_{g_{i,j,k}} = \left[\frac{\sum\limits_{n \in g} \int\limits_{V_{i,j,k}} d\underline{r}\ D_n^{-1}(\underline{r})\ \phi_n(\underline{r})}{\phi_{g_{i,j,k}}\ V_{i,j,k}} \right]^{-1} \tag{2.18}$$

where $D_n(\underline{r})$ is the diffusion coefficient of the real problem, the one dimensional homogenized flux equations become

$$-\hat{D}_{g_{\ell,m,n}} \frac{\partial^2}{\partial u^2} \hat{\phi}^u_{g_{\ell,m,n}}(u) + \hat{\Sigma}_{t_{g_{\ell,m,n}}} \hat{\phi}^u_{g_{\ell,m,n}}(u)$$

$$-\sum_{g'=1}^{G} (\hat{\Sigma}_{gg'_{\ell,m,n}} + \frac{1}{\lambda}\hat{M}_{gg'_{\ell,m,n}})\ \hat{\phi}^u_{g'_{\ell,m,n}}(u)$$

$$= -\hat{S}^u_{g_{\ell,m,n}}(u); \qquad u = x,y,z;\ g = 1,2,\ldots G \tag{2.19}$$

where

$$\hat{\phi}^u_{g_{\ell,m,n}}(u) = \frac{\int_{V_m}^{V_{m+1}} dV \int_{W_n}^{W_{n+1}} dW\ \hat{\phi}_g(u,v,w)}{h^v_m\ h^n_w}$$

and the $\hat{S}^u_{g_{\ell,m,n}}$ (u) represent the leakage rates on those four surfaces of thickness du which are transverse to direction u. Equation (2.19) can be solved analytically if the u-dependence of $S^u_{g_{\ell,m,n}}$ (u) is known. QUANDRY expresses this dependence to be either a flat or a quadratic function of u. It is important to recognize that neither expression will result in error if the discontinuity factors are found exactly. The detailed derivations of this model and corresponding equivalence equations are described in Reference 2 and 3. Only two equations, which are useful in determining discontinuity factors $f^{u\pm}_{g_{\ell,m,n}}$ when a reference solution is known, are reproduced in the following:

$$[\hat{\phi}^u_{\ell-1,m,n}(u_\ell)] = [B^u_{\ell-1,m,n}][\hat{\bar{\phi}}_{\ell-1,m,n}] - [A^u_{\ell-1,m,n}][\hat{J}^u_{\ell-1,m,n}(u_\ell)]$$

$$- \{[C^{u+}_{\ell-1,m,n}]a^{u-}_{\ell-1} + [D^{u+}_{\ell-1,m,n}]b^{u-}_{\ell-1} + [E^{u+}_{\ell-1,m,n}]c^{u-}_{\ell-1}\}[\hat{\bar{S}}^u_{\ell-2,m,n}]$$

$$- \{[C^{u+}_{\ell-1,m,n}](1 - a^{u-}_{\ell-1} - a^{u+}_{\ell-1}) + [D^{u+}_{\ell-1,m,n}](-b^{u-}_{\ell-1} - b^{u+}_{\ell-1})$$

$$+ [E^{u+}_{\ell-1,m,n}](-c^{u-}_{\ell-1} - c^{u+}_{\ell-1})\}[\hat{\bar{S}}^u_{\ell-1,m,n}]$$

$$- \{[C^{u+}_{\ell-1,m,n}]a^{u+}_{\ell-1} + [D^{u+}_{\ell-1,m,n}]b^{u+}_{\ell-1} + [E^{u+}_{\ell-1,m,n}]c^{u+}_{\ell-1}\}[\hat{\bar{S}}^u_{\ell,m,n}]$$

$$(2.20a)$$

$$[\hat{\phi}^u_{\ell,m,n}(u_\ell)] = [B^u_{\ell,m,n}][\hat{\bar{\phi}}_{\ell,m,n}] + [A^u_{\ell,m,n}][\hat{J}_{\ell,m,n}(u_\ell)]$$

$$- \{[C^{u-}_{\ell,m,n}]a^{u-}_\ell + [D^{u-}_{\ell,m,n}]b^{u-}_\ell + [E^{u-}_{\ell,m,n}]c^{u-}_\ell\}[\hat{\bar{S}}^u_{\ell-1,m,n}]$$

$$+ \{[C^{u-}_{\ell,m,n}](1 - a^{u-}_\ell - a^{u+}_\ell) + [D^{u-}_{\ell,m,n}](-b^{u-}_\ell - b^{u+}_\ell)$$

$+ [E_{\ell,m,n}^{u-}] (-c_\ell^{u-} - c_\ell^{u+}) \quad [\hat{\bar{S}}_{\ell,m,n}^{u}]$

$- \{[C_{\ell,m,n}^{u-}] a_\ell^{u+} + [D_{\ell,m,n}^{u-}] b_\ell^{u+} + [E_{\ell,m,n}^{u-}] c_\ell^{u+}\} \quad [\hat{\bar{S}}_{\ell+1,m,n}^{u}]$ (2.20b)

where

$[\hat{\bar{\phi}}_{\ell,m,n}]$ is a G-element column vector of homogenized node-averaged group fluxes for node (ℓ,m,n),

$[\hat{\phi}_{\ell,m,n}^{u}(u_\ell)]$ is a G-element column vector of homogenized surface-averaged fluxes for node (ℓ,m,n) at $u = u_\ell$,

$[\hat{J}_{\ell,m,n}^{u}(u_\ell)]$ is a G-element column vector of homogenized surface-averaged currents of node (ℓ,m,n) and direction u at $u = u_\ell$,

$[\hat{\bar{S}}_{\ell,m,n}^{u}]$ is a G-element column vector of homogenized node-averaged transverse leakages for node (ℓ,m,n) and direction u, defined by

$$\hat{\bar{S}}^{u}_{g_{\ell,m,n}} = \frac{1}{h_u^\ell} \int_{u_\ell}^{u_{\ell+1}} du \; \hat{S}^{u}_{g_{\ell,m,n}}(u) .$$

The GxG matrices $[A_{\ell,m,n}^{u}]$, $[B_{\ell,m,n}^{u}]$, $[C_{\ell,m,n}^{u\pm}]$, $[D_{\ell,m,n}^{u\pm}]$, and $[E_{\ell,m,n}^{u\pm}]$ are called coupling matrices and are defined in Appendix 2 of Reference 2; they depend only on the homogenized cross sections, homogenized diffusion coefficients, $\hat{D}_{g_{\ell,m,n}}$, mesh spacing and $\hat{\lambda}$. The $a_\ell^{u\pm}$, $b_\ell^{u\pm}$, and $c_\ell^{u\pm}$ are transverse leakage expansion coefficients which depend only on the nodal mesh spacing; they are defined in Appendix 1 of Reference 2 for the quadratic expansion, and they are zero for the flat expansion.

The accuracy of equivalence theory need not be limited by the diffusion theory approximation, and the presence of $\hat{D}_{g_{\ell,m,n}}$ in (2.19) should not imply necessarily that that approximation has been made. Instead the homogenized diffusion constants are introduced in order to make the resultant equivalence equations have a form nearly the same as the equations associated with diffusion theory so that diffusion theory codes can be easily extended to solve them. In this connection, however, it is important to have an accurate numerical method for solving the global equations. Exact equivalence parameters can be obtained only if an exact solution is already known, thus estimation of them is always necessary in practical cases. Among these parameters, homogenized cross sections are model-independent so that there is no way we can alter their values. On the other hand, discontinuity factors are model-dependent and it is expected that a good model will make global solutions less sensitive to their exact values so that a simple approximation can be made. To demonstrate this situation a third model in QUANDRY which is called coarse-mesh finite difference method (CMFD) is also used in this thesis. In this method the $f^{u\pm}_{g_{\ell,m,n}}$ are obtained from the conventional mesh-centered finite difference equations given by

$$\hat{J}^u_{g_{\ell-1,m,n}}(u_\ell) = -\hat{D}_{g_{\ell-1,m,n}} \frac{2}{h_{\ell-1}} (\hat{\phi}^u_{g_{\ell-1,m,n}}(u_\ell) - \bar{\hat{\phi}}_{g_{\ell-1,m,n}}),$$

$$J^u_{g_{\ell},m,n}(u_\ell) = -\hat{D}_{g_{\ell},m,n} \frac{2}{h_\ell} (\hat{\bar{\phi}}_{g_{\ell},m,n} - \hat{\phi}^u_{g_{\ell},m,n}(u_\ell));$$

$$u = x, y, z; \quad g = 1, 2, \ldots G. \tag{2.21}$$

Noting that (2.21) can be recast into a form similar to the original QUANDRY equations, Kord Smith also incorporated this model into QUANDRY by choosing the coupling matrices $[A^u_{\ell,m,n}]$, $[B^u_{\ell,m,n}]$, $[C^{u\pm}_{\ell,m,n}]$, $[D^{u\pm}_{\ell,m,n}]$ and $[E^{u\pm}_{\ell,m,n}]$ in (2.20) in order to match (2.21).

The resultant equivalence equations of all three models (quadratic, flat, CMFD) described above have the following mathematical form:

$$[H]\,[X] = \frac{1}{\hat{\lambda}}\,[P]\,[X] \tag{2.22}$$

where

[H] is a $(4*G*I*J*K)*(4*G*I*J*K)$ square matrix whose elements are linear combinations of the coupling matrices and thus functions of $\hat{\lambda}$,

[P] is a $(4*G*I*J*K)*(4*G*I*J*K)$ square matrix whose elements are zero except in the first $(G*I*J*K)*(G*I*J*K)$ submatrix where it is equal to the fission production matrix,

[X] is a $4*G*I*J*K$-element column vector whose elements are homogenized node-averaged fluxes and face-averaged net leakages in each direction.

Because [H] is dependent on $\hat{\lambda}$, (2.22) is a nonlinear eigenvalue problem. In QUANDRY, the maximum eigenvalue is found by fission source iteration accelerated by Wielandt's frac-

tional iteration method.[4] Within each outer iteration a

modified Gauss-Seidel method[5] is used for the inner itera-

tions and the cyclic Cheybyshev Semi-Iterative method[5] is

used for the flux iterations. These strategies are fully

described in Reference 2. It is important to realize that

even without the use of discontinuity factors and the

Wielandt scheme, and in the limit as the nodal volume $V_{i,j,k}$

approaches zero, so that the equations for the homogenized

node-averaged fluxes $\hat{\phi}_{g_{i,j,k}}$ become the linear mesh-centered

finite difference approximation to the two-group diffusion

equation, the flux iteration scheme is still not guaranteed

to converge because both groups are solved simultaneously

and thus diagonal dominance is not ensured. The Wielandt

scheme will make the lack of diagnonal dominance even more

pronounced and the effect of discontinuity factors on diagonal

dominance is problem dependent as can be seen by using the

CMFD model. Moreover, the nodal volume $V_{i,j,k}$ is not zero

so that [H] depends on $\hat{\lambda}$, and the whole process becomes

nonlinear. Thus there is no guarantee that QUANDRY will

converge. Past experience, however, has shown that it does

converge if proper nodal sizes are chosen. Reasons for

raising these issues will become clearer in Chapter 4.

In the rest of this thesis, all discussions will be

based on the models used in QUANDRY.

2.4 ASSEMBLY EQUIVALENCE PARAMETERS

Exact equivalence parameters can be obtained only if a

reference solution is known for the heterogeneous nodes. Thus for all practical cases, approximations must be made. Kord Smith,[3] because of his finding that discontinuity factors are insensitive to position, suggested an approximation based on an assembly calculation with $\underline{n} \cdot \hat{\underline{J}}_g = 0$ on assembly boundaries. This is an eigenvalue calculation and is the same kind of approximation used to determine conventional flux weighted constants. Because $\underline{n} \cdot \hat{\underline{J}}_g = 0$ on boundaries, the homogenized fluxes for these assembly problems will be constant over the entire assembly including the boundary surfaces. Equation (2.10) then shows that the homogenized surface-averaged fluxes will be equal to the heterogeneous node-averaged flux. Thence the heterogeneous node-averaged and surface-averaged fluxes from the assembly calculation can be used in (2.14) to estimate the discontinuity factors. Discontinuity factors so determined will be called assembly discontinuity factors (ADF). It is important to recognize that, unlike exact discontinuity factors, assembly discontinuity factors are independent of the model used in the global calculations. Equation (2.4), (2.8) along with the heterogeneous fluxes obtained from the assembly calculation provide estimations of homogenized cross sections $\hat{\Sigma}_{t_g}$, $\hat{\Sigma}_{gg'}$, and $\hat{M}_{gg'}$. These will be called assembly homogenized cross sections (AHCS). The conventional flux weighted constants (FWC) consist of assembly homogenized cross sections along with 1 for the discontinuity factors. In the rest of this thesis, when ADF are used, AHCS are implied. ADF have

been tested on all three benchmarks described in Chapter One by Kord Smith[3] and Richard Loretz.[6] A summary of their results is shown in Table (2.1) to (2.3). The columns marked ADF show that that approximation is much more accurate than the FWC method. But if higher accuracy is desired, more sophisticated methods for determining equivalence parameters are required.

TABLE 2.1   SUMMARY OF RESULTS OF THE CISE BWR BENCHMARK

	FWC	ADF	Single-Assembly[1] Flat-Currents Fixed-Source Calculations	Five-Assembly[2] Flat-Currents Fixed-Source Calculations
Error in Eigenvalue	-0.16%	-0.03%	+0.16%	-0.06%
Maximum error in assembly power	+9.86%	-3.06%	-2.76%	+0.77%
Average error in assembly power	4.19%	0.90%	0.97%	0.29%

[1] Results of first global-local iteration using ADF solution as initial estimate.

[2] Results of first global-local iteration using reference solution as initial estimate.

TABLE 2.2   SUMMARY OF RESULTS OF THE HAFAS BWR BENCHMARK

	FWC	ADF	Single-Assembly[1] Flat-Currents Fixed-Source Calculations	Five-Assembly[2] Flat-Currents Fixed-Source Calculations
Error in Eigenvalue	-0.44%	-0.06%	+0.12%	-0.04%
Maximum error in assembly power	+16.95%	-5.29%	+2.21%	+1.07%
Average error in assembly power	6.14%	1.33%	0.86%	0.52%

[1] Results of first global-local iteration using ADF solution as initial estimate.

[2] Results of first global-local iteration using reference solution as initial estimate.

TABLE 2.3   SUMMARY OF RESULTS FOR THE LSHBWR BENCHMARK

	FWC	ADF	Single Assembly[1] Shaped Incoming Partial Currents Fixed Source Calculations
Error in eigenvalue	- 0.29%	-0.08%	0.22%
Maximum error in assembly power	+22.6%	+9.48%	+2.78%
Average error in assembly power	5.90%	3.16%	1.31%

[1] The fixed source calculations were done only for those assemblies surrounding a control rod.

2.5 EVALUATION OF APPROXIMATE EQUIVALENCE PARAMETERS FROM FIXED SOURCE CALCULATIONS

The inaccuracies of ADF arise from the fact that zero current boundary conditions are imposed for the assembly calculations. Because of this, many of the interassembly effects are neglected. However, if the actual boundary conditions that exist on the surfaces of an assembly as well as the global eigenvalue were known, a local fixed-source assembly calculation could be performed for every assembly to obtain equivalence parameters. Equivalence parameters so determined will be exact. Unfortunately, determining these boundary conditions is just as difficult as solving the full heterogeneous problem. Nevertheless, the observation that such fixed-source calculations can produce the desired equivalence parameters suggests an iterative method to improve estimation on the equivalence parameters. We can first solve the global homogenized problem using approximate homogenized parameters (e.g. ADF). From this solution, we can extract approximate boundary conditions needed for each fixed-source calculation. By performing such fixed-source calculations, we can then obtain approximate equivalence parameters which will reflect many of the interassembly effects. Then the global homogenized problem can be solved again but this time using the updated equivalence parameters. Presumably, this latter homogenized solution will be more accurate than its predecessor because the equivalence parameters used to

generate it reflect many of the interassembly effects. This process can be repeated if it appears that greater accuracy will thereby be attained.

Since only average quantities are given by the global homogenized solution, the spatial shapes on the assembly surfaces of any quantity (fluxes, net currents, partial currents, etc.) which is involved in the boundary conditions of the fixed-source calculations need to be specified. The simplest approximation is to assume that they are flat. This will be called "flat" approximation. A more sophisticated approximation is to assume that they have the shape of the same quantity on the same surface in an eigenvalue assembly calculation. For example, if partial currents are used, an assembly calculation with $\underline{n} \cdot \underline{J}_g = 0$ on all surfaces can be performed and it will provide the shape of partial currents on the surfaces. This will be called an "eigenvalue" approximation. If net currents are used, this assembly calculation ($\underline{n} \cdot \underline{J}_g = 0$) does not provide any information about the shape of currents on the surfaces of the assembly. A different assembly calculation which has albedo boundary conditions on all surfaces could be performed and it would provide the needed information. But there is no guarantee that these more sophisticated approximations will give better results than the simple flat approximation.

A more systematic way to improve the approximation on the shapes is to include more assemblies in the fixed-source

calculations and move the approximate surface conditions farther away from the assembly of interest. For example, an assembly with its four nearest neighbors (in 2-D) can be used for the fixed-source calculation. With the approximate boundary conditions moved to the outer boundaries of adjoining assemblies, no explicit limitations on the shapes of the surface quantities need be made for the center assembly. Consequently, the equivalence parameters for the center assembly are less sensitive to the boundary conditions of this fixed-source problem than they are for the case of a single assembly fixed-source calculation. If more assemblies are included in the fixed-source calculations, corresponding equivalence parameters will be even more accurate (although more expensive to obtain).

Because of the approximations about the spatial shapes on the assembly surfaces of those quantities involved in the boundary conditions of the fixed-source problems, the above global-local iteration process (if it converges) will not converge exactly to the reference solution. However, if shapes obtained from previous local fixed-source calculations were used to determine shapes on the boundaries for the next local calculations, the global-local iteration process could converge to the reference solution. Needless to say, if such a strategy were used, more than one assembly would be needed in each fixed-source problem in order to obtain the desired information about the shapes.

Methods using single or five assemblies (an assembly

with its four nearest neighbors) with flat currents on the

boundaries of each fixed-source problem have been applied

to the "CISE" and "HAFAS" problems by Smith.[3] He used the

nodal method to solve every fixed-source problem. For the

method using five assemblies in each fixed-source problem,

because of the cost, he actually used the reference solution

as the initial estimate and assumed that the iteration proc-

ess starting with ADF result would converge to that answer.

Loretz[6] has applied to the "LSHBWR" problem the method

using single assembly and incoming partial currents as bound-

ary conditions in each fixed-source calculation. The shapes

of the incoming partial currents on the boundary surfaces

of the assembly were obtained from a $\underline{n} \cdot \underline{J}_g = 0$ assembly

calculation. The magnitude of these incoming partial cur-

rents were obtained by a double-P_o (DP_o) approximation with

net currents and fluxes on the surfaces of the assembly

given by previous global results. He used the finite dif-

ference method to solve each fixed-source problem. Also

because of the cost, he did the fixed-source calculations

to improve the equivalence parameters only for those assemblies

surrounding a control rod. Their results are shown in the

last two columns of Table (2.1) to (2.3). They do lead to

improved accuracies. However, the cost of the overall com-

putation[7] is comparable to, or even greater than that incurred

by solving the entire problem without homogenization. Thus

unless some efficient method can be developed for solving the fixed source problems, this global-local iteration process is of little interest.

2.6 SUMMARY

In this chapter, equivalence theory was formally presented. It shows that equivalence parameters can be defined such that they will reproduce any reference solution. However, that reference solution must be known in order to generate the exact equivalence parameter. A simple method (ADF) to estimate equivalence parameters was then introduced. Numerical tests show that, if greater accuracy is needed, more sophisticated methods to estimate equivalence parameters are needed. Some more accurate methods (all of them involving fixed-source calculations) were then discussed. However, in terms of computational efficiency, these methods are of little interest unless an efficient method can be developed to solve the fixed-source problems.

The response matrix method, because it provides information of interest directly and because it makes use of parameters (response matrices) which can be precalculated and stored as functions of state variables (exposure, void, etc.), is believed to be most efficient in solving the fixed-source problems. In the next chapter, a method using the conventional partial current response matrices will be discussed.

CHAPTER THREE

THE RESPONSE MATRIX METHOD USING PARTIAL

CURRENT RESPONSE MATRICES

3.1 INTRODUCTION

A global-local iteration procedure to improve estimation of equivalence parameters was proposed in the last chapter. Because of reactor symmetry, the global calculation may not involve the whole core. But, in general, no two nodes in that portion of reactor analyzed will have the same surface quantities (net currents, partial currents, etc.) on their surfaces even if they are geometrically and materially identical. Thus a fixed-source calculation would have to be done for every node (or node with its nearest neighbors) to determine equivalence parameters. If the nodal method or the finite difference method is used to solve each fixed-source problem, the computational expense may become even greater than that incurred by solving the entire problem without homogenization. Thus the use of the response matrix method is strongly suggested because it provides information of interest directly and because it makes use of response matrices which can be precalculated and stored as functions of state variables.

Depending on the symmetry of the assembly and the accuracy with which the spatial shape of surface quantities on the faces of the assembly is to be described, the cost of generating response matrices can be ten or so times that of performing a single fixed-source calculation for an assembly. However,

considering that there are only ten or so different types of assembly in a quarter core which has more than one hundred assemblies, the response matrix approach should be less expensive even if only one iteration is performed. If the same library of response matrices can be used for several problems or if three-dimensional calculations are performed, the response matrix method becomes substantially cheaper. In this chapter, the response matrix method using conventional partial current response matrices will be presented.

3.2 PARTIAL CURRENT RESPONSE MATRICES[8]

3.2.1 DEFINITION

In the response matrix method, the reactor is divided into a number of regions. Each region can be represented by a response matrix which is an operator that defines fully the output of the region by operating on the input imposed on that region. Conventional response matrices use group incoming partial currents on the surfaces of a region as input. Output can be group outgoing partial currents on the surfaces of that region as well as any other information of interest (integrated reaction rates, fluxes at hot spots, etc.) for that region. Conventionally, the response matrices are defined by

$$[J^{out}] = [R] [J^{in}] \quad ,$$
$$[IR] = [R'] [J^{in}]$$

(3.1)

where

$[J^{in}]$ is an N-element column vector whose elements are

group incoming partial currents on the surfaces of

the region of interest,

$[J^{out}]$ is an N-element column vector whose elements are

group outgoing partial currents on the surfaces of

the region of interest,

[IR]   is an M-element column vector whose elements are any

information of interest for the region of interest,

[R]   is an N x N square response matrix,

[R']   is an M x N nonsquare response matrix.

The dimensions of these column vectors and response matrices

(M and N) depend on the accuracy and the amount of informa-

tion wanted. They will be defined after the next section.

3.2.2 GENERATION: ANGULAR AND SPATIAL APPROXIMATION

From equation (3.1), we can see that if $[J^{in}]$ is set to

zero except for the i-th element where it is set to 1, the

corresponding $[J^{out}]$ and [IR] are just the i-th columns of

[R] and [R'], respectively. Thus the generation of the i-th

column of [R] and [R'] is equivalent to solving a problem

defined by putting the region of interest into a vacuum and

imposing on it a unit group incoming partial current for the

surface and group corresponding to the i-th element of $[J^{in}]$.

A series of such fixed source calculations are needed to gen-

erate the whole [R] and [R']. These fixed source problems

can be solved by any method available (transport theory,

multi-group diffusion theory, etc.) to obtain $[J^{out}]$ and [IR].

However, to set up these problem it is insufficient to know

only that the group incoming partial current is 1. We must
also know the angular distribution as well as the spatial dis-
tribution of the neutrons comprising that partial current.
Unfortunately, this information is not available unless a
multigroup transport solution for the whole reactor is known.
In order to make response matrices independent a full-core
solution and thus precalculable, assumptions about the angular
and spatial distributions of this partial current must be made.
In this chapter angular distribution (^DP_o or P-1) is assumed
to be such that heterogeneous surface net currents and surface
fluxes can be expressed in terms of the partial currents on
that surface by

$$[\phi] = 2 \ [J^{in}] + 2 \ [J^{out}]$$
$$[J] = [J^{out}] - [J^{in}]$$

(3.2)

where

    $[\phi]$ is an N-element column vector whose elements are hetero-
       geneous group fluxes on the surfaces of the region of
       interest,

    $[J]$ is an N-element column vector whose elements are hetero-
       geneous group net currents in the outward normal direc-
       tion on the surfaces of the region of interest.

With respect to the spatial shape of this partial current,
the simplest approximation is to assume that it is uniform
over the surface where it is applied. This will be called the
"flat" approximation. Another possibility is to assume that
it is distributed over the surface where it is applied accord-

ing to the shape of the incoming partial current given by
an eigenvalue problem performed by applying the (usually
incorrect) boundary condition $\underline{n} \cdot \underline{J}_g = 0$ on all boundaries
of the region of interest. This procedure will be called
the "eigenvalue" approximation. Since, for many regions
in a reactor, the net currents on their surfaces are small,
the inter-region effects are better simulated by the eigen-
value approximation. Thus that approximation should be supe-
rior to the flat approximation. However, this argument does
not apply to all subregions of a reactor. Accordingly, a
more systematic procedure is to increase the size of $[J^{in}]$
by dividing each surface into smaller subsurfaces and asso-
ciating each element of $[J^{in}]$ with one group and one subsurface.
On each subsurface, the spatial shape of the unit incoming
partial current can be approximated as flat or as that given
by the eigenvalue calculation. In this way the spatial
approximation is applied to smaller areas so that the real
spatial shape is better simulated. In the limit as the areas
of the subsurfaces approach zero, the real spatial shape
will be correctly represented. However, going toward this
limit increases the number of columns of response matrices
and thus increases the number of fixed-source calculations
needed to generate the whole response matrices.

3.2.3 DIMENSION OF RESPONSE MATRICES

In Equation (3.1) and (3.2), the dimensions N and M of
those column vectors and response matrices were not defined.

From the discussion of the last section, "N" should be given
by

$$N = NS * G \qquad\qquad (3.3)$$

where

NS is the total number of subsurfaces on the total bound-
ary of a region,

G is the total number of energy groups.

In this thesis, because all problems considered are two groups
in two dimensional Cartesian coordinates and all boundary
lines are divided into equal numbers of segments (1 or 2),
N = NSEG * 8 where NSEG is the number of segments on each
boundary line. Because the purpose of this investigation is
to determine equivalence parameters, the information needed
consists of the heterogeneous volume-integrated reaction rates,
the heterogeneous volume-integrated fluxes, the heterogeneous
surface-averaged fluxes, and the heterogeneous surface-aver-
aged net currents. The first two are needed to determine
homogenized cross sections as can be seen from equations (2.4)
and (2.8). The last three together with the homogenized cross
sections and eigenvalue are needed to generate discontinuity
factors as can been seen from equations (2.9), (2.10), (2.14)
and (2.20). Because of the angular approximation, surface
values of fluxes and net currents can be obtained provided
both incoming and outgoing partial currents are knwon. Thus
[IR] need not include these surface values but merely all
volume-integrated values. In our investigation fission spectra

are assumed to be the same for all isotopes so that $\hat{M}_{gg'_{i,j,k}}$ can be rewritten as $\hat{\chi}_g \nu \hat{\Sigma}_{f_{g'_{i,j,k}}}$. With this simplification it turns out that the total number of elements M needed in the vector [IR] equals 12.

3.2.4 TABULATION AND INTERPOLATION

Throughout our investigation, in order to be consistent with our numerical reference cases which are generated using diffusion theory, response matrices will always be generated by the multi-group diffusion theory, mesh-centered, finite difference code "CITATION".[9] The details of how to use this code to solve problems with incoming partial currents as boundary conditions are given in Appendix B.1.

With spatial and angular approximations made for a unit incoming partial current, response matrices for a region become independent of its outside environment and thus can be pretabulated as parametric functions of all state variables (exposure, temperature, void, eigenvalue, etc.) It is important to realize that the eigenvalue must be included in the list of state variables. The response matrices used in each local calculation should be those associated with the global eigenvalue which is obtained from previous global calculations and updated as the global-local iteration proceeds.

With this table created, whenever we wish to perform a local calculation, we can obtain the response matrices corresponding to the present state variables by interpolation. This multi-dimensional interpolation is not studied in this

thesis. However, it is by no means a trivial problem.

3.2.5 SIZE OF THE REGION USED TO DEFINE RESPONSE MATRICES

In order to make interpolation of response matrices possible, the size of the region used to define response matrices must be small enough so that the state variables inside that region will be rather uniform. On the other hand, its size should be reasonably large so that the number of fixed source calculations can be kept within bounds. Because of these considerations the horizontal cross section of a single BWR assembly is always chosen as the region to define response matrices throughout our investigations.

3.3 FIXED-SOURCE CALCULATIONS USING PARTIAL CURRENT RESPONSE MATRICES

3.3.1 RESPONSE MATRICES FOR A NODE

With response matrices defined and generated we can now discuss the fixed-source problems which are used to improve the estimation of equivalence parameters. To define these problems first the size of the node which constitutes the area we want to homogenize must be chosen. Since response matrices are generated for assemblies, the node can only be a single assembly or a cluster of assemblies. The larger the node is, fewer nodes there will be making up the reactor and the faster the global calculation will be. However, at the same time the local calculations will become less efficient since the state variables of a node larger than an assembly will not be uniform and response matrices for such nodes can

not be precalculated. Instead they must be obtained through

a local calculation by lengthy arithmetic manipulation of

the response matrices of those assemblies comprising that

node. Moreover, the overall procedure will become less

accurate because spatial approximations for those local

problems will be applied to larger areas. In this thesis,

two kinds of size for a node will be used, namely; a single

assembly as a node and four assemblies as a node. The former

will be called "assembly homogenization" and the latter will

be called "cluster homogenization". These configurations

and some notation needed for later derivations are shown

on Figure 3.1 and 3.2. For assembly homogenization, response

matrices of a node are just those of an assembly and are

pretabulated. However, for cluster homogenization, the

response matrices of the cluster (node) are not precalculated
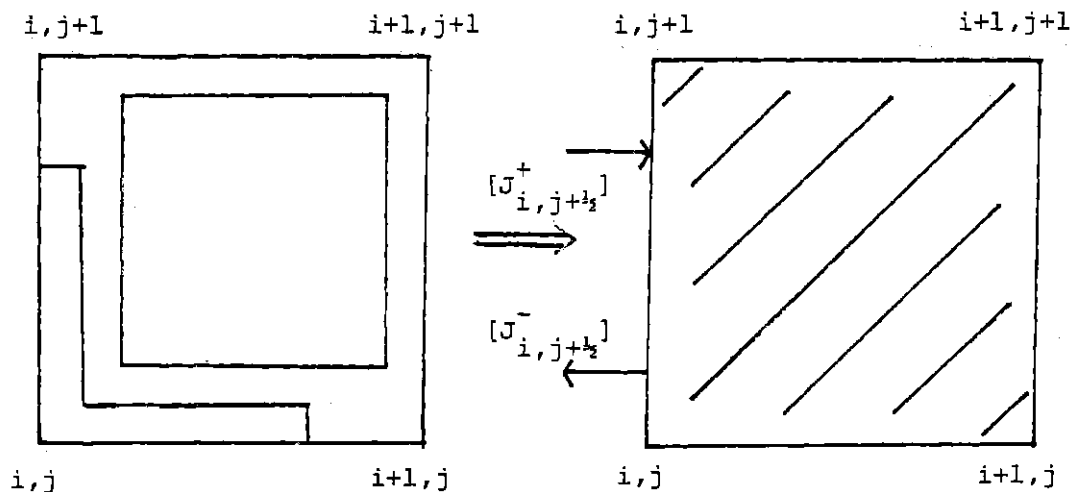
FIGURE 3.1 CONFIGURATION AND NOTA-

TION OF THE ASSEMBLY HOMOGENIZATION
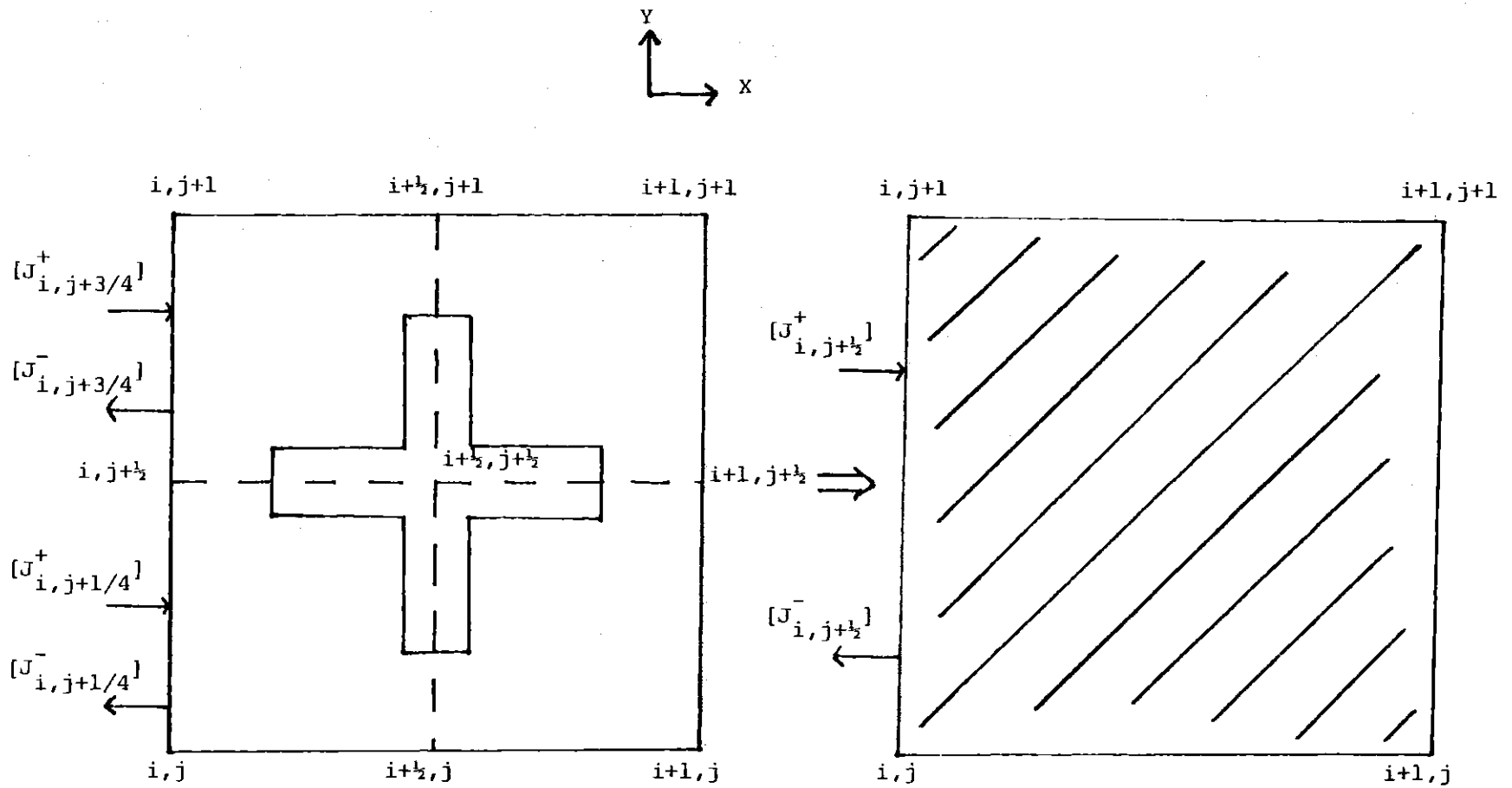
FIGURE 3.2 CONFIGURATION AND NOTATION OF THE CLUSTER HOMOGENIZATION

and need to be determined. Knowing the state variables within each assembly in the node, we can obtain by inter-polation from a table of precalculated values response matri-ces for each assembly.

If each assembly of a 4-assembly node is represented by the grid index at its left-bottom corner (Fig. 3.2), equation (3.1) becomes

$$\begin{bmatrix} [J^-_{\alpha,\beta+1/4}] \\ [J^-_{\alpha+1/4,\beta}] \\ [J^+_{\alpha+1/2,\beta+1/4}] \\ [J^+_{\alpha+1/4,\beta+1/2}] \end{bmatrix} = \begin{bmatrix} [R^{\alpha,\beta}_{11}] & [R^{\alpha,\beta}_{12}] & [R^{\alpha,\beta}_{13}] & [R^{\alpha,\beta}_{14}] \\ [R^{\alpha,\beta}_{21}] & [R^{\alpha,\beta}_{22}] & [R^{\alpha,\beta}_{23}] & [R^{\alpha,\beta}_{24}] \\ [R^{\alpha,\beta}_{31}] & [R^{\alpha,\beta}_{32}] & [R^{\alpha,\beta}_{33}] & [R^{\alpha,\beta}_{34}] \\ [R^{\alpha,\beta}_{41}] & [R^{\alpha,\beta}_{42}] & [R^{\alpha,\beta}_{43}] & [R^{\alpha,\beta}_{44}] \end{bmatrix} \begin{bmatrix} [J^+_{\alpha,\beta+1/4}] \\ [J^+_{\alpha+1/4,\beta}] \\ [J^-_{\alpha+1/2,\beta+1/4}] \\ [J^-_{\alpha+1/4,\beta+1/2}] \end{bmatrix}$$

$$\alpha = i, \ i + 1/2,$$

$$\beta = j, \ j + 1/2,$$

$$i = 1, \ 2,\ldots I,$$

$$j = 1, \ 2,\ldots J$$

(3.4)

where

$[J^\pm_{\gamma,\delta+1/4}]$ are (G*NSEG)-element column vectors whose elements are total group partial currents of each segment on the line connecting points (γ,δ) to $(\gamma,\delta+1/2)$ if $\gamma = \alpha, \ \alpha+1/2$, or (δ,γ) to $(\delta+1/2,\gamma)$ if $\gamma = \beta, \ \beta+1/2$,

$[R^{\alpha,\beta}_{\gamma\delta}]$ is a (G*NSEG)*(G*NSEG) square matrix whose elements are the elements of the (γ,δ) submatrix of the response matrix for assembly (α,β); $\gamma,\delta = 1,2,3,4$,

NSEG is the number of segments on each boundary line

of an assembly,

G   is the total number of groups.

In this equation, the (+) and (−) are used to represent the partial currents in the positive and negative u-direction (u = x or y), respectively. With the definition

$$[J^{\pm}_{\ell,m+1/2}] \;=\; \begin{bmatrix} [J^{\pm}_{\ell,m+1/4}] \\ [J^{\pm}_{\ell,m+3/4}] \end{bmatrix} \tag{3.5}$$

manipulation of (3.4) will give

$$[A_{i,j}]\;[J^{INNER}_{i,j}] \;=\; [B_{i,j}]\;[J^{in}_{i,j}] \tag{3.6}$$

$$[J^{out}_{i,j}] \;=\; [C_{i,j}]\;[J^{in}_{i,j}] \;+\; [D_{i,j}]\;[J^{INNER}_{i,j}] \tag{3.7}$$

where

$$[J^{in}_{i,j}] = \mathrm{col}\{[J^{+}_{i,j+1/2}],[J^{+}_{i+1/2,j}],[J^{-}_{i+1,j+1/2}],[J^{-}_{i+1/2,j+1}]\},$$

$$[J^{out}_{i,j}] = \mathrm{col}\{[J^{-}_{i,j+1/2}],[J^{-}_{i+1/2,j}],[J^{+}_{i+1,j+1/2}],[J^{+}_{i+1/2,j+1}]\},$$

$$[J^{INNER}_{i,j}] = \mathrm{col}\{[J^{-}_{i+1/2,j+1/4}],[J^{-}_{i+1/2,j+3/4}],[J^{-}_{i+1/4,j+1/2}],$$

$$[J^{-}_{i+3/4,j+1/2}],[J^{+}_{i+1/2,j+1/4}],[J^{+}_{i+1/2,j+3/4}],$$

$$[J^{+}_{i+1/4,j+1/2}],[J^{+}_{i+3/4,j+1/2}]\},$$

$$[A_{ij}] = \begin{bmatrix}
[I] & [0] & [0] & -[R_{14}^{i+\frac{1}{2},j}] & -[R_{11}^{i+\frac{1}{2},j}] & [0] & [0] & [0] \\
[0] & [I] & [0] & [0] & [0] & -[R_{11}^{i+\frac{1}{2},j+\frac{1}{2}}] & [0] & -[R_{12}^{i+\frac{1}{2},j+\frac{1}{2}}] \\
[0] & -[R_{23}^{i,j+\frac{1}{2}}] & [I] & [0] & [0] & [0] & -[R_{22}^{i,j+\frac{1}{2}}] & [0] \\
[0] & [0] & [0] & [I] & [0] & -[R_{21}^{i+\frac{1}{2},j+\frac{1}{2}}] & [0] & -[R_{22}^{i+\frac{1}{2},j+\frac{1}{2}}] \\
-[R_{33}^{i,j}] & [0] & -[R_{34}^{i,j}] & [0] & [I] & [0] & [0] & [0] \\
[0] & -[R_{33}^{i,j+\frac{1}{2}}] & [0] & [0] & [0] & [I] & -[R_{32}^{i,j+\frac{1}{2}}] & [0] \\
-[R_{43}^{i,j}] & [0] & -[R_{44}^{i,j}] & [0] & [0] & [0] & [I] & [0] \\
[0] & [0] & [0] & -[R_{44}^{i+\frac{1}{2},j}] & -[R_{41}^{i+\frac{1}{2},j}] & [0] & [0] & [I]
\end{bmatrix}$$

$$[B_{ij}] = \begin{bmatrix}
[0] & [0] & [0] & [R_{12}^{i+\frac{1}{2},j}] & [R_{13}^{i+\frac{1}{2},j}] & [0] & [0] & [0] \\
[0] & [0] & [0] & [0] & [0] & [R_{13}^{i+\frac{1}{2},j+\frac{1}{2}}] & [0] & [R_{14}^{i+\frac{1}{2},j+\frac{1}{2}}] \\
[0] & [R_{21}^{i,j+\frac{1}{2}}] & [0] & [0] & [0] & [0] & [R_{24}^{i,j+\frac{1}{2}}] & [0] \\
[0] & [0] & [0] & [0] & [0] & [R_{23}^{i+\frac{1}{2},j+\frac{1}{2}}] & [0] & [R_{24}^{i+\frac{1}{2},j+\frac{1}{2}}] \\
[R_{31}^{i,j}] & [0] & [R_{32}^{i,j}] & [0] & [0] & [0] & [0] & [0] \\
[0] & [R_{31}^{i,j+\frac{1}{2}}] & [0] & [0] & [0] & [0] & [R_{34}^{i,j+\frac{1}{2}}] & [0] \\
[R_{41}^{i,j}] & [0] & [R_{42}^{i,j}] & [0] & [0] & [0] & [0] & [0] \\
[0] & [0] & [0] & [R_{42}^{i+\frac{1}{2},j}] & [R_{43}^{i+\frac{1}{2},j}] & [0] & [0] & [0]
\end{bmatrix}$$

$$[C_{i,j}] = \begin{bmatrix} [R_{11}^{i,j}] & [0] & [R_{12}^{i,j}] & [0] & [0] & [0] & [0] & [0] \\ [0] & [R_{11}^{i,j+\frac{1}{2}}] & [0] & [0] & [0] & [0] & [R_{14}^{i,j+\frac{1}{2}}] & [0] \\ [R_{21}^{i,j}] & [0] & [R_{22}^{i,j}] & [0] & [0] & [0] & [0] & [0] \\ [0] & [0] & [0] & [R_{22}^{i+\frac{1}{2},j}] & [R_{23}^{i+\frac{1}{2},j}] & [0] & [0] & [0] \\ [0] & [0] & [0] & [R_{32}^{i+\frac{1}{2},j}] & [R_{33}^{i+\frac{1}{2},j}] & [0] & [0] & [0] \\ [0] & [0] & [0] & [0] & [0] & [R_{33}^{i+\frac{1}{2},j+\frac{1}{2}}] & [0] & [R_{34}^{i+\frac{1}{2},j+\frac{1}{2}}] \\ [0] & [R_{41}^{i,j+\frac{1}{2}}] & [0] & [0] & [0] & [0] & [R_{44}^{i,j+\frac{1}{2}}] & [0] \\ [0] & [0] & [0] & [0] & [0] & [R_{43}^{i+\frac{1}{2},j+\frac{1}{2}}] & [0] & [R_{44}^{i+\frac{1}{2},j+\frac{1}{2}}] \end{bmatrix}$$

$$[D_{i,j}] = \begin{bmatrix} [R_{13}^{i,j}] & [0] & [R_{14}^{i,j}] & [0] & [0] & [0] & [0] & [0] \\ [0] & [R_{13}^{i,j+\frac{1}{2}}] & [0] & [0] & [0] & [0] & [R_{12}^{i,j+\frac{1}{2}}] & [0] \\ [R_{23}^{i,j}] & [0] & [R_{24}^{i,j}] & [0] & [0] & [0] & [0] & [0] \\ [0] & [0] & [0] & [R_{24}^{i+\frac{1}{2},j}] & [R_{21}^{i+\frac{1}{2},j}] & [0] & [0] & [0] \\ [0] & [0] & [0] & [R_{34}^{i+\frac{1}{2},j}] & [R_{31}^{i+\frac{1}{2},j}] & [0] & [0] & [0] \\ [0] & [0] & [0] & [0] & [0] & [R_{31}^{i+\frac{1}{2},j+\frac{1}{2}}] & [0] & [R_{32}^{i+\frac{1}{2},j+\frac{1}{2}}] \\ [0] & [R_{43}^{i,j+\frac{1}{2}}] & [0] & [0] & [0] & [0] & [R_{42}^{i,j+\frac{1}{2}}] & [0] \\ [0] & [0] & [0] & [0] & [0] & [R_{41}^{i+\frac{1}{2},j+\frac{1}{2}}] & [0] & [R_{42}^{i+\frac{1}{2},j+\frac{1}{2}}] \end{bmatrix}$$

$[R_{\gamma\delta}^{\alpha,\beta}]$ in this equation are defined in (3.4). [I] and [0] are (G*NSEG) by (G*NSEG) identity and null matrices, respectively.

From (3.6) we get

$$[J_{i,j}^{INNER}] = [A_{i,j}]^{-1} [B_{i,j}] [J_{i,j}^{in}] \qquad (3.8)$$

Substituting it into (3.7) gives

$$[J_{i,j}^{out}] = \{[C_{i,j}] + [D_{i,j}][A_{i,j}]^{-1}[B_{i,j}]\} [J_{i,j}^{in}]. \qquad (3.9)$$

Thus the response matrix [R] of the cluster (i,j) is given by

$$[R_{i,j}] = [C_{i,j}] + [D_{i,j}] [A_{i,j}]^{-1} [B_{i,j}]. \qquad (3.10)$$

The response matrix [R'] of the cluster can be obtained in a similar way. However, we choose another way to obtain the information needed. Knowing $[J_{i,j}^{in}]$ from (3.8), we can calculate $[J_{i,j}^{INNER}]$. By permuting $[J_{i,j}^{in}]$ together with $[J_{i,j}^{INNER}]$, the incoming partial currents for each assembly can be found. Then all the information needed can be obtained by using the response matrix [R'] of each assembly. Since this information consists of volume-integrated quantities, the column vector [IR] for the entire cluster will be given by

$$[IR_{i,j}] = \sum_{\alpha} [IR_{i,j}^{\alpha}] \qquad (3.11)$$

where

$[IR_{i,j}]$ is an M-element column vector whose elements are
     cluster volume-integrated values for node (i,j),

$[IR_{i,j}^{\alpha}]$ is an M-element column vector whose elements are

assembly volume-integrated values of assembly α in
node (i,j) with α running through all four assemblies
in node (i,j).

$[IR^{\alpha}_{i,j}]$ in this equation is obtained from (3.1). Note that
since $[A_{i,j}]$, $[B_{i,j}]$, $[C_{i,j}]$, and $[D_{i,j}]$ depend on the
response matrices of all the assemblies comprising node (i,j),
they can not be determined until the state variables in each
assembly are known. Thus the response matrices of a cluster
cannot be precalculated.

In each local calculation, it is necessary to invert
a (8*G*NSEG) X (8*G*NSEG) matrix and do some matrix multi-
plication to obtain the response matrix $[R_{i,j}]$. Thus using a
cluster as a node, we have shifted the computational burden
from global problems to local problems.

In order to make the calculation of $[R_{i,j}]$ efficient,
advantage can be taken of the sparseness of $[A_{i,j}]$, $[B_{i,j}]$,
$[C_{i,j}]$, and $[D_{i,j}]$. Details are described in Appendix C.

3.3.2 SETTING UP LOCAL FIXED-SOURCE PROBLEMS

In our investigation, either a single node or five nodes
(the node to be homogenized and its nearest neighbors) will
be used as the defining domain of each fixed-source problem.
On every boundary line of an assembly (no matter whether the
node is an assembly or a cluster) we can have either 1 or 2
segments. Thus for either assembly of cluster homogenization
four kinds of local problems can be defined. They are speci-
fied in Table 3.1.

Method	Number of Nodes* in Each Fixed-Source Problem	Number of Segments on the Boundary Line of Each Assembly
N5S2	5	2
N5S1	5	1
N1S2	1	2
N1S1	1	1

*Node can be either an assembly or a cluster

TABLE 3.1   METHOD DEFINITION

It is important to realize that all fixed-source problems
for a given local calculation in our investigation will be
carried out using the same method. For cluster homogeniza-
tion the number of segments on each boundary line of a
cluster is actually twice the number of segments on each
boundary line of an assembly (i.e., for 2-segment methods,
there are four segments on each boundary line of a cluster).

Because only the magnitude of the net surface currents
(obtained from (2.9)) and surface fluxes (obtained from
(2.14)) on each surface of a node can be deduced from pre-
vious global results, equation (3.2), which is consistent
with the angular approximation used in generating the response
matrices, will be needed to obtain as boundary conditions the
magnitude of the incoming partial currents on boundaries of
the domain included in each fixed-source problem. Because
this magnitude is that of the partial currents over an entire
nodal surface, spatial approximations are also needed (except
for assembly homogenization using 1-segment methods) to de-
fine fully the boundary conditions for each fixed-source

problem. For assembly homogenization using 2-segment methods, either the flat or the eigenvalue approximation will be used along with total magnitudes over the whole nodal boundary to determine the incoming partial currents for each segment. For cluster homogenization the flat approximation can be used directly to determine the incoming partial currents for each segment. However, because cluster eigenvalue calculations cannot be carried out beforehand (for the same reason that the response matrices of a cluster cannot be precalculated), incoming partial current distributions must be found from the ratios of partial currents for the individual assemblies making up the cluster. Accordingly, with the magnitude of the incoming partial current for a given cluster face having four segments found as described above, we assume that the partial current is split equally between the lower and upper pairs of segments. Then within each pair the ratio of partial currents can be found from an assembly eigenvalue calculation.

3.3.3 SOLUTION TECHNIQUES

For assembly homogenization, if incoming partial currents $[J_{i,j}^{in}]$ of node (i,j) are known, outgoing partial currents $[J_{i,j}^{out}]$ and the information column vector $[IR_{i,j}]$ can be obtained directly by applying equation (3.1) to that assembly.

For cluster homogenization, if incoming partial currents $[J_{i,j}^{in}]$ of node (i,j) are known and the response matrix $[R_{i,j}]$ of the node has been determined by (3.10), outgoing partial

currents $[J_{i,j}^{out}]$ can be obtained by applying (3.1) to that cluster. $[J_{i,j}^{INNER}]$, which are partial currents on assembly boundary lines not common to cluster boundaries, can be determined from (3.8). Knowing $[J_{i,j}^{in}]$ and $[J_{i,j}^{INNER}]$, the incoming partial currents for each assembly comprising the cluster can be established and then $[IR_{i,j}]$ can be determined according to (3.11).

Once $[J_{i,j}^{in}]$, $[J_{i,j}^{out}]$, and $[IR_{i,j}]$ are determined, procedures to calculate equivalence parameters for node (i,j) are the same for both assembly or cluster homogenization. By using $[IR_{i,j}]$ which contains heterogeneous node volume-integrated reaction rates and heterogeneous node volume-integrated group fluxes, homogenized cross sections and heterogeneous node volume-averaged group fluxes can be obtained according to (2.4) and (2.8). Equations (3.2) yield heterogeneous surface-averaged group fluxes and heterogeneous surface-averaged net currents. Since all heterogeneous values except heterogeneous surface-averaged group fluxes are equal to the corresponding homogenized values, equation (2.20) together with equation (2.14) can be used to obtain discontinuity factors. It is important to realize that if the quadratic transverse leakage model is used, the transverse leakages of neighboring nodes are needed to determine discontinuity factors. Thus discontinuity factors must be generated after fixed-source calculations for all nodes have been done.

The remaining problem is how to get incoming partial currents $[J^{in}_{i,j}]$ for node (i,j).

For 1-node fixed-source calculations (1 or 2 segments), they are just the given boundary conditions because boundaries of the domain of the fixed-source problem coincide with boundaries of the node to be homogenized.

For 5-node fixed-source calculations, since only incoming partial currents on boundaries of the domain of the fixed-source problem are given by previous global results, incoming partial currents on boundaries of the center node which is the node to be homogenized need to be determined. The configuration and some notation for 5-node fixed-source problems are shown in Figure 3.3. Writing out equation (3.1) for each node and regrouping gives

$$\begin{bmatrix} [I] & -[D_{i,j}] \\ -[R_{i,j}] & [I] \end{bmatrix} \begin{bmatrix} [J^{in}_{i,j}] \\ [J^{out}_{i,j}] \end{bmatrix} = \begin{bmatrix} [Y_{i,j}] \\ [0] \end{bmatrix} \qquad (3.12)$$

where

$[0]$ is an N-element column vector with elements equal to zero,

$[I]$ is an N*N identity matrix,

$[R_{i,j}]$ is the N*N response matrix for node (i,j),

$[D_{i,j}]$ is an N*N diagnonal matrix associated with node (i,j) and given by

$$[D_{i,j}] = \text{Diag}\{[R^{i-1,j}_{33}], \ [R^{i,j-1}_{44}], \ [R^{i+1,j}_{11}], \ [R^{i,j+1}_{22}]\} \qquad (3.13)$$

	(i,j+1)	
(i-1,j)	(i,j)	(i+1,j)
	(i,j-1)	

$$[R_{\ell,m}] = \begin{bmatrix} [R_{11}^{\ell,m}] & [R_{12}^{\ell,m}] & [R_{13}^{\ell,m}] & [R_{14}^{\ell,m}] \\ [R_{21}^{\ell,m}] & [R_{22}^{\ell,m}] & [R_{23}^{\ell,m}] & [R_{24}^{\ell,m}] \\ [R_{31}^{\ell,m}] & [R_{32}^{\ell,m}] & [R_{33}^{\ell,m}] & [R_{34}^{\ell,m}] \\ [R_{41}^{\ell,m}] & [R_{42}^{\ell,m}] & [R_{43}^{\ell,m}] & [R_{44}^{\ell,m}] \end{bmatrix}$$

surface labelling for any given node
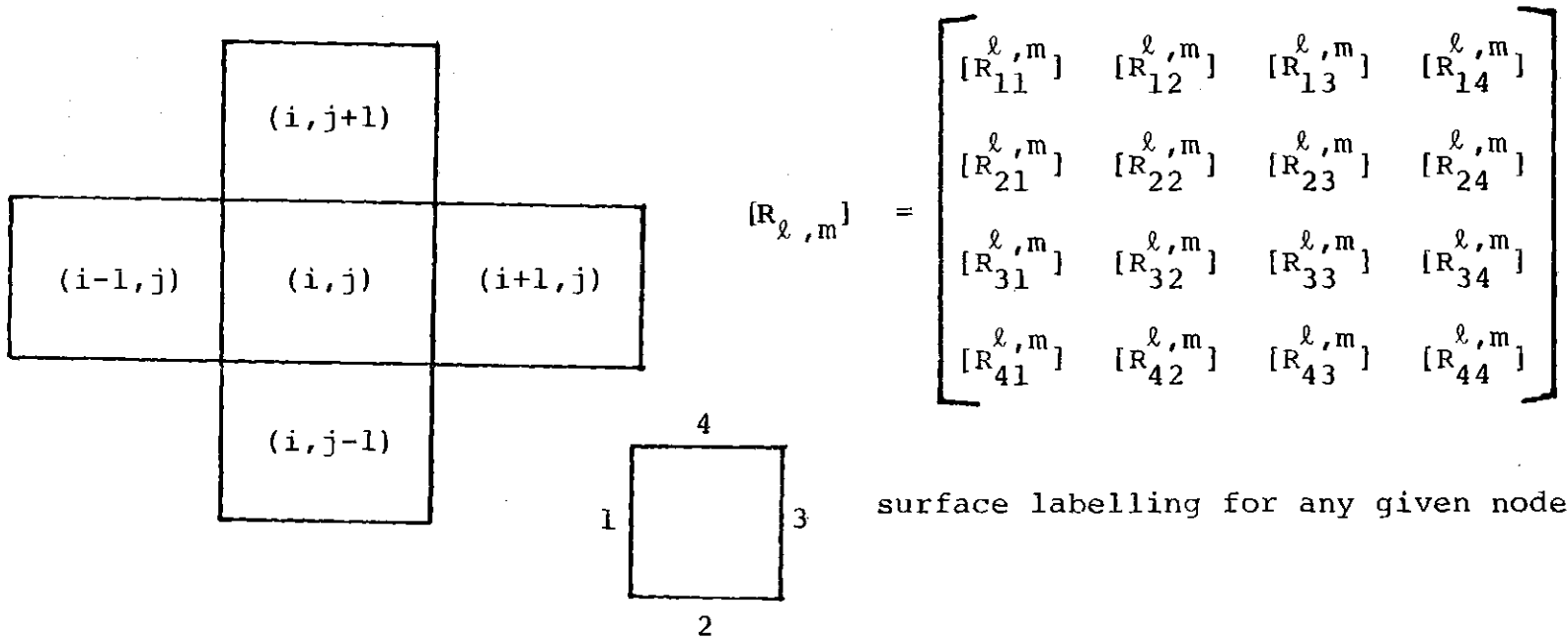
$[R_{\alpha\beta}^{\ell,m}]$ is a P * P matrix of matrix elements connecting outgoing partial currents on face α to incoming partial currents on face β; $\alpha,\beta=1,2,3,4$,

P   = 2 * NSEG * G for cluster homogenization,

P   = NSEG * G for assembly homogenization

FIGURE 3.3   CONFIGURATION AND NOTATION FOR 5-NODE FIXED SOURCE PROBLEMS USING PARTIAL CURRENT RESPONSE MATRICES.

$[J_{i,j}^{in}]$ and $[J_{i,j}^{out}]$ are N-element column vectors whose elements are group partial currents of node (i,j), $N = 4 * P$, P and $[R_{\alpha\alpha}^{l,m}]$ with $\alpha = 1,2,3,4$ are defined in Figure 3.3.

The $[Y_{i,j}]$ in the above equation are given by

$$[Y_{i,j}] = \text{Col}\{[Y_{i,j}^1], [Y_{i,j}^2], [Y_{i,j}^3], [Y_{i,j}^4]\} \qquad (3.14)$$

where

$$[Y_{i,j}^1] = [Z_{i,j}^1][J_{i-1,j}^{in}],$$

$$[Y_{i,j}^2] = [Z_{i,j}^2][J_{i,j-1}^{in}],$$

$$[Y_{i,j}^3] = [Z_{i,j}^3][J_{i+1,j}^{in}],$$

$$[Y_{i,j}^4] = [Z_{i,j}^4][J_{i,j+1}^{in}],$$

$$[Z_{i,j}^1] = \{[R_{31}^{i-1,j}][R_{32}^{i-1,j}][0][R_{34}^{i-1,j}]\},$$

$$[Z_{i,j}^2] = \{[R_{41}^{i,j-1}][R_{42}^{i,j-1}][R_{43}^{i,j-1}][0]\},$$

$$[Z_{i,j}^3] = \{[0][R_{12}^{i+1,j}][R_{13}^{i+1,j}][R_{14}^{i+1,j}]\},$$

$$[Z_{i,j}^4] = \{[R_{21}^{i,j+1}][0][R_{23}^{i,j+1}][R_{24}^{i+1,j}]\},$$

[0]   is a P * P null matrix,

P and $[R_{\alpha\beta}^{l,m}]$ with $\alpha,\beta = 1,2,3,4$ are defined on Figure 3.3. Equation (3.12) is solved by a block Gauss-Seidel iteration method. Because the coefficient matrix may not be diagonally dominant, the iteration cannot be proved by the standard mathematical method to be convergent. However, the physics of the situation suggests that it will in fact always converge. Iterations can be considered as neutron generations and a region with a fixed source in a vacuum will reach an asymptotic

state provided that region itself in a vacuum is subcritical.
Thus this iteration method will converge as long as the
total domain of the fixed-source problem is subcritical
in a vacuum. Since this requirement is always met in prac-
tical cases, there is no problem in solving (3.12) by the
Gauss-Seidel method.

The overall procedure for local calculations are shown
on Figure 3.4. A computer code "RESPONSE" was developed
to carry out the local calculations according to that flow
chart.

3.4 NUMERICAL TESTS

3.4.1 A PRELIMINARY TEST PROBLEM

In order to see whether the response matrices method
can provide a good estimation of equivalence parameters,
a core consisting of very heterogeneous assemblies was
analyzed as a preliminary test of the method. This test
zone is described in Appendix A.4 and Figure A.4.1 shows
the layout. The central cluster of the test zone was the
node homogenized. In each assembly fuel pins, water rods,
gadolinium rods, control blades, wide and narrow water gaps
were explicitly modeled. The test zone was assumed to be
part of a reactor with eigenvalue equal to 1. Two standard
solutions characteristic of the test zone present in dif-
ferent environments were generated by CITATION. (How to
use CITATION to obtain these standards is described at the
end of Appendix B.1.) The first environment simulated the
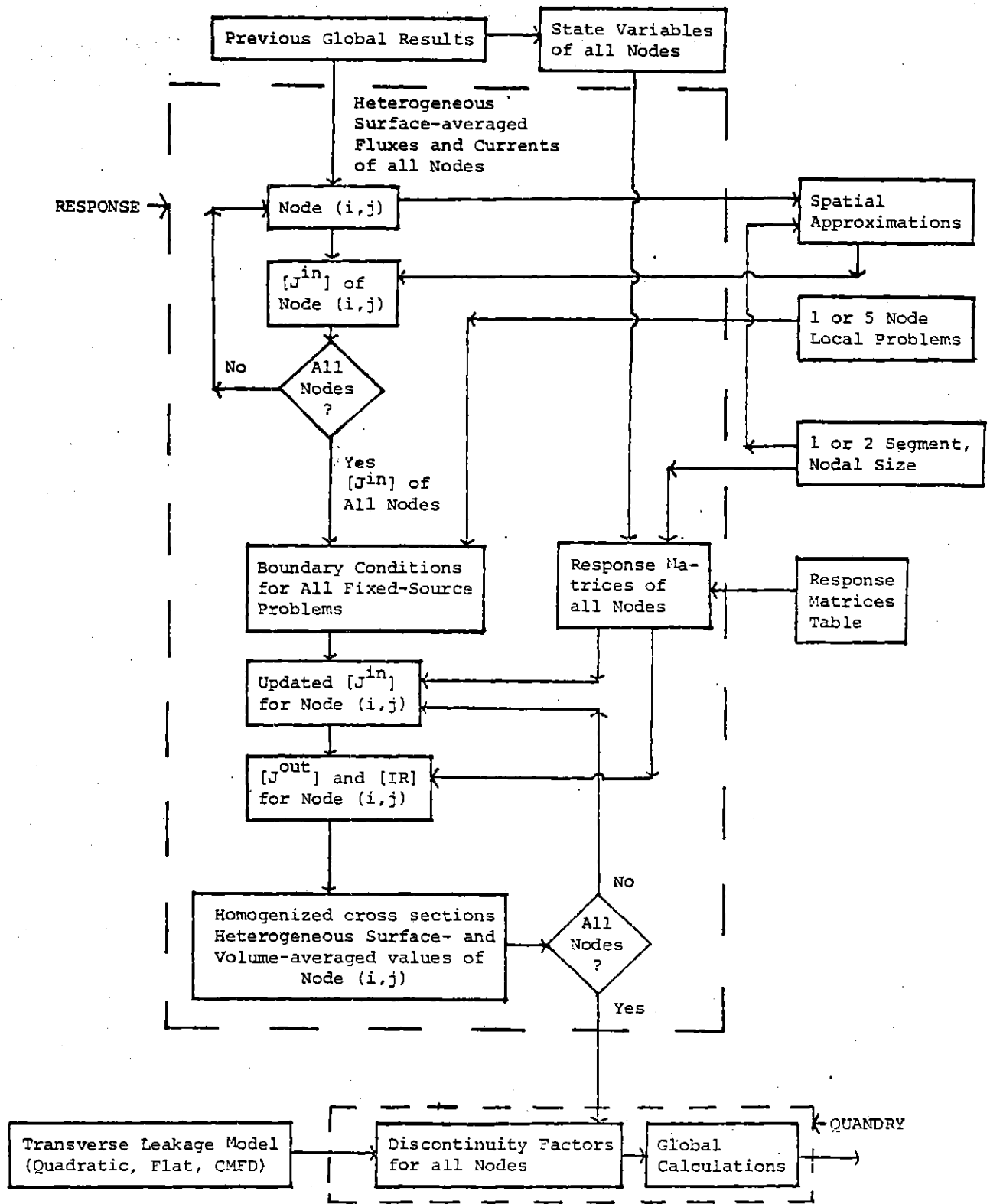
FIGURE 3.4   LOCAL CALCULATION PROCEDURES

central part of the core so that the spatial shape of
incoming partial currents was asymptotic (i.e., it approaches
the eigenvalue distribution). The second environment was
assumed to be such that the spatial shape of incoming
partial currents was flat. For both problems, discontinuity
factors were for the flat transverse leakage model.

Response matrices for this problem were generated with
either flat or eigenvalue spatial approximation. The cor-
rect eigenvalue (1) was used to generate them. To define
the local fixed-source calculation, initial estimates of
the magnitude of surface-averaged group incoming partial
currents on boundaries of the fixed-source problem were
obtained from the standard. The spatial approximation used
to determine the partial currents on those assembly boundary
lines that constitute each cluster boundary line was flat
(which is exact because of the symmetry of this problem).
The spatial approximation (if needed) used to determine
the partial currents of each segment on boundaries of the
fixed-source problem was chosen for consistency to be that
used to generate the response matrices. Discontinuity factors
were generated using the flat transverse leakage model.

All four cluster homogenization methods were tested,
and results are shown in Table 3.2. They suggest that
using the eigenvalue spatial approximation yields better
results than using the flat spatial approximation no matter
what standard is considered. Also with the eigenvalue approx-

Case:	I	II	III	IV	V	VI	VII
Method:	N5S2	N1S2	N5S2	N1S2	N5S1	N1S1	ADF[1]
Spatial Approximation In Generating Response Matrices (F = Flat, E = Eigenvalue)	F	F	E	E	E	E	
Spatial Approximation in Local Fixed-Source Calculations	F	F	E	E			

% Error		I	II	III	IV	V	VI	VII
	$\nu\hat{\Sigma}_{f_1}$	-0.66	-0.58	-0.15	-0.11	-0.13	-0.12	-0.36
	$\nu\hat{\Sigma}_{f_2}$	-0.10	-0.12	-0.26	-0.13	-0.06	-0.07	0.696
	$\hat{\Sigma}_{R_1}=\hat{\Sigma}_{a_1}+\hat{\Sigma}_{21}$	0.35	0.42	0.09	0.14	0.19	0.19	0.30
	$\hat{\Sigma}_{a_2}$	1.43	1.55	0.18	0.50	0.85	0.85	2.18
	$\hat{\Sigma}_{21}$	0.02	-0.05	0.00	-0.05	-0.07	-0.07	-0.32
	$f_1^{\pm}$	-3.91	-5.63	-1.23	-2.66	-3.24	-3.24	3.59
	$f_2^{\pm}$	-4.73	-9.05	-1.53	-3.60	-4.38	-4.38	5.39

[1] This column gives the errors for ADF.

TABLE 3.2.A RESULTS FOR THE PRELIMINARY TEST PROBLEM USING EIGENVALUE SHAPES FOR STANDARD

Case:	I	II	III	IV	V	VI	VII
Method:	N5S2	N1S2	N5S2	N1S2	N5S1	N1S1 ·	ADF[1]
Spatial Approximation In Generating Response Matrices (F = Flat, E = Eigenvalue)	F	F	E	E	E	E	
Spatial Approximation in Local Fixed-Source Calculations	F	F	E	E			

		I	II	III	IV	V	VI	VII
	$\nu\hat{\Sigma}_{f_1}$	-0.63	-0.58	-0.12	-0.10	-0.09	-0.12	0.39
	$\nu\hat{\Sigma}_{f_2}$	-0.29	-0.13	-0.45	-0.14	-0.25	-0.08	0.51
	$\hat{\Sigma}_{R_1}$	0.33	0.40	0.07	0.12	0.17	0.17	0.29
% Error	$\hat{\Sigma}_{R_2}$	1.04	1.44	-0.20	0.40	0.47	0.70	1.79
	$\hat{\Sigma}_{21}$	0.02	-0.04	0.00	-0.04	-0.07	-0.06	-0.33
	$f_1^{\pm}$	-3.44	-5.36	-0.76	-2.20	-2.78	-2.78	4.09
	$f_2^{\pm}$	-4.16	-7.80	-0.95	-2.20	-3.81	-2.92	6.01

[1] This column gives the errors in ADF.

TABLE 3.2.B   RESULTS FOR THE PRELIMINARY TEST PROBLEM USING FLAT SHAPES FOR STANDARD

imation, errors in all equivalence parameters are smaller than those associated with ADF.

Because the magnitudes of partial currents used to define the fixed-source problem were obtained from the respective standards, these results are the best the various methods can yield.

3.4.2 CISE BENCHMARK

For the CISE benchmark, response matrices for all multiplying assemblies were generated using the eigenvalue approximation, and response matrices for reflector were generated with the flat approximation. Because of the cost, they are generated with the reference eigenvalue and were never updated during the global-local iterations. Both assembly and cluster homogenizations were tested. For the cluster homogenization response matrices of a vacuum assembly are needed as can be seen from Figure A.1.2 in Appendix A. They are given by

$$[R'] = \text{null matrix}$$

$$[R] = \begin{bmatrix} [0] & [0] & [I] & [0] \\ [0] & [0] & [0] & [I] \\ [I] & [0] & [0] & [0] \\ [0] & [I] & [0] & [0] \end{bmatrix} \tag{3.14}$$

where [0] and [I] are (NSEG*G)*(NSEG*G) null and identity matrices, respectively. Equation (3.14) is just the statement that neutrons coming in through a face will continue through and emerge across the opposite face.

For cluster homogenization the spatial shape used to determine the partial currents on those assembly boundary lines that constitute each cluster boundary line was assumed to be flat. For either assembly or cluster homogenization, if 2-segment methods were used, the spatial approximation used to determine the partial currents at each segment for an assembly was that used to generate the response matrices of that assembly. Both the "flat" and the "quadratic" transverse leakage model were examined with one or the other model used consistently throughout the global-local iterations to determine discontinuity factors and to solve the global equations. The procedures are outlined in Figure 3.5. Results, shown in Table 3.3 and Figure F.1 and F.2 of Appendix F, indicate that errors are very large.

To understand better why for this problem the response matrix method does not work, a detailed examination of all equivalence parameters for all nodes was made. It showed:

1. for any local method the errors in homogenized cross sections obtained by the response matrix method are smaller than 0.7% everywhere in the reactor while assembly homogenized cross sections (AHCS) have errors around 2% and even larger than 3% in a number of nodes,

2. the errors in discontinuity factors in the central part of the reactor are around 3% which is comparable
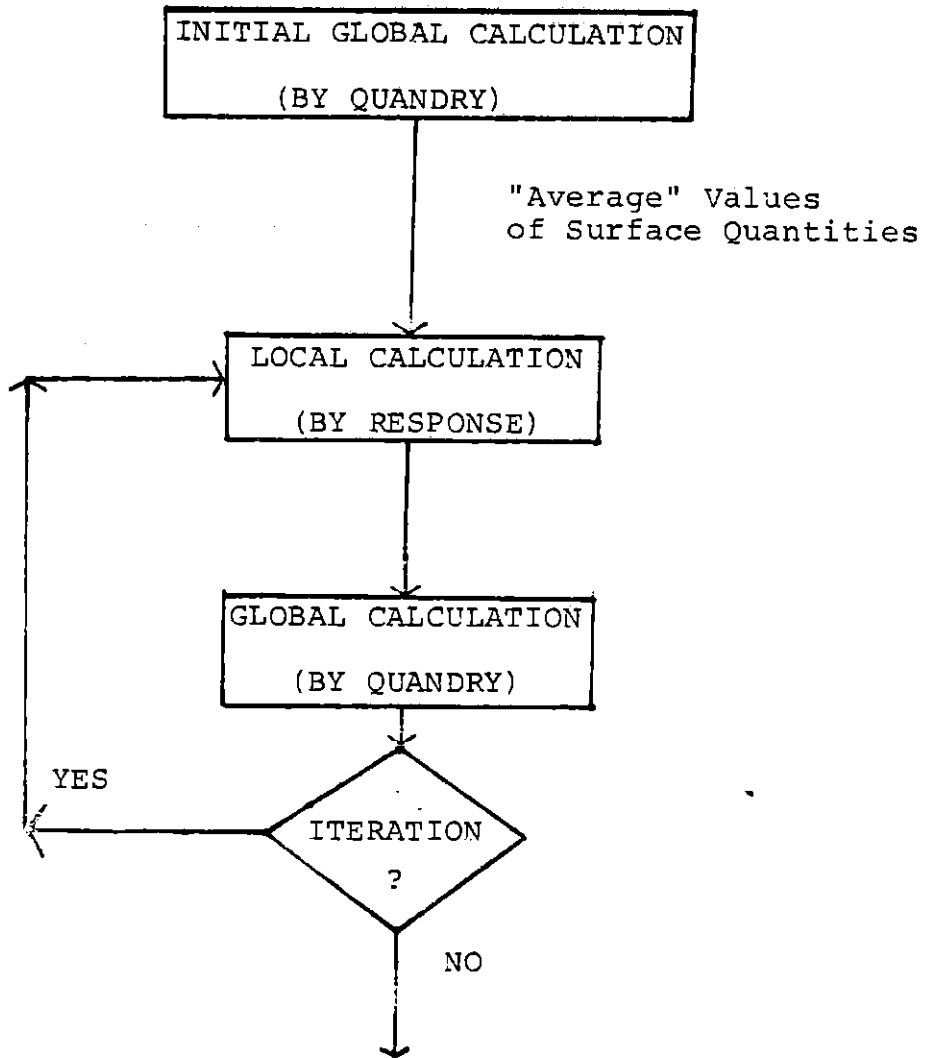
FIGURE 3.5   GLOBAL-LOCAL ITERATION PROCEDURES

Case	I (ADFF)[1]	II (ADFQ)[2]	III	IV	V	VI	VII
Model in Global Calculation (F = flat, Q = quadratic)	F	Q	F	F	F	Q	Q
Initial Estimation			ADFF	ADFF	ADFF	ADFQ	Reference[3]
Nodal Size	Cluster	Cluster	Cluster	Cluster	Cluster	Cluster	Assembly
Method in Local Calculation			N1S2	N5S2	N5S2	N5S2	N5S2
Nth Iteration			1	1	$2^{(5)}$	1	1
Error % [4] λ	0.02	-0.05	-1.67	-1.23	-1.12	-1.25	-1.08
ε_{max}	-2.63	-2.05	47.8	28.1	9.54	29.0	24.53
ε_{av}	1.19	0.82	15.2	6.39	3.50	6.88	8.58

[1] ADFF is the result obtained by solving the global equations with the flat transverse leakage model using ADF.

[2] ADFQ is the result obtained by solving the global equations with the quadratic transverse leakage model using ADF.

[3] Reference solution provided only the magnitude of the surface quantities.

[4] λ = eigenvalue, ε_{max} is the maximum error in nodal power, ε_{av} is the average of volume-weighted absolute errors in nodal power.

[5] Response matrices used for the 2nd iteration are still those associated with the reference eigenvalue.

TABLE 3.3 RESULTS FOR THE CISE BENCHMARK USING PARTIAL CURRENT RESPONSE MATRICES

to the errors incurred using assembly discontinuity
factors,

3. the errors in discontinuity factors on the periphery
of the core are quite large (over 30% for fuel assem-
blies and 100% for adjacent reflector nodes).

It thus appears that the error in power comes largely from
the errors in discontinuity factors of nodes near the reac-
tor boundaries. To demonstrate further this conclusion a
simple problem described in Appendix A.5 was solved. The
eigenvalue approximation which is flat was used to generate
response matrices. Results are shown in Table 3.4. Since
each node is initially homogeneous, the error in power comes
entirely from errors in the discontinuity factors.

It seems clear that the response matrix method using
partial current response matrices cannot predict accurately
discontinuity factors for nodes near reactor boundaries.
Moreover, for a large reactor the errors near the periphery
of the core will cause large errors in power. The main
reason for this shortcoming is the spatial approximation
for the incoming partial currents used to generate the re-
sponse matrices. In these fixed-source problems for gener-
ating response matrices, the resultant outgoing partial
currents will have different spatial shapes from those of
the incoming partial currents (e.g., if a flat approximation
is used for the incoming partial currents, the resultant
outgoing partial currents will not be flat). Using these

Case		I
Model		Q
Initial Estimation		ADFQ[1]
Nodal Size		Assembly
Method in Local Calculation		N5S2
Nth iteration		1
	λ	-2.0
% Error	ε_{max}	1.98
	ε_{av}	1.48
	$DF^{[2]}$	38.0

[1] For this problem using ADF will reproduce the reference solution because it is actually a 1-D problem and every node is initially homogeneous.

[2] This is the error in the discontinuity factor for the thermal group on the $J_{in} = 0$ face. It is also the maximum error in the discontinuity factors.

TABLE 3.4   RESULTS OF THE HOMOGENEOUS
PROBLEM IN APPENDIX A.5.

response matrices for the local fixed-source calculations
thus implies a net current which may not be good enough for
simulating the real spatial shapes. Our results show that
they are not adequate for nodes near the reactor boundaries.
As an example, for the problem in Appendix A.5 the fluxes
and x-direction net currents on the line LL' should be
flat in y and the y-direction net currents on the line MM'
should be zero. But the response matrix method gives non-
flat fluxes and non-flat x-direction net currents on the
line LL' and the y-direction net currents on the line MM'
are zero only in an average sense.

Because homogenized cross sections are associated with
the whole node, they are not so sensitive to an approxima-
tion applied at the surfaces of the node. Thus they can
be predicted accurately by the response matrix method with
partial current response matrices. On the other hand, dis-
continuity factors are the ratio of heterogeneous to homog-
enized surface fluxes which are surface quantities. Accord-
ingly they are very sensitive to the validity of the approx-
imation applied on the surfaces. Thus for nodes near the
periphery discontinuity factors obtained by the partial
current response matrix method will have large errors. Con-
sequently, the next global calculation will result in large
errors in power.

We have mentioned in section 2.5 that Loretz did obtain
improvements by using a fixed-source problem with partial

currents as boundary conditions to update equivalence parameters. His method corresponds to our N1S1 method using response matrices generated with the eigenvalue approximation. However, he did only local fixed-source calculations for nodes surrounding a control rod. These nodes are not in the periphery of the reactor so that the fact that he could obtain improvements is not contradictory to our results.

Another important result obtained from this benchmark is that assembly homogenization is much faster than cluster homogenization. A comparison of execution time is shown in Table 3.5. It shows that the time saved in the global calculation by using a cluster as a node is far less than the extra time needed for the local calculation using cluster homogenization methods. The reason is that it is very time consuming to obtain response matrices [R] for all clusters. (It takes over 75% of the total local calculation time.)

3.5 SUMMARY

In this chapter the definition and characteristics of partial current response matrices were first presented. Then we discussed various methods for solving fixed-source problems by using tabulated partial current response matrices. Numerical tests show that because of the validity of the spatial approximation, discontinuity factors for peripheral nodes will be greatly in error and this results in a large error in power and eigenvalue in the next global calculation.

Global or Local Calculation	Nodal Size	Method in Local Calculation	CPU Time (Sec)
Local	Cluster	N5S2	8.00
Local	Assembly	N5S2	2.32
Global	Cluster		0.90
Global	Assembly		3.35

TABLE 3.5   EXECUTING TIME OF CLUSTER AND ASSEMBLY

HOMOGENIZATIONS FOR CISE BENCHMARK

Because the spatial distribution of net currents is smoother and less sensitive to position than the spatial distribution of partial currents is, simulating by a single predetermined shape the spatial distribution of net currents for one type of assembly regardless of its location in the reactor is believed to be able to yield better results. As mentioned in section 2.5, Kord Smith did obtain good results by using a fixed-source calculation with flat net currents as boundary conditions. These suggest the use of a different response matrix which relates surface fluxes and nodal volume integrals to net currents. Such response matrices will be called "net current response matrices" and will be discussed in the next chapter.

CHAPTER FOUR

THE RESPONSE MATRIX METHOD USING NET

CURRENT RESPONSE MATRICES

4.1 INTRODUCTION

We have pointed out in the last chapter that it is inadequate to use the response matrix method with partial current response matrices to evaluate discontinuity factors because of the spatial shape of the assembly surface fluxes and outgoing partial currents implied by the shape of an incoming partial current. Because the spatial distribution of net currents is smoother, it is believed that the response matrix method based on net current response matrices can give better results. The test problems of Kord Smith given in Section 2.5 strongly suggest that the net current method will work. In this chapter, we shall discuss first net current response matrices and then local fixed-source calculations using these response matrices.

4.2 NET CURRENT RESPONSE MATRICES

4.2.1 DEFINITION

Just as with a partial current response matrix, a net current response matrix is an operator that defines fully the output from a region by operating on the input imposed on that region. However instead of using group incoming partial currents as input, group net currents on boundary surfaces of the region are used as input. Output can be group surface fluxes on boundaries of that region as well as information of interest about the interior of the region.

In mathematical form, net current response matrices are given by

$$[\phi] = [R][J] \ ,$$
$$[IR] = [R'][J] \qquad\qquad (4.1)$$

where

> $[\phi]$ is an N-element column vector whose elements are heterogeneous group surface fluxes on boundaries of the region of interest,
>
> $[J]$ is an N-element column vector whose elements are heterogeneous group net currents in the direction of the outward normal on boundaries of the region of interest,
>
> $[IR]$ is an M-element column vector whose elements are any information of interest for the region of interest,
>
> $[R]$ is an N*N square response matrix,
>
> $[R']$ is an M*N non-square response matrix.

M and N in this equation will be shown in the next section to be the same as those defined in Section 3.2.3.

4.2.2   GENERATION: ANGULAR AND SPATIAL APPROXIMATION

As partial current response matrices, the i-th column of $[R]$ and $[R']$ are equal respectively to $[\phi]$ and $[IR]$ obtained from a problem with zero $[J]$ except for its i-th element where it is equal to 1. Thus we also need a series

of fixed-source problems to generate whole $[R]$ and $[R']$.
However this time each fixed-source problem is equivalent
to a problem defined by the region adjacent to a perfect
reflector except for the group and surface corresponding
to i-th element of $[J]$. For that group and surface, the
net current is set to 1. For each fixed-source problem,
without any knowledge of the full-core solution we need
both angular and spatial approximation of the unit net
current to define fully that problem. With them, each
fixed-source problem can be solved by any method available
(transport theory, multi-group diffusion theory, etc.).
Since our references are generated with diffusion theory
code, for consistency each fixed-source problem will also
be solved under diffusion theory approximation and thus
no further angular approximation will be needed. With
respect to the spatial approximation, unless otherwise
specified we shall assume that the unit net current is
uniformly distributed over the surface through which it
is passing. This will be called the 'flat' approximation.
As with partial current response matrices, the spatial
approximation can be improved by dividing each surface of
the region into several sub-surfaces and associating each
element of $[J]$ with one group and one sub-surface. The
flat approximation is then applied on each sub-surface.

There is no reason why we cannot make use of an eigen-
value approximation as with the partial current response
matrices. However an eigenvalue calculation with $\underline{n} \cdot \underline{J}_g = 0$

on all boundaries will not be able to provide the needed
information. An eigenvalue calculation with albedo boundary
condition imposed on one segment will be needed. However
without any knowledge of the full-core solution, the correct
value of the albedo to be used is unknown so that this
approximation is less attractive. Thus only the flat approxi-
mation will be used in this chapter for the net current
response matrices.

4.2.3 DIMENSION OF THE RESPONSE MATRICES

In view of the discussions in the last section and in
Section 3.2.3, we choose the dimensions N and M of the net
current response matrices to be the same as those of the
partial current response matrices. Thus M is equal to 12
and N is given by 8*NSEG where NSEG is the number of segments
(1 or 2) on each boundary line of the region.

4.2.4 TABULATION AND INTERPOLATION

In order to be consistent with our numerical reference
cases which are generated using diffusion theory, net current
response matrices will always be generated by the diffusion
theory code CITATION. The details of using CITATION to
generate net current response matrices are described in
Appendix B.2.

With the spatial approximation and diffusion theory
approximation made for the unit net current, net current
response matrices can be precalculated and tabulated as
functions of state variables just as partial current
response matrices are. However if the region of interest,

after being made consistent with the global eigenvalue, is just critical in an infinite lattice composed of its own material, net current response matrices for this state will not exist. This situation happens whenever the estimated global eigenvalue is exactly equal to the infinite multiplication factor of the region of interest. This situation is not a practical problem since the probability that it will arise is of measure zero. However, for states near this singular condition, elements of net current response matrices will approach positive or negative infinite depending on which side (supercritical or subcritical) of the singularity they are on. The multi-variable interpolation of net current response matrices is particularly complicated by this phenomenon. This problem is presently being investigated by H. Khalil [10] and will not be discussed further in the present thesis.

4.2.5 SIZE OF THE REGION USED TO DEFINE RESPONSE MATRICES

For the same reasons as the case of partial current response matrices (described in Section 3.2.5) BWR assemblies are chosen as the region to be used to define net current response matrices.

4.3 FIXED-SOURCE CALCULATION USING NET CURRENT RESPONSE MATRICES

4.3.1 RESPONSE MATRICES FOR A NODE

In Section 3.4.2, we concluded that the time saved in a global calculation by using a cluster as a node is far less than the extra time needed for the local calculation with

cluster homogenization because response matrices of a cluster cannot be precalculated. This situation is the same for net current response matrices. Accordingly in this chapter we shall use only assembly homogenization. Thus response matrices for a node are just those of an assembly and are pretabulated.

4.3.2 SETTING UP LOCAL FIXED-SOURCE PROBLEMS

As in Section 3.3.2, either 1 node or 5 nodes (the node to be homogenized and its four nearest neighbors) will be used as the defining domain of each local fixed-source problem. And on each boundary line of an assembly, we can have either 1 or 2 segments. Combination of them yields four methods which will be designated by the same names as those used in Table 3.1 (except that now a node can only be an assembly).

Unlike the situation in Section 3.3.2, defining each local fixed-source problem does not require use of Eq (3.2) to generate incoming partial currents. Previous global homogenized results give heterogeneous net surface current directly through Equation (2.9). Moreover, if 1-segment methods are used, no spatial approximation is needed. However, if 2-segment methods are used, spatial approximation are needed to determine the net currents for each segment on boundaries of the defining domain of each fixed-source problem. In order to be consistent with the spatial approximation used to generate net current response matrices, the flat approximation will be used.

Because a node is an assembly and consistent spatial approximations are used to generate response matrices and to define local fixed-source problems, Methods N1S1 and N1S2 are the same for all nodes except boundary nodes (for which Method N1S1 satisfies the boundary conditions in an average sense while Method N1S2 satisfies them for each individual segment). Equivalence parameters obtained from the two methods will then not be the same for peripheral nodes, and thus global iterations will yield different results.

4.3.3 SOLUTION TECHNIQUES

Once heterogeneous net surface currents $[J_{ij}]$ of the node to be homogenized are known, heterogeneous surface fluxes $[\phi_{i,j}]$ and the information vector $[IR_{i,j}]$, which contains heterogeneous node volume-integrated reaction rates and fluxes, can be obtained directly by applying Equation (4.1) to that node. Then homogenized cross sections can be obtained according to (2.4) and (2.8). Using the global eigenvalue from the previous global calculation, discontinuity factors can be obtained from (2.20).

The sole problem, then, is to determine $[J_{i,j}]$ for the node to be homogenized. For the 1-node methods (1 or 2 segments), it is obtained directly from the previous global results. For 5-node methods, it has to be calculated from net currents on the outermost boundaries of the adjoining assemblies obtained from previous global results. The configuration and some notation for 5-node fixed-source

problems are shown in Figure 4.1. Writing out Equation (4.1)

for all nodes and regrouping yields

$$
\begin{bmatrix} [I] & [D_{i,j}] \\ [I] & -[R_{i,j}] \end{bmatrix} \begin{bmatrix} [\phi_{i,j}] \\ [J_{i,j}] \end{bmatrix} = \begin{bmatrix} [Y_{i,j}] \\ [0] \end{bmatrix}
$$

(4.2)

where

$[\phi_{i,j}]$ is an N-element column vector whose elements
are heterogeneous group surface currents of
segments on the boundaries of the central
node (i,j),

$[J_{i,j}]$ is an N-element column vector whose elements
are heterogeneous group surface net currents
of a segment in the outward direction on the
boundaries of the central node (i,j),

$[R_{i,j}]$ is the N*N response matrix for node (i,j),

$[Y_{i,j}]$ is an N-element column vector whose elements
are the fluxes on the surfaces of node (i,j)
due to net currents across those faces of
its four neighboring nodes that are not
common to node (i,j),

$[D_{i,j}]$ is an N*N diagonal matrix associated with the
surfaces of node (i,j) but depending on the
properties of its neighbors. It is given by

$$[D_{i,j}] = \text{Diag } \{[R_{33}^{i-1,j}], [R_{44}^{i,j-1}], [R_{11}^{i+1,j}], [R_{22}^{i,j+1}]\}$$

SURFACE LABELLING
FOR ANY GIVEN NODE:
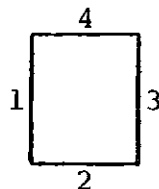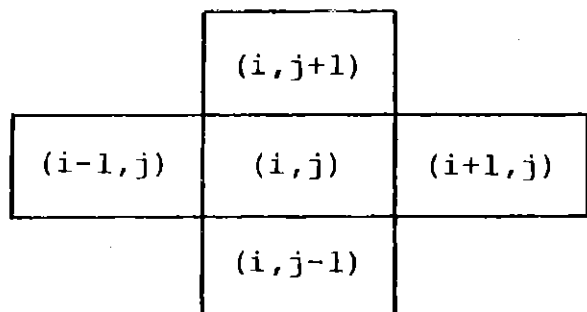
$$[R_{\ell,m}] = \begin{bmatrix} [R_{11}^{\ell,m}] & [R_{12}^{\ell,m}] & [R_{13}^{\ell,m}] & [R_{14}^{\ell,m}] \\ [R_{21}^{\ell,m}] & [R_{22}^{\ell,m}] & [R_{23}^{\ell,m}] & [R_{24}^{\ell,m}] \\ [R_{31}^{\ell,m}] & [R_{32}^{\ell,m}] & [R_{33}^{\ell,m}] & [R_{34}^{\ell,m}] \\ [R_{41}^{\ell,m}] & [R_{42}^{\ell,m}] & [R_{43}^{\ell,m}] & [R_{44}^{\ell,m}] \end{bmatrix}$$

$[R_{\alpha\beta}^{\ell,m}]$ is an $(NSEG*G)*(NSEG*G)$ square matrix of matrix elements connecting fluxes on face α to net currents on face β, $\alpha,\beta = 1,2,3,4$,

where
   NSEG is the number of segments on each boundary line of node (ℓ,m),
   G is the total number of groups.

FIGURE 4.1 CONFIGURATION AND NOTATION FOR 5-NODE FIXED SOURCE
PROBLEMS USING NET CURRENT RESPONSE MATRICES

$[I]$ is the N*N identity matrix,

$[0]$ is an N-element column vector whose elements are zero,

N = 4 * NSEG * G,

$[R_{\alpha\alpha}^{\ell,m}]$ $(\alpha = 1,2,3,4)$ are defined on Figure 4.1.

The surface flux source term $[Y_{i,j}]$ in this equation is given by

$$[Y_{i,j}] = \text{Col}\{[Y_{i,j}^1], [Y_{i,j}^2], [Y_{i,j}^3], [Y_{i,j}^4]\} \qquad (4.3)$$

where

$$[Y_{i,j}^1] = [Z_{i,j}^1][J_{i-1,j}] \ ,$$

$$[Y_{i,j}^2] = [Z_{i,j}^2][J_{i,j-1}] \ ,$$

$$[Y_{i,j}^3] = [Z_{i,j}^3][J_{i+1,j}] \ ,$$

$$[Y_{i,j}^4] = [Z_{i,j}^4][J_{i,j+1}] \ ,$$

$$[Z_{i,j}^1] = \{[R_{31}^{i-1,j}][R_{32}^{i-1,j}][0][R_{34}^{i-1,j}]\},$$

$$[Z_{i,j}^2] = \{[R_{41}^{i,j-1}] [R_{42}^{i,j-1}] [R_{43}^{i,j-1}][0]\} \ ,$$

$$[Z_{i,j}^3] = \{[0][R_{12}^{i+1,j}][R_{13}^{i+1,j}][R_{14}^{i+1,j}]\} \ ,$$

$$[Z_{i,j}^4] = \{[R_{21}^{i,j+1}][0][R_{23}^{i,j+1}][R_{24}^{i,j+1}]\} \ ,$$

$[0]$ is an (NSEG*G)*(NSEG*G) null matrix,

$[R_{\alpha\beta}^{\ell,m}]$ $(\alpha,\beta=1,2,3,4)$ are defined on Figure 4.1.

Equation (4.2) has almost the same form as Equation (3.12).
However it cannot be solved by the Gauss-Seidel iteration
method as was done earlier because that method will not
converge for this case. In fact, we can prove (see
Appendix D) that for a one-dimensional one-group problem
the spectral radius of the Gauss-Seidel iteration matrix
will be larger than 1 except under very limited conditions.
For two-dimensional two-group problems, we can anticipate
that the possibility of convergence will become even less.
Thus in order to be able to solve all local fixed-source
problems throughout the reactor, we abandon iteration
methods and solve (4.2) directly. Substituting the second
sub-matrix equation (4.2) into the first yields

$$[J_{i,j}] = \{[D_{i,j}] + [R_{i,j}]\}^{-1}[Y_{i,j}] \qquad (4.4)$$

where $[D_{i,j}] + [R_{i,j}]$ is inverted directly.

The overall procedures for local calculations using net
current response matrices are the same as those shown in
Figure 3.1 except that $[J_{i,j}^{in}]$ and $[J_{i,j}^{out}]$ are replaced by
$[J_{i,j}]$ and $[\phi_{i,j}]$ and the nodal size is always an assembly.
A new version of RESPONSE was developed to carry out the
local calculations using net current response matrices
according to that flow chart.

4.4 NUMERICAL TESTS

4.4.1 CISE BENCHMARK

The global-local iteration procedure was the same as that shown in Figure 3.5. In order to reduce the cost of global-local iterations, response matrices were generated for the reference eigenvalue and were never updated during the global-local iterations. All four methods (N1S1, N1S2, N5S1, and N5S2) for the local calculations and three models, quadratic (Q), flat (F), and CMFD, were examined for the global calculations. Throughout a sequence of global-local iterations the same model was used for all global calculations. Results are shown in Table 4.1 to 4.3 and Figure F.3 to F.5 of Appendix F.

In Case VI of Table 4.1, we started the global-local iteration with the results obtained by using ADF and the quadratic model. Using the surface currents resulting from this step we did an N1S2 local calculation to update the equivalence parameters. Another global calculation with these new equivalence parameters was performed followed by an N5S2 local calculation using net currents for each fixed-source problem resulting from this newest global result. Finally, with the equivalence parameters predicted by the N5S2 problem we solved the global problem again.

This procedure will be called Method A. The steps involved are shown in Figure 4.2. The reason for examining Method A will become clearer in the next section.

CASE	I (ADFQ)	II	III	IV	V	VI
Model for Global Calculation	Q	Q	Q	Q	Q	Q
Initial Estimation		ADFQ	ADFQ	ADFQ	ADFQ	ADFQ
Method for Local Calculation		N1S1	N1S2	N5S1	N5S2	$A^{(2)}$
% Errors (after 1st iteration) — λ	-0.05	0.09	0.09	0.10	-0.10	-0.11
$HCS_m^{(1)}$	3.03	0.65	0.65	0.85	0.72	0.79
ε_{max}	3.04	2.87	2.93	2.88	1.09	1.64
ε_{av}	0.90	0.97	1.00	0.92	0.33	0.90
No. of Iterations to Converge		4	3	3	Failed to Converge	
% Errors (after convergence) — λ		0.10	0.10	0.11		
HCS_m		0.68	0.68	0.92		
ε_{max}		3.05	3.11	3.23		
ε_{av}		0.95	0.98	0.94		

[1] HCS_m is the maximum error in homogenized cross sections.

[2] Explained in the text.

TABLE 4.1   RESULTS FOR THE CISE BENCHMARK USING
NET CURRENT RESPONSE MATRICES AND THE QUADRATIC TRANSVERSE LEAKAGE MODEL

CASE		I (ADFF)	II	III	IV	V
Model for Global Calculation		F	F	F	F	F
Initial Estimation			ADFF	ADFF	ADFF	ADFF
Method for Local Calculation			N1S1	N1S2	N5S1	N5S2
% Errors (after 1st iteration)	λ	0.02	0.09	0.08	0.11	-0.12
	HCS_m	3.03	0.66	0.57	1.05	0.81
	ε_{max}	3.46	2.97	3.03	2.77	1.48
	ε_{av}	1.31	0.97	1.00	0.90	1.55
No. of Iterations to Converge			4	4	4	Failed to Converge
% Errors (after convergence)	λ		0.10	0.10	0.11	
	HCS_m		0.68	0.68	0.87	
	ε_{max}		3.05	3.11	2.92	
	ε_{av}		0.95	0.98	0.94	

TABLE 4.2 RESULTS FOR THE CISE BENCHMARK USING
NET CURRENT RESPONSE MATRICES AND FLAT MODEL

CASE		I (ADFC)[1]	II	III
Model for Global Calculation		CMFD	CMFD	CMFD
Initial Estimation			ADFC	REFERENCE
Method for Local Calculation			N5S2	N5S2
% Errors (after 1st iteration)	λ	2.27	0.10	-0.10
	HCS_m	3.03	3.04	0.72
	ε_{max}	37.6	8.01	2.54
	ε_{av}	15.4	2.91	0.55
Convergency			Failed to Converge	Failed to Converge

[1] ADFC is the result obtained by using ADF with CMFD model.

TABLE 4.3   RESULTS FOR THE CISE BENCHMARK USING
NET CURRENT RESPONSE MATRICES AND CMFD MODEL

```
        ┌─────────────────────┐
        │     ADF RESULTS     │
        └─────────────────────┘
                   │
                   ▼
   ┌──────────────────────────────┐
   │   N1S2 LOCAL CALCULATION     │
   └──────────────────────────────┘
                   │
                   ▼
     ┌──────────────────────────┐
     │   GLOBAL CALCULATION     │
     └──────────────────────────┘
                   │
                   ▼
   ┌──────────────────────────────┐
   │   N5S2 LOCAL CALCULATION     │
   └──────────────────────────────┘
                   │
                   ▼
     ┌──────────────────────────┐
     │   GLOBAL CALCULATION     │
     └──────────────────────────┘
                   │
                   ▼
```
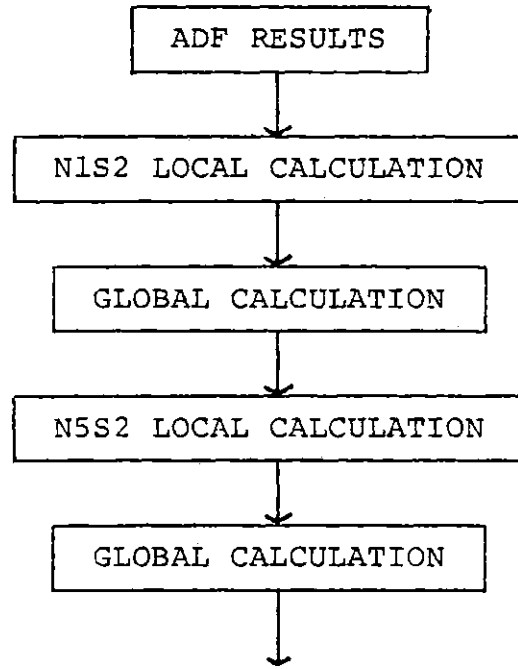
FIGURE 4.2   PROCEDURES IN METHOD A

As is noted in the tables, several cases failed to converge. This happened because of a divergence of the global calculations performed by QUANDRY. In Section 2.3, we discussed possible reasons why QUANDRY may diverge. For the present problem, there are three possible sources of divergence. First, the nonlinear global-local iteration procedure itself may simply be divergent. Secondly, even if the non-linear procedure is convergent there may be a stage during the global-local iterations at which one of the iteration matrices in QUANDRY becomes divergent. Finally, because the response matrices used during the global-local iteration process are not updated in accordance with the estimated global eigenvalue, there may result a condition that makes QUANDRY diverge. (The local and global problems are trying to converge to different results.) Unless the response matrices are updated according to the global eigenvalue obtained from the previous global calculation, the convergent solutions shown in Table 4.1 and 4.2 are not truly convergent in the sense that the local calculations have converged to one result and the global ones to another. All these points are brought out more fully by two simpler test problems described in Appendix E.

Table 4.1 and 4.2 show that except for N5S2 none of the methods provide much improvement over the ADF results. Detailed examination of the results from all global-local iterations shows that one global-local iteration for any method yields nearly the best result that that method can give. For

the N1S1 and N5S1 methods, the convergent solutions are the same as the solution obtained from solving the entire reactor according to the 1-segment net current response matrix technique based on the flat approximation. (The reason that the convergent solution of N1S1 method is different from that of N5S1 method by a small amount is that we did not update response matrices according to the newest estimation of the global eigenvalue.) For this problem, because the errors of ADF results are evidently the same order as those of a response matrix solution involving flat net currents over each assembly face. Hence the results obtained from the convergent solutions of the N1S1, N5S1, and N1S2 methods cannot be expected to yield much improvement. On the other hand the N5S2 method, because it not only accounts for the effect of nearest neighbors but also relaxes the limitation of completely flat spatial shapes on the surfaces of each node by having 2-segments on each boundary line of a node, is expected to yield better results.

Table 4.1 and 4.2 also show that the convergent solutions (if they exist) for various methods using different transverse leakage models are the same (as they should be). However, the first global-local iteration results obtained from using the quadratic transverse leakage model are better than the results obtained from using the flat transverse leakage model. This is because a more sophisticated model will make the global solution less sensitive to the exact values of discontinuity factors.

This point is further demonstrated by the results shown on Table 4.3. From Case III on that table, it seems that even for such a crude model as CMFD we can obtain quite good results provided the input currents for the local problem are correct. However, Case I and II of that same table show that without a very good estimate of the magnitude of boundary conditions for each fixed-source problem the results of the first global-local iteration still have large errors. Moreover, the non-linear global-local iteration will not converge so that we cannot improve results by taking more iterations.

It seems clear that the response matrix method using net current response matrices based on the flat approximation works for this problem. In order to understand more why the response matrix method using partial current response matrices as shown in Section 3.4.2 did not yield good results and to demonstrate the effect of generating the net current response matrices with another spatial approximation, we generated the net current response matrices from the partial current response matrices according to

$$[\bar{R}] = 2 \{[R] + [I]\}\{[R] - [I]\}^{-1} \tag{4.5}$$

where

$[\bar{R}]$ is the N*N net current response matrix for an assembly,

[R] is the corresponding N*N partial current response matrix which is generated using the eigenvalue spatial approximation and the reference eigenvalue (as described in Section 3.4.2),

[I] is an N*N identity matrix,

N = 4*NSEG*G.

This equation is obtained by using Equation (3.2) along with the definitions of response matrices. The net current response matrices of an assembly so determined are not the same as those generated directly using the flat spatial approximation because Equation (4.5) implies a different spatial approximation for the net currents. A detailed examination of this implied spatial distribution shows that it has a shape that is not at all smooth.

The CISE benchmark was rerun but this time using the response matrices (4.5) to solve each fixed-source problem. Various local methods and global models were tried. The poor results, shown in Table 4.4 and Figure F.6 and F.7 of Appendix F, indicate that it is not adequate to use net current response matrices generated with unsmooth spatial approximation.

Because partial and net current response matrices are just mathematical transformation of each other, the converged solutions obtained from using the N1S1 method with net current

CASE		I	II	III	IV	V	VI
Model for Global Calculation		F	Q	Q	F	F	Q
Initial Estimation		ADFF	ADFQ	ADFQ	ADFF	ADFF	ADFQ
Method for Local Calculation		N1S1	N1S1	N1S2	N5S1	N5S2	N5S2
	λ	-1.06	-1.06	-0.65	-1.14	-0.94	-0.99
% Errors	HCS_m	0.80	0.72	0.63	1.25	1.20	1.27
(after 1st	ε_{max}	23.1	23.0	15.9	25.5	20.8	22.3
iteration)	ε_{av}	8.60	8.60	6.16	9.56	7.96	8.73
No. of Iterations to Converge		5	5	5	Failed to Converge	Failed to Converge	Failed to Converge
	λ	-1.22	-1.23	-0.72			
% Errors	HCS_m	0.60	0.60	0.85			
(after	ε_{max}	19.6	19.9	14.7			
convergence)	ε_{av}	7.44	7.51	5.76			

TABLE 4.4   RESULTS FOR THE CISE BENCHMARK USING NET CURRENT
RESPONSE MATRICES GENERATED FROM PARTIAL
CURRENT RESPONSE MATRICES

response matrices should be the same as that obtained from
using the same method but with partial current response
matrices. Thus Case I and II of Table 4.4 further demon-
strate that the spatail approximation is the reason why the
response matrix method using partial current response matrices
does not work.

4.4.2 HAFAS BENCHMARK

Because of the finding that the quadratic transverse
leakage model yielded the best result, only this model was
used in analyzing the HAFAS benchmark. Response matrices
for this problem were generated with the flat approximation.
The global eigenvalue used to generate these response
matrices was that obtained from the ADF result which was the
best estimation of the solution available without solving
the full-core problem. All four methods (N1S1, N1S2, N5S1,
N5S2) were tried but only one global-local iteration was
performed. Results are shown in Table 4.5 and Figure F.8
of Appendix F.

Case II and III of Table (4.5) indicate that 1-node
methods improve the ADF results. However, Case IV and V
on that table indicate that, in contrast to the CISE bench-
mark, 5-node methods starting with the ADF result yield
poor results.

To try to understand these results, detailed examination
of the net currents on the boundaries of each fixed source
problem, the resultant net currents on the boundaries of the
node homogenized and the resultant equivalence parameters

CASE	I (ADFQ)	II	III	IV	V	VI	VII	VIII
Model for Global Calculation	Q	Q	Q	Q	Q	Q	Q	Q
Initial Estimation		ADFQ	ADFQ	ADFQ	ADFQ	REFERENCE	REFERENCE	ADFQ
Method for Local Calculation		N1S1	N1S2	N5S1	N5S2	N5S2	N5S1	A
λ	-0.06	0.04	0.04	0.36	-0.08	-0.09	-0.05	-0.15
% Errors (after 1st iteration) HCS_m	6.43	0.56	0.56	6.79	3.52	0.60	7.48	0.92
ε_{max}	5.29	2.07	2.08	25.6	9.67	0.96	23.31	1.30
ε_{av}	1.33	0.92	0.92	4.74	4.84	0.24	6.15	0.40

TABLE 4.5   RESULTS FOR THE HAFAS BENCHMARK USING
NET CURRENT RESPONSE MATRICES

was made. It showed that because of the complexity of this problem, the net currents on the surfaces of each node given by QUANDRY employing assembly discontinuity factors had large errors. Thus the boundary conditions for each fixed-source problem for the next local iterate also had large errors. For 1-node methods, because the boundary conditions for each fixed-source problem are just the net currents on the surfaces of the node homogenized, the estimated surface derivative, given by the global calculation, for that node are preserved after the local calculation. Because of this preservation, the global flux tilts are predicted quite accurately. A good estimation on equivalence parameters is then expected and thus the next global calculation will yield good results. However, for 5-node methods, because the net currents on the surfaces of the node homogenized (central node) are determined by the local calculation and because the limitation on the shapes of the net currents on the boundaries of the central node imposed by the spatial approximation in response matrices, the surface derivatives for the central node so determined may yield very bad prediction on the global flux tilt across that node. Thus unless the estimation of the net currents on the boundaries of the defining domain of a 5-node fixed-source problem is very good, the resultant spatial tilts in fluxes for the central node may be quite wrong and result in large errors in equivalence parameters.

Table 4.5 shows that 5-node methods starting with ADF results do give large errors in homogenized cross sections so that it is not surprising that the next global calculation yielded poor results.

The explanation of this behavior is further confirmed by Case VI and VII of Table 4.5. In Case VII, although reference solution was used to give the magnitude of the net currents on the boundaries of each fixed-source problem, the errors in equivalence parameters are still very large because of the lack of flexibility of the shape for the net currents on the boundaries of the central node. On the other hand, in Case VI because there are two segments on each boundary line of the center node, the limitation on the shape of the net currents is relaxed. The results show that errors in equivalence parameters are then very small, and the next global calculation thus yielded good results.

Although these cases are of no practical interest (since the reference solution is not known a priori) they do suggest the use of Method A which is described on Figure 4.2 in the last section. Because the global results obtained by using equivalence parameters from the results of an N1S2 local calculation (using the ADF results as an initial estimation) yield an estimation of net currents better than that given directly by the ADF results, using them to define the N5S2 local fixed-source problems is expected to yield better equivalence parameters and global results than those obtained by using the ADF results directly to define the N5S2 local

fixed-source problems. Case VIII on Table 4.5 shows that Method A gives the best results of all the practical methods tested. For Method A, the response matrices used in the N5S2 local calculation should be that corresponding to the eigenvalue given by the global calculation after the N1S2 local calculation. However, in Case VIII of Table 4.5 to reduce the cost the response matrices used were still those associated with the eigenvalue given by the ADF results. Our experience has shown that because the difference between the two eigenvalues was only 0.1% and because we were not trying to iterate more than once, the effects due to not updating the eigenvalue are very small.

4.4.3   LSHBWR BENCHMARK

For the same reasons as for the HAFAS problem, only the quadratic transverse leakage model was used in this problem. Employing the flat net current approximation, two sets of response matrices were generated. One of them corresponded to the eigenvalue given by the ADF results and the other corresponded to the eigenvalue given by the global calculation after the N1S2 local calculation. All the various methods for performing the local calculation were tried. Results are shown in Table 4.6 and Figure F.9 in Appendix F. As in the HAFAS problem, Methods N5S2 and N5S1 with the ADF result as the initial estimation were not able to give a good estimation for the spatial tilts of fluxes for the central node and as a consequence yield inaccurate results. In contrast to situation for the CISE and HAFAS problems,

CASE		I (ADFQ)	II	III	IV	V	VI	VII [1]
Model for Global Calculation		Q	Q	Q	Q	Q	Q	Q
Initial Estimation			ADFQ	ADFQ	ADFQ	ADFQ	ADFQ	ADFQ
Method for Local Calculation			N1S1	N1S2	N5S1	N5S2	A	N1S2
% Errors (after 1st iteration)	λ	-0.05	0.05	0.05	0.39	-0.16	0.07	0.15
	ε_{max}	9.61	3.42	3.42	35.8	38.8	5.42	4.09
	ε_{av}	3.26	1.06	1.06	7.36	12.2	1.01	1.28

4-27

[1] In this column, the errors are for the convergent solution which was obtained by using updated (in accordance with the eigenvalue given by the previous global calculation) response matrices in the local calculations.

TABLE 4.6   RESULTS FOR THE LSHBWR BENCHMARK USING
NET CURRENT RESPONSE MATRICES

Method A did not give quite as good results as Methods
N1S1 and N1S2. This is because in this problem, with its
unrealistic flux tilt, the shape of the net currents on the
boundary surfaces cannot be well-simulated by a flat distri-
bution. This fact is demonstrated by the error that existed
in the convergent solution for Method N1S2 (Case VII of
Table 4.6). Because that solution is very close to the
solution obtained by solving the entire problem using response
matrices based on flat net surface currents, the errors that
result imply that the real shape is quite different from flat.
Method A did, however, improve significantly results obtained
using the ADF parameters.

4.4.4 EXECUTION TIME COMPARISON

The execution times (in CPU seconds of IBM 370/168)
for the various methods applied to all three benchmarks
are given in Table 4.7. The time which might be needed for
interpolating response matrices is not included in the execu-
tion times for the local calculations since no systematic
interpolation was carried out in this thesis. It is believed
however that for one local calculation one or two CPU
seconds will be sufficient for the interpolation.

The last column of Table 4.7 gives the execution time
needed for the first global-local iteration. For all methods
except Method A, it involves two global calculations (the
first global calculation is to yield the ADF results) and
one local calculation. For Method A, it involves three
global calculations and two local calculations. The execu-

PROBLEM EXECUTION TIME FOR HETEROGENEOUS RUN	EXECUTION TIME PER GLOBAL CALCULATION	METHOD FOR LOCAL CALCULATION	EXECUTION TIME PER LOCAL CALCULATION	TOTAL EXECUTION TIME FOR THE FIRST GLOBAL-LOCAL ITERATION
CISE (500)	2.4	N1S1	0.5	5.3
		N1S2	1.0	5.8
		N5S1	0.7	5.5
		N5S2	2.0	6.8
		A		10.2
HAFAS (700)	4.4	N1S1	0.9	9.7
		N1S2	1.7	10.5
		N5S1	1.3	10.1
		N5S2	2.8	11.6
		A		17.7
LSHBWR	3.7	N1S1	0.8	8.2
		N1S2	1.2	8.6
		N5S1	1.0	8.4
		N5S2	2.2	9.6
		A		14.5

TABLE 4.7   EXECUTION TIME COMPARISON
(ALL TIMES IN SECONDS)

tion times needed to obtain the full core heterogeneous standard solutions are given in the first column. It is clear that our methods improve significantly the computational efficiency.

4.5 SUMMARY

In this chapter, net current response matrices were introduced, and the use of them to solve fixed source problems was discussed. All three benchmarks were tested. The results show that the Methods N1S1 and N1S2 using flat net current response matrices consistently reduce the maximum power error to a level of $\sim 3\%$. Whether they improve the ADF results depends on the complexity of the problem. Method A consistently improves the ADF results. However, for problems involving extremely large tilts in the net currents, it may not give quite as good results as Methods N1S2 and N1S1. Results also show that the computational efficiency for all three methods is very attractive. The execution time needed is one to two orders of magnitude smaller than that needed to solve the entire problem by a fine mesh method that treats all heterogeneous regions explicitly.

It is clear in retrospect that the response matrix method using flat net current response matrices works well provided any one of the three schemes, N1S1, N1S2 or A, is used for the local calculations. Since both the N1S2 and A methods use 2-segment response matrices, while the N1S1 method uses 1-segment response matrices, the storage requirement and data management problems for the tabulation and

interpolation of response matrices for the former methods are considerably more severe than those for the latter method. Thus we strongly suggest that the N1S1 method be used for all problems.

CHAPTER FIVE

SUMMARY AND CONCLUSIONS

5.1 OVERVIEW OF THE INVESTIGATION

The objective of this research effort was to develop

accurate and efficient homogenization methods for coarse

mesh analysis of boiling water reactors.

Initially the existence of exact homogenized parameters

which will reproduce all of the integrated properties of a

known reference solution was discussed. It was shown that

because of the lack of degrees of freedom for the equations

embodying the diffusion theory model, exact, spatially flat

homogenized parameters for that model do not exist in

general. However, exact homogenized parameters based on

equivalence theory which is an extension of diffusion theory

do exist. As a consequence, equivalence theory homogenization

methods instead of conventional flux-weighting techniques

were used for cross section homogenization.

In Chapter 2, equivalence theory was formally derived.

The unique feature of this method is the introduction of two

additional degrees of freedom per direction and group to

the conventional diffusion theory equations. With them, it

is possible to define exact homogenized parameters (for any

approximate method used to solve the homogenized problem)

to match any known reference solution. However, since the

exact solution is needed to define these parameters, approxi-

mations for these exact parameters must be made in practical

cases.

Some methods for estimating these parameters suggested by Smith[3] and Loretz[6] were reviewed. These authors showed that the ADF method is cheap and simple. However, if greater accuracy is required, more sophisticated methods involving nonlinear iterations between global homogenized reactor calculations and local fixed-source calculations (to compute the equivalence parameters) are needed. If, however, nodal methods or finite-difference methods are used to solve the fixed-source problems for the local calculations, the cost is comparable to and even higher than that incurred by solving the entire problem heterogeneously. Consequently, a method which can solve each fixed-source problem more efficiently is in demand.

Since the response matrix method can give information of interest directly and since it uses parameters (response matrices) which can be pretabulated, it is believed to be the most efficient method for solving fixed-source problems.

In Chapter 3, the application of conventional partial current response matrices was examined. Various methods for defining fixed-source problems and the procedures for solving them were discussed. However, numerical tests showed that because of the spatial approximation imposed on the incoming partial currents used to generate the response matrices, predicted discontinuity factors for peripheral nodes are greatly in error and this results in a large error

in power and eigenvalue when the next global calculation
is performed.

In Chapter 4, a different response matrix which
directly relates information of interest and surface fluxes
to net surface currents was introduced. Various methods
for defining fixed-source problems with these net current
response matrices and solution techniques were discussed.
Numerical tests show that the 1-node methods using flat net
current response matrices consistently reduce the maximum
assembly power error to a level of 3% in one global-local
iteration. Whether they improve the ADF results depends
on the complexity of the problem. The procedure designated
as Method A consistently improves the ADF results. How-
ever, for problems involving extremely large global flux
tilts in the net currents, it may not give quite as good
results as 1-node methods.

The results also show that the computational efficiency
for these methods is neraly two orders of magnitude greater
than that achieved by solving the entire problem without
homogenization.

Since the N1S1 method uses 1-segment response matrices,
the generation, storage and interpolation of response
matrices for this method will be much easier and cheaper
than for the 2-segment methods which use 2-segment response
matrices. Thus we strongly suggest that the N1S1 method be
used for all BWR analysis.

5.2 RECOMMENDATIONS FOR FUTURE RESEARCH

5.2.1 STEADY-STATE THERMAL ANALYSIS

The problems analyzed in this thesis are actually zero-power reactors (i.e. no thermal-hydraulic feedback is represented). In order to analyze full-power reactors, feedbacks must be taken into account. In principle, there is no problem of using response matrix methods to analyze these reactors. However with feedback the cost of the global calculation becomes rather expensive. Thus the possibility of starting the local calculation with a sufficiently, but not completely converged global solution, so that the cost can be reduced must be studied.

5.2.2 FUEL MANAGEMENT STUDIES

For fuel management studies, the history of a reactor (exposure, control history, void history) must be taken into account. In order to pretabulate response matrices as functions of these variables, approximations for the spatial distribution within an assembly must be made for these state variables. A thorough study is needed to ensure that the approximations used are acceptable and thus that response matrix methods can be used for such studies.

5.2.3 TRANSIENT ANALYSIS

Basically, transient studies are similar to steady-state thermal analyses. However, the uniform spatial distributions of state variables (temperature, void, etc.), within an assembly which are assumed in generating response matrices, becomes questionable. Moreover, for large power excursions,

because of the Doppler effect (which is instantaneous) in the fuel within an assembly, the response matrices for the assembly may not be stationary (i.e., the response at time t to an input at time t_o may depend on what happens within the time interval $t - t_o$). Thus the use of response matrix methods for transient analysis needs careful study.

5.2.4 TABULATION AND INTERPOLATION OF THE NET CURRENT RESPONSE MATRICES

In view of the discussion in Section 4.2.4 and in the preceding three sections, the tabulation and interpolation of the net current response matrices are by no means trivial problems. They involve not only multivariable (fuel temperature, void, exposure, control history, etc.) tabulations and interpolations but are further complicated by the singular behavior of the net current response matrices. In this thesis no systematic methods for tabulation and interpolation were studied. However in order to use efficiently and accurately the response matrix method to predict the power distribution for steady-state thermal analyses, depletion analyses, and transient analyses, a thorough study of the tabulation and interpolation problems must be pursued.

5.2.5 3-D EFFECTS

All of the analysis in this thesis was restricted to two-dimensional radial planes. Although the axial flux shape is rather smooth, exceptions such as partially inserted control blades do exist. The extension of the response

matrix method to three-dimensional problems seems rather straightforward. However it needs to be examined.

5.2.6 ENERGY HOMOGENIZATION

As discussed in Section 2.2, it is possible to reduce the number of energy groups without loss of accuracy provided exact equivalence parameters are used to solve the global homogenized problem. If good estimation of these parameters can be made, the global homogenized problem can be further simplified. Although such a simplification may not be attractive for 2-group global calculation, it is attractive in collapsing many-group calculations to fewer group calculations. This scheme has not been investigated.

5.2.7 TRANSPORT THEORY

It was shown in Section 2.2 that it is possible to define exact equivalence parameters for any reference solution. In this thesis, however, the two-group fine-mesh diffusion theory results were used as reference solutions. Thus the response matrices were also generated with the diffusion theory approximation. The effects of using transport theory solutions as the reference solution and generating the response matrices with transport theory needs to be investigated.

REFERENCES

1. A.F. Henry, Nuclear Reactor Analysis, M.I.T. Press, Cambridge, Mass. (1975).

2. K.S. Smith, "An Analytic Nodal Method for Solving the Two-Group, Multidimensional, Static and Transient Neutron Diffusion Equation", Nuclear Engineer's Thesis, Department of Nuclear Engineering, M.I.T., Cambridge, Mass. (March 1979).

3. K.S. Smith, "Spatial Homogenization Methods for Light Water Reactor Analysis", Ph.D. Thesis, Department of Nuclear Engineering, M.I.T., Cambridge, Mass (June 1980).

4. E.L. Wachspress, Iterative Solution to Elliptic Systems and Applications to the Neutron Diffusion Equations of Reactor Physics, Prentice-Hall, Englewood Cliffs, N.J. (1966).

5. R.S. Varga, Matrix Iterative Analysis, Prentice-Hall, Englewood Cliffs, N.J. (1962).

6. R.A. Loretz, "The Determination of Equivalent Diffusion Theory Parameters by Local Implementation of the Koebke Method", S.M. Thesis, Department of Nuclear Engineering, M.I.T., Cambridge, Mass. (August 1980).

7. K.S. Smith, personal communication (1980).

8. A. Shimuzu and K. Aoki, Application of Invariant Embedding to Reactor Physics, Academic Press, New York, (1972).

9. Nuclear Reactor Core Analysis Code: CITATION, Computer Code developed at Oak Ridge National Laboratory.

10. Hussein Khalil, personal communication (1981).

11. J.R. Lamarsh, Nuclear Reactor Theory, Addison-Wesley Publishing Company, Reading, Mass. (1972).

12. G.I. Bell and S. Glasstone, Nuclear Reactor Theory, Van Nostrand-Reihold, New York, (1970).

13. A.F. Henry, B.A. Worley, and A.A. Morshed, "Spatial Homogenization of Diffusion Theory Parameters", Paper presented at the IAEA Technical Committee Meeting on Homogenization Methods in Reactor Physics, Lugano, Switzerland (November 1978).

14. H. Finnemann, F. Bennewitz and M.R. Wagner, "Interface Current Techniques for Multidimensional Reactor Calculations", Atomkernenergie (ATKE) Bd. 30 (1977).

15. R.D. Lawrence, "A Nodal Green's Function Method for Multidimensional Neutron Diffusion Calculations", Ph.D. Thesis, Department of Nuclear Engineering, University of Illinois at Urbana-Champaign (1979).

16. C.M. Kang and K.F. Hansen, "Finite Element Methods for Reactor Analysis", Nucl. Sci. Eng., 51, 456 (1973).

17. G.P. Bottoni, R. Guandalini, G. Vimercati, and P. Peroni, "Neutronic Aspects of the LWR Core Simulator CETRA", ANS/ENS (May 1979).

18. S. Borresen, "A Simplified, Coarse-Mesh, Three-Dimensional Diffusion Scheme for Calculating Gross Power Distributions in a BWR", Nucl. Sci. Eng. 44 (1971)

19. G. Pierini, "A Consistent Homogenization Procedure to Obtain Few-Group Cell Parameters", Atomkernenergie (ATKE) Bd. 34 (1970).

20. R.A. Bonalumi, "A Rigorous Calculation of Homogenized Diffusion Theory Parameters", Trans. Am. Nucl. Soc., 30 (1978).

21. R.A. Bonalumi, F. La Briola, and G.C. Pierini, "Homogenized Cell Diffusion Parameters from Transport Codes", Trans. Am. Nucl. Soc., 26 (1977).

22. K. Koebke, "A New Approach to Homogenization and Group Condensation", Paper presented at the IAEA Technical Committee Meeting on Homogenization Methods in Reactor Physics, Lugano, Switzerland (November 1978).

APPENDIX A

DESCRIPTION OF BWR TEST PROBLEMS

A.1   THE CISE BWR BENCHMARK PROBLEM

A.2   THE HAFAS BWR BENCHMARK PROBLEM

A.3   THE LSHBWR BENCHMARK PROBLEM

A.4   THE PRELIMINARY TEST PROBLEM

A.5   THE HOMOGENEOUS TEST PROBLEM

A.1   THE CISE BWR BENCHMARK PROBLEM
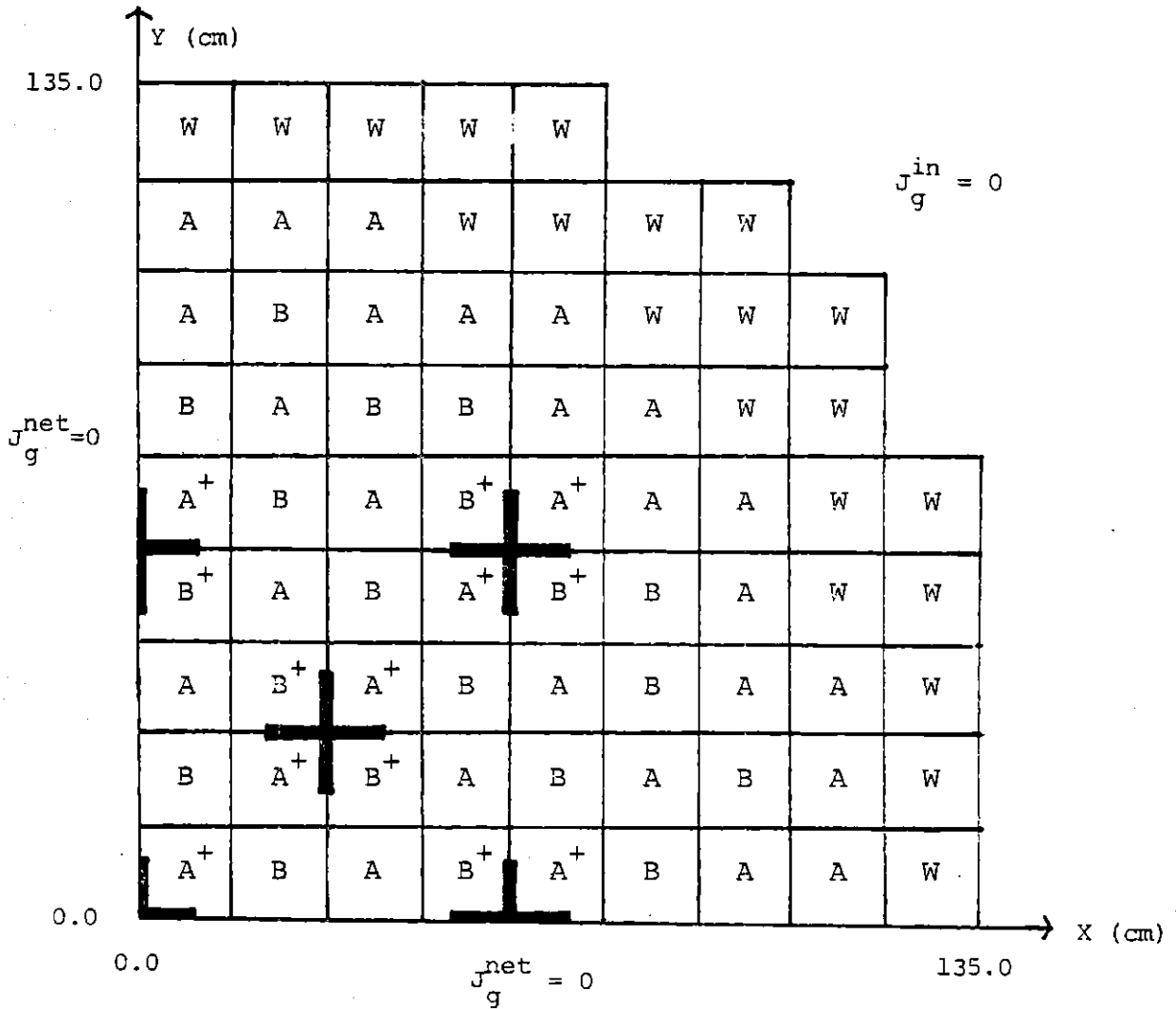
FIGURE A.1.1   CORE LAYOUT OF THE CISE BENCHMARK FOR
ASSEMBLY HOMOGENIZATION
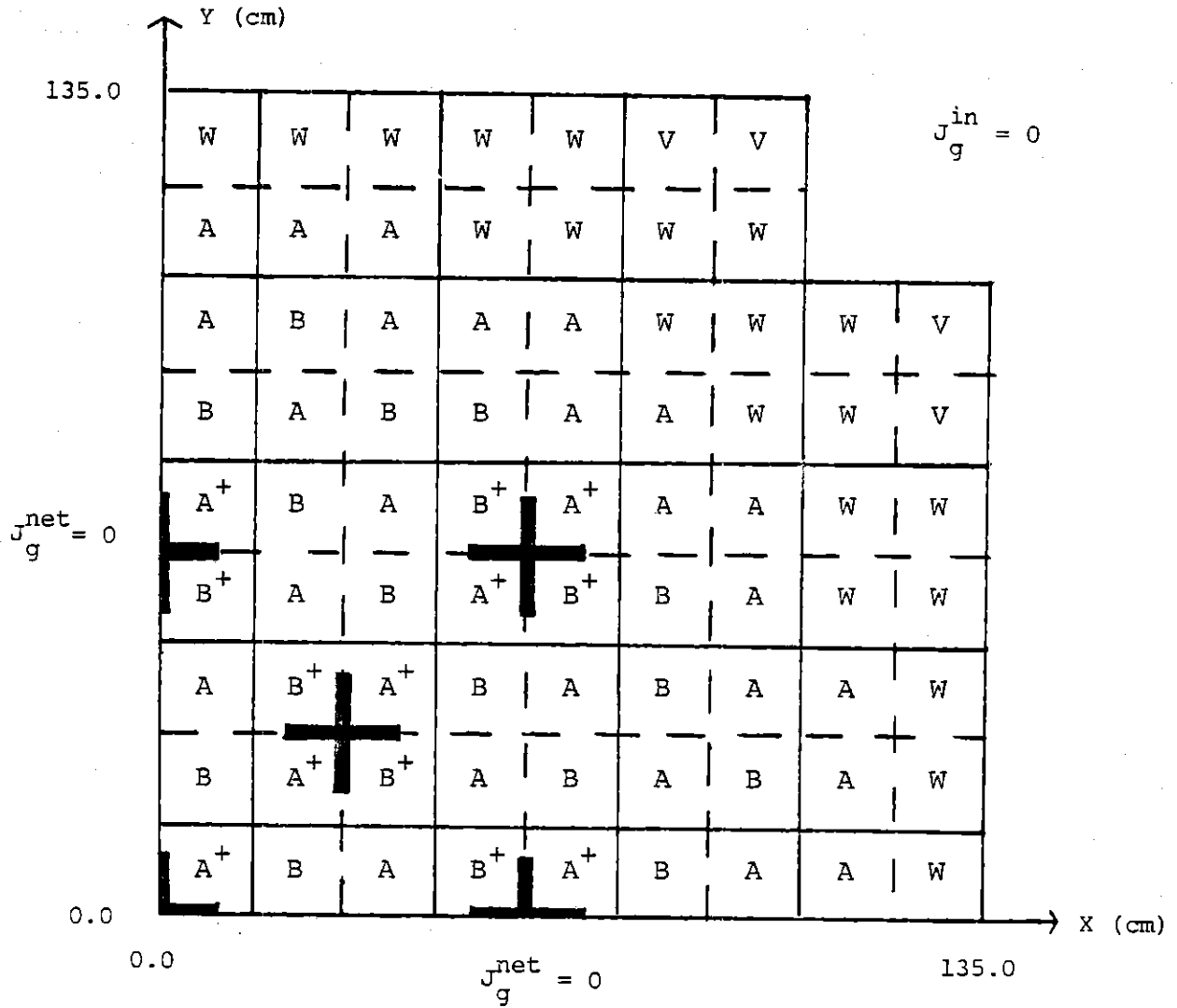
FIGURE A.1.2   CORE LAYOUT OF THE CISE BENCHMARK FOR
CLUSTER HOMOGENIZATION
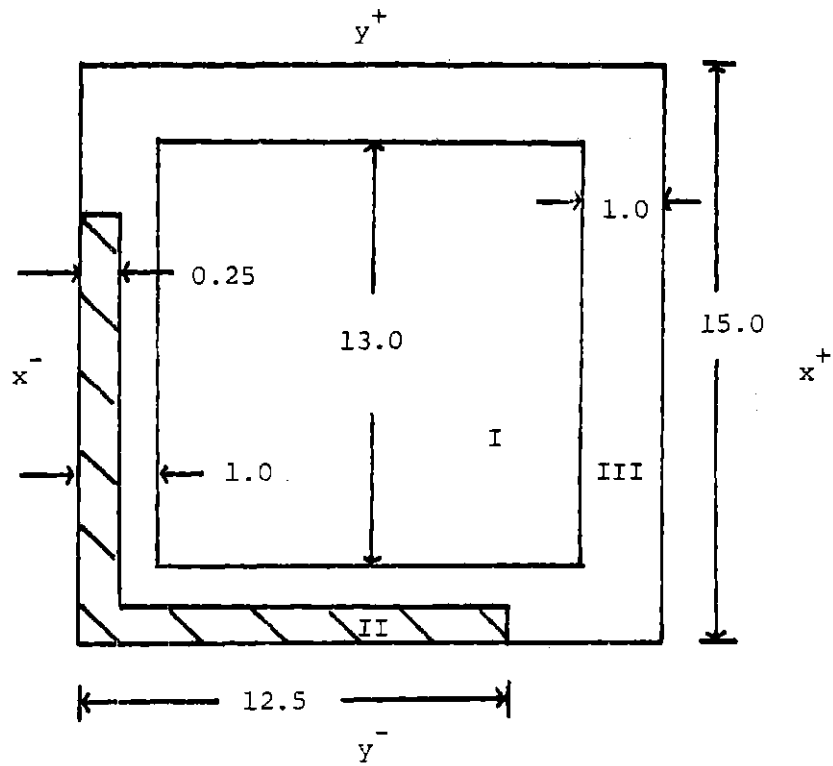
FIGURE A.1.3   ASSEMBLY DESCRIPTION AND SURFACE ORIENTA-
TION FOR THE CISE BENCHMARK

Assembly Type

Zone	A	A$^+$	B	B$^+$	W	V
I	3	3	4	4	2	5
II	2	1	2	1	2	5
III	2	2	2	2	2	5

TABLE A.1.1   MATERIAL POSITIONS FOR ASSEMBLIES OF THE CISE
BENCHMARK

Composition	Group, g	D_g (cm)	Σ_{a_g} (cm^{-1})	$\nu\Sigma_{f_g}$ (cm^{-1})	$\Sigma_{gg'}$ (cm^{-1})
1	1	3.00	0.08	0.0	0.0
(Control blade)	2	0.15	1.00	0.0	
2	1	2.00	0.0	0.0	0.04
(Water)	2	0.30	0.01	0.0	
3	1	1.80	0.008	0.006	0.012
(Fresh fuel)	2	0.55	0.085	0.110	
4	1	1.80	0.008	0.005	0.012
(Depleted fuel)	2	0.55	0.085	0.100	

$$\chi_1 = 1.0$$
$$\chi_2 = 0.0$$
$$\nu = 2.5$$

TABLE A.1.2 HETEROGENEOUS CROSS SECTIONS FOR THE CISE BENCH-MARK

Assembly Type	Group, g	$\hat{D}_g$ (cm)	$\hat{\Sigma}_{a_g}$ (cm^{-1})	$\nu\hat{\Sigma}_{f_g}$ (cm^{-1})	$\hat{\Sigma}_{gg'}$ (cm^{-1})
A	1	1.8440	0.00607	0.004556	0.01874
(Fresh fuel)	2	0.4284	0.05946	0.07254	0.0
B	1	1.8440	0.00608	0.003796	0.01874
(Depleted fuel)	2	0.4284	0.05946	0.06595	0.0
A$^+$	1	1.8580	0.00804	0.004565	0.01772
(Fresh fuel, controlled)	2	0.4283	0.07416	0.07558	0.0
B$^+$	1	1.8580	0.00804	0.003804	0.01772
(Depleted fuel controlled)	2	0.4283	0.07415	0.06870	0.0
W	1	2.0000	0.0	0.0	0.04
(Water)	2	0.3000	0.01	0.0	0.0

$\chi_1 = 1.0$

$\chi_2 = 0.0$

$\nu = 2.5$

TABLE A.1.3   FLUX-WEIGHTED CONSTANTS FOR THE CISE BWR BENCHMARK

Assembly Type	Group, g	$f_g^{x^-}$	$f_g^{x^+}$	$f_g^{y^-}$	$f_g^{y^+}$
A	1	0.9623	0.9623	0.9623	0.9623
	2	1.4510	1.4510	1.4510	1.4510
B	1	0.9625	0.9625	0.9625	0.9625
	2	1.4510	1.4510	1.4510	1.4510
A^+	1	0.8955	1.0150	0.8955	1.0150
	2	0.6492	1.8880	0.6492	1.8880
B^+	1	0.8949	1.0160	0.8949	1.0160
	2	0.6488	1.8890	0.6488	1.8890
W	1	1.0	1.0	1.0	1.0
	2	1.0	1.0	1.0	1.0

TABLE A.1.4   ASSEMBLY DISCONTINUITY FACTORS FOR THE CISE BENCHMARK

A.2   THE HAFAS BWR BENCHMARK PROBLEM
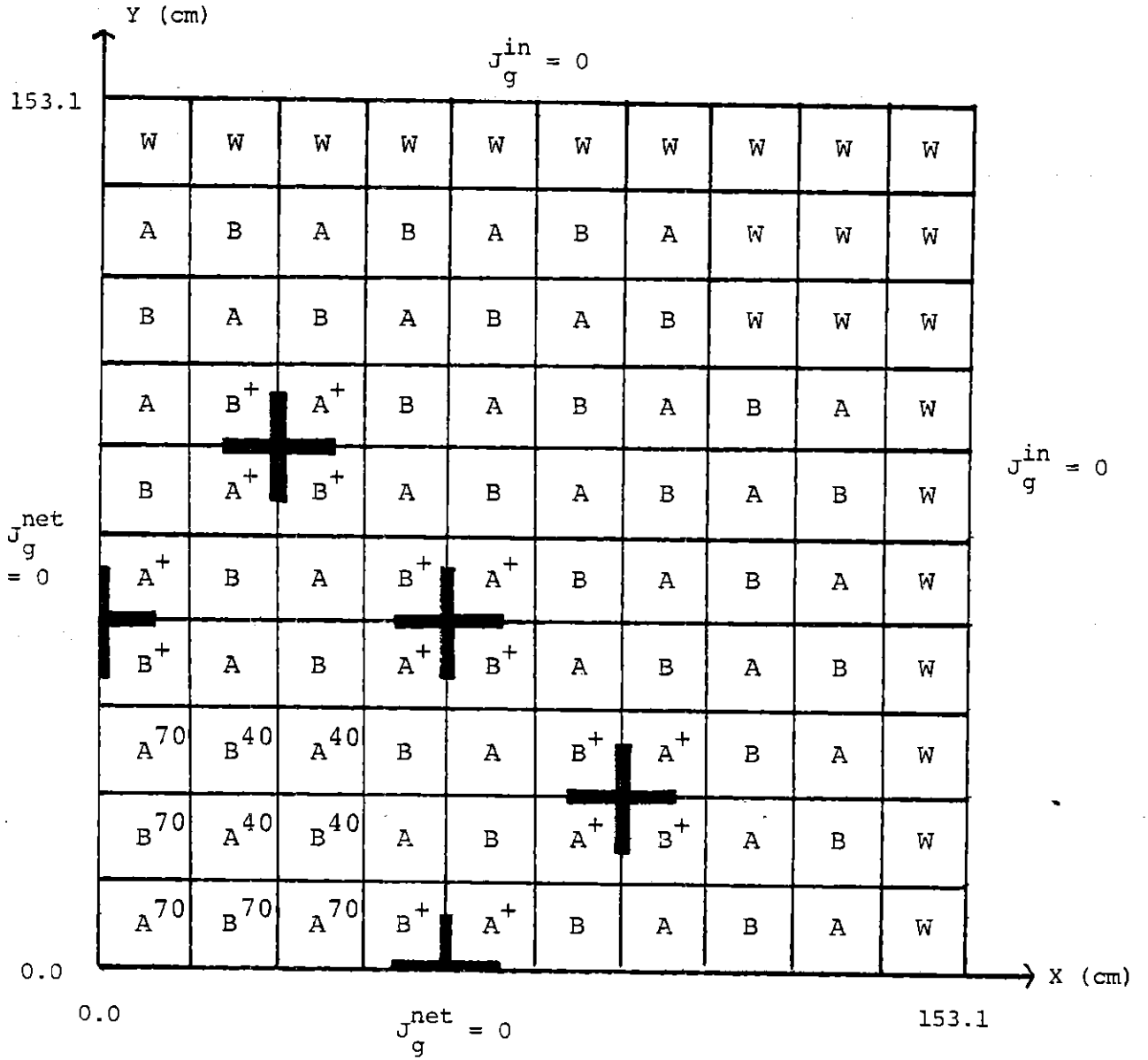
FIGURE A.2.1   CORE LAYOUT OF THE HAFAS BENCHMARK
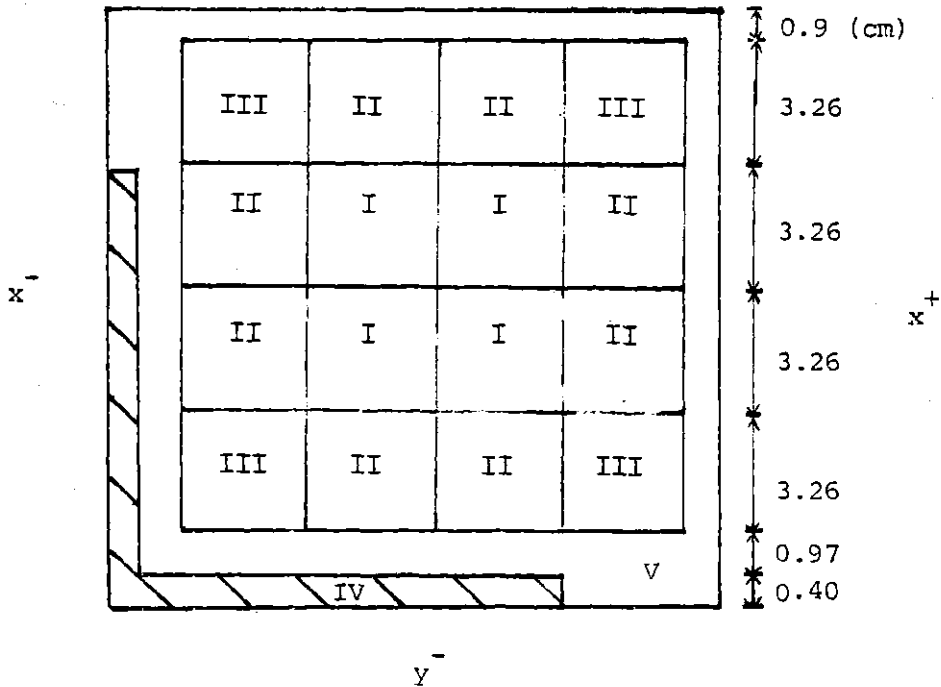
FIGURE A.2.2   ASSEMBLY DESCRIPTION AND SURFACE ORIENTATION FOR THE HAFAS BENCHMARK

Zone	A	A^{40}	A^{70}	A^{+}	B	B^{40}	B^{70}	B^{+}	W
Assembly Type
I	1	5	9	1	2	6	10	2	15
II	2	6	10	2	3	7	11	3	15
III	3	7	11	3	4	8	12	4	15
IV	13	13	13	14	13	13	13	14	15
V	13	13	13	13	13	13	13	13	15

TABLE A.2.1   MATERIAL POSITIONS FOR ASSEMBLIES OF THE HAFAS BENCHMARK

Composition	Group, g	D_g (cm)	Σ_{a_g} (cm^{-1})	$\nu\Sigma_{f_g}$ (cm^{-1})	Σ_{21} (cm^{-1})
1	1	1.400	0.009	0.0065	0.016
(Fuel a, void=0%)	2	0.375	0.080	0.1220	
2	1	1.400	0.009	0.0057	0.017
(Fuel b, void=0%)	2	0.375	0.070	0.1000	
3	1	1.400	0.009	0.0051	0.018
(Fuel c, void=0%)	2	0.375	0.060	0.0800	
4	1	1.400	0.009	0.0051	0.018
(Fuel d, void=0%)	2	0.375	0.050	0.0700	
5	1	1.680	0.008	0.0063	0.010
(Fuel a, void=40%)	2	0.530	0.077	0.1180	
6	1	1.680	0.0085	0.0055	0.0105
(Fuel b, void=40%)	2	0.530	0.067	0.0960	
7	1	1.680	0.009	0.0049	0.0110
(Fuel c, void=40%)	2	0.530	0.057	0.0780	
8	1	1.680	0.009	0.0049	0.0110
(Fuel d, void=40%)	2	0.530	0.047	0.0680	

(continued)

TABLE A.2.2 HETEROGENEOUS CROSS SECTIONS FOR THE HAFAS BENCHMARK

Composition	Group, g	D_g (cm)	Σ_{a_g} (cm^{-1})	$\nu\Sigma_{f_g}$ (cm^{-1})	Σ_{21} (cm^{-1})
9	1	2.000	0.0078	0.0061	0.0052
(Fuel a, void=70%)	2	0.800	0.073	0.1140	
10	1	2.000	0.0082	0.0053	0.0053
(Fuel b, void=70%)	2	0.800	0.0630	0.0920	
11	1	2.000	0.0086	0.0047	0.0054
(Fuel c, void=70%)	2	0.800	0.0530	0.0720	
12	1	2.000	0.0086	0.0047	0.0054
(Fuel d, void=70%)	2	0.800	0.043	0.0620	
13	1	1.530	0.0005	0.000	0.031
(Fuel can and water)	2	0.295	0.0090	0.000	
14	1	1.110	0.08375	0.000	0.00375
(Control blade)	2	0.185	0.950	0.000	
15	1	2.00	0.000	0.000	0.04
(Water)	2	0.300	0.010	0.000	

$\chi_1 = 1.0$

$\chi_2 = 0.0$

$\nu = 2.5$

TABLE A.2.2 HETEROGENEOUS CROSS SECTIONS FOR THE HAFAS

BENCHMARK

Assembly type	Group, g	$\hat{D}_g$ (cm)	$\hat{\Sigma}_{a_g}$ (cm^{-1})	$\nu\hat{\Sigma}_{f_g}$ (cm^{-1})	$\hat{\Sigma}_{gg'}$ (cm^{-1})
A	1	1.4320	0.00678	0.004255	0.02065
(Fresh fuel, 0% void)	2	0.3414	0.04713	0.06249	0.0
A^{40}	1	1.6380	0.00639	0.004099	0.01588
(Fresh fuel, 40% void)	2	0.4097	0.04486	0.05972	0.0
A^{70}	1	1.8500	0.00616	0.003946	0.01208
(Fresh fuel, 70% void)	2	0.4890	0.04221	0.05661	0.0
A^{+}	1	1.4160	0.00927	0.004304	0.01974
(Fresh fuel, controlled)	2	0.3441	0.06099	0.06894	0.0
B	1	1.4320	0.00678	0.003879	0.02121
(Depleted fuel, 0% void)	2	0.3424	0.04144	0.05255	0.0
B^{40}	1	1.6380	0.00667	0.003725	0.01617
(Depleted fuel, 40% void)	2	0.4128	0.0392	0.05052	0.0
B^{70}	1	1.8500	0.00638	0.003573	0.01214
(Depleted fuel, 70% void)	2	0.4955	0.03655	0.04677	0.0

(continued)

TABLE A.2.3   FLUX-WEIGHTED CONSTANTS FOR THE HAFAS BWR BENCH-
MARK

Assembly Type	Group, g	$\hat{D}_g$ (cm)	$\hat{\Sigma}_{a_g}$ (cm^{-1})	$\nu\hat{\Sigma}_{f_g}$ (cm^{-1})	$\hat{\Sigma}_{gg'}$ (cm^{-1})
B$^+$	1	1.4160	0.00926	0.003924	0.02031
(Depleted fuel, controlled)	2	0.3451	0.05405	0.05773	
W	1	2.0	0.0	0.0	0.04
(Water)	2	0.3	0.01	0.0	0.0

$\chi_1 = 1.0$

$\chi_2 = 0.0$

$\nu = 2.5$

TABLE A.2.3   FLUX-WEIGHTED CONSTANTS FOR THE HAFAS BWR
BENCHMARK (CONTINUED)

Assembly Type	Group, g	$f_g^{x^-}$	$f_g^{x^+}$	$f_g^{y^-}$	$f_g^{y^+}$
A	1	0.9311	0.9677	0.9311	0.9677
	2	1.4740	1.2470	1.4740	1.2470
A^{40}	1	0.9368	0.9709	0.9368	0.9709
	2	1.5330	1.2550	1.5330	1.2550
A^{70}	1	0.9406	0.9739	0.9406	0.9739
	2	1.5830	1.2560	1.5830	1.2560
A^+	1	0.8169	1.0570	0.8169	1.0570
	2	0.6264	1.7320	0.6264	1.7320
B	1	0.9313	0.9694	0.9313	0.9694
	2	1.4070	1.2130	1.4070	1.2130
B^{40}	1	0.9372	0.9724	0.9372	0.9724
	2	1.4610	1.2200	1.4610	1.2200
B^{70}	1	0.9407	0.9750	0.9407	0.9750
	2	1.5060	1.2210	1.5060	1.2210
B^+	1	0.8151	1.0610	0.8151	1.0610
	2	0.5902	1.6830	0.5902	1.6830
W	1	1.0	1.0	1.0	1.0
	2	1.0	1.0	1.0	1.0

TABLE A.2.4   ASSEMBLY DISCONTINUITY FACTORS FOR THE HAFAS BENCHMARK

A.3   THE LSHBWR BENCHMARK PROBLEM

Y (cm)

$\underline{J}^{in} \cdot \underline{n} = 0$

35	35	35	35						
35	35	35	35						
0	0	35	35	35	35				
0	0	35	35	35	35				
0^+	0^+	0	0	35	35	35	35		
0^+	0^+	0	0	35	35	35	35		
40	40	40	0	0	0	35	35	35	35
70	70	70	40	0	0	35	35	35	35
70	70	70	40	0^+	0^+	0	0	35	35
70	70	70	40	0^+	0^+	0	0	35	35

$\underline{J}^{in} \cdot \underline{n} = 0$

$\underline{J} \cdot \underline{n} = 0$

15.31

$\underline{J} \cdot \underline{n} = 0$

X (cm)
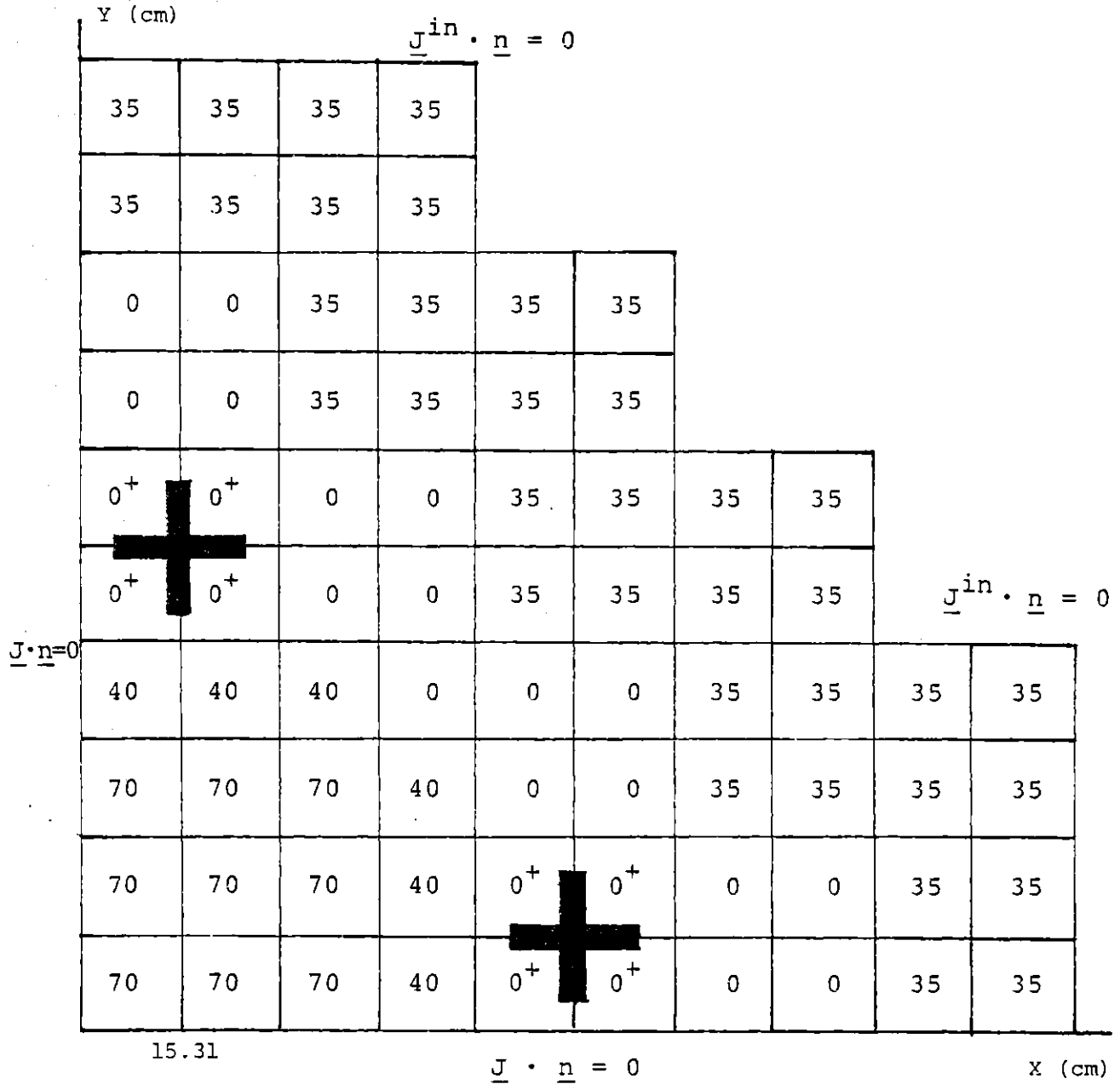
FIGURE A.3.1   CORE LAYOUT FOR THE LSHBWR BENCHMARK
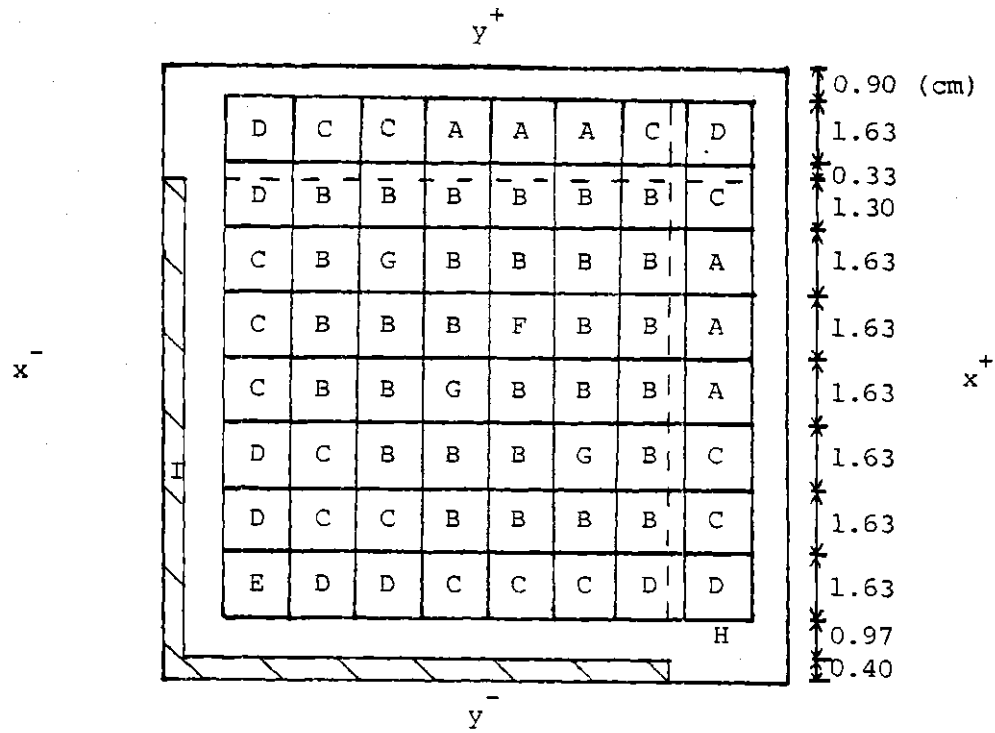
FIGURE A.3.2   ASSEMBLY DESCRIPTION AND SURFACE ORIENTATION FOR THE LSHBWR BENCHMARK

Zone \ Assembly	0^+	0	40	70
A	1	10	18	26
B	2	11	19	27
C	3	12	20	28
D	4	13	21	29
E	5	14	22	30
F	6	15	23	31
G	7	16	24	32
H	8	17	25	33
I	9	17	25	33

TABLE A.3.1   MATERIAL POSITIONS FOR ASSEMBLIES OF THE LSHBWR BENCHMARK

TABLE A.3.2 HETEROGENEOUS CROSS SECTIONS FOR THE LSHBWR BENCHMARK PROBLEM

COMPOSITION	GROUP	DIFF. COEFF.	REMOVAL X-S	OUTSCATTER X-S	NU-FISSION X-S
1	GROUP 1	0.142700E+01	0.262550E-01	0.166990E-01	0.665270E-02
	GROUP 2	0.368080E+00	0.779120E-01	0.0	0.126440E+00
2	GROUP 1	0.141060E+01	0.255200E-01	0.162170E-01	0.651540E-02
	GROUP 2	0.379930E+00	0.751790E-01	0.0	0.121890E+00
3	GROUP 1	0.139490E+01	0.257680E-01	0.166060E-01	0.559700E-02
	GROUP 2	0.378210E+00	0.637000E-01	0.0	0.971490E-01
4	GROUP 1	0.137490E+01	0.262460E-01	0.171350E-01	0.491400E-02
	GROUP 2	0.380550E+00	0.546390E-01	0.0	0.779920E-01
5	GROUP 1	0.134160E+01	0.259190E-01	0.167510E-01	0.427110E-02
	GROUP 2	0.391690E+00	0.461690E-01	0.0	0.610660E-01
6	GROUP 1	0.158160E+01	0.281970E-01	0.277330E-01	0.0
	GROUP 2	0.307530E+00	0.869100E-02	0.0	0.0
7	GROUP 1	0.139730E+01	0.290910E-01	0.162010E-01	0.589980E-02
	GROUP 2	0.271070E+00	0.444140E+00	0.0	0.268800E-01
8	GROUP 1	0.152290E+01	0.268460E-01	0.262490E-01	0.0
	GROUP 2	0.312270E+00	0.875880E-02	0.0	0.0
9	GROUP 1	0.111330E+01	0.874190E-01	0.375290E-02	0.0
	GROUP 2	0.184010E+00	0.967260E+00	0.0	0.0
10	GROUP 1	0.141630E+01	0.263780E-01	0.167780E-01	0.662050E-02
	GROUP 2	0.368490E+00	0.800900E-01	0.0	0.125430E+00

COMPOSITION	GROUP	DIFF. COEFF.	REMOVAL X-S	OUTSCATTER X-S	NU-FISSION X-S
11	GROUP 1	0.141780E+01	0.254260E-01	0.162050E-01	0.651950E-02
	GROUP 2	0.376890E+00	0.779900E-01	0.0	0.122110E+00
12	GROUP 1	0.141410E+01	0.262910E-01	0.172090E-01	0.569940E-02
	GROUP 2	0.371370E+00	0.668700E-01	0.0	0.984880E-01
13	GROUP 1	0.140190E+01	0.271220E-01	0.181040E-01	0.507070E-02
	GROUP 2	0.371680E+00	0.576770E-01	0.0	0.795880E-01
14	GROUP 1	0.139030E+01	0.281730E-01	0.191260E-01	0.458180E-02
	GROUP 2	0.371310E+00	0.504670E-01	0.0	0.646670E-01
15	GROUP 1	0.158420E+01	0.278650E-01	0.274030E-01	0.0
	GROUP 2	0.309230E+00	0.864970E-02	0.0	0.0
16	GROUP 1	0.140970E+01	0.287200E-01	0.160240E-01	0.588620E-02
	GROUP 2	0.267700E+00	0.449050E+00	0.0	0.265000E-01
17	GROUP 1	0.153100E+01	0.313090E-01	0.307390E-01	0.0
	GROUP 2	0.294170E+00	0.916000E-02	0.0	0.0
18	GROUP 1	0.168930E+01	0.191380E-01	0.999040E-02	0.633850E-02
	GROUP 2	0.527170E+00	0.760250E-01	0.0	0.121900E+00
19	GROUP 1	0.169710E+01	0.181410E-01	0.955690E-02	0.621530E-02
	GROUP 2	0.538430E+00	0.737680E-01	0.0	0.118220E+00
20	GROUP 1	0.168950E+01	0.189620E-01	0.103320E-01	0.546480E-02
	GROUP 2	0.531530E+00	0.634410E-01	0.0	0.961500E-01

COMPOSITION	GROUP	DIFF. COEFF.	REMOVAL X-S	OUTSCATTER X-S	NU-FISSION X-S
21	GROUP 1	0.167460E+01	0.195930E-01	0.109500E-01	0.485350E-02
	GROUP 2	0.532680E+00	0.546350E-01	0.0	0.779930E-01
22	GROUP 1	0.166130E+01	0.204500E-01	0.116880E-01	0.438500E-02
	GROUP 2	0.532230E+00	0.477090E-01	0.0	0.636410E-01
23	GROUP 1	0.197400E+01	0.198060E-01	0.194180E-01	0.0
	GROUP 2	0.408610E+00	0.658170E-02	0.0	0.0
24	GROUP 1	0.169900E+01	0.211310E-01	0.933020E-02	0.562870E-02
	GROUP 2	0.360680E+00	0.438710E+00	0.0	0.279270E-01
25	GROUP 1	0.160950E+01	0.282650E-01	0.277210E-01	0.0
	GROUP 2	0.316570E+00	0.854980E-02	0.0	0.0
26	GROUP 1	0.168940E+01	0.148870E-01	0.571000E-02	0.630570E-02
	GROUP 2	0.525170E+00	0.780170E-01	0.0	0.123400E+00
27	GROUP 1	0.169750E+01	0.140690E-01	0.546140E-02	0.619450E-02
	GROUP 2	0.536580E+00	0.756550E-01	0.0	0.119800E+00
28	GROUP 1	0.169000E+01	0.145590E-01	0.590060E-02	0.543910E-02
	GROUP 2	0.529360E+00	0.654030E-01	0.0	0.980660E-01
29	GROUP 1	0.167550E+01	0.149260E-01	0.624900E-02	0.483840E-02
	GROUP 2	0.530250E+00	0.567280E-01	0.0	0.804220E-01
30	GROUP 1	0.166280E+01	0.154660E-01	0.666170E-02	0.437940E-02
	GROUP 2	0.529560E+00	0.499330E-01	0.0	0.665090E-01

COMPOSITION	GROUP	DIFF. COEFF.	REMOVAL X-S	OUTSCATTER X-S	NU-FISSION X-S
31	GROUP 1	0.197440E+01	0.114830E-01	0.110950E-01	0.0
	GROUP 2	0.408850E+00	0.657670E-02	0.0	0.0
32	GROUP 1	0.170050E+01	0.157160E-01	0.414920E-02	0.565780E-02
	GROUP 2	0.370520E+00	0.419950E+00	0.0	0.338370E-01
33	GROUP 1	0.160990E+01	0.282560E-01	0.277120E-01	0.0
	GROUP 2	0.316700E+00	0.854670E-02	0.0	0.0
34	GROUP 1	0.127370E+01	0.737700E-02	0.566690E-02	0.0
	GROUP 2	0.956900E+00	0.507830E-02	0.0	0.0
35	GROUP 1	0.201000E+01	0.356870E-01	0.351600E-01	0.0
	GROUP 2	0.325900E+00	0.996300E-02	0.0	0.0

$\nu = 2.5$ Removal X-S Group 1 $\equiv \Sigma_{a_1} + \Sigma_{21}$

$\chi_1 = 1.0$ Removal X-S Group 2 $\equiv \Sigma_{a_2}$

$\chi_2 = 0.0$ Outscatter X-S Group 1 $\equiv \Sigma_{21}$

Zone	Material
A	2.50 w/o fuel adjacent to zircaloy can
B	2.50 w/o fuel in the interior
C	1.90 w/o fuel
D	1.49 w/o fuel
E	1.18 w/o fuel - corner rod
F	The water rod
G	The gadolinium rods
H	Channel walls and wide and narrow gaps
I	Control rod (if present)

TABLE A.3.3 MATERIAL DESCRIPTION FOR THE LSHBWR BENCHMARK

Constants	Type of Assembly			
	0^+	0	40	70
$\bar{D}_1$	1.423	1.447	1.673	1.673
$\bar{\Sigma}_{R_1}$	0.02815	0.02753	0.02133	0.01810
$\bar{\Sigma}_{21}$	0.01839	0.02059	0.01480	0.01157
$\nu\bar{\Sigma}_{f_1}$	0.00444	0.00441	0.00420	0.004184
$\bar{D}_2$	0.3486	0.3361	0.4192	0.4137
$\bar{\Sigma}_{a_2}$	0.07038	0.05187	0.04968	0.04834
$\nu\bar{\Sigma}_{f_2}$	0.07362	0.06304	0.06117	0.05965
$f_1^{x^-} f_1^{y^-}$	0.7979	0.9233	0.9380	0.9414
$f_2^{x^-} f_2^{y^-}$	0.5084	1.580	1.615	1.758
$f_1^{x^+} f_1^{y^+}$	1.102	0.9941	0.9911	0.9879
$f_2^{x^+} f_2^{y^+}$	1.828	1.293	1.280	1.338

TABLE A.3.4   FLUX-WEIGHTED PARAMETERS AND ASSEMBLY DISCON-
TINUITY FACTORS FOR THE LSHBWR BENCHMARK

A.4   THE PRELIMINARY TEST PROBLEM
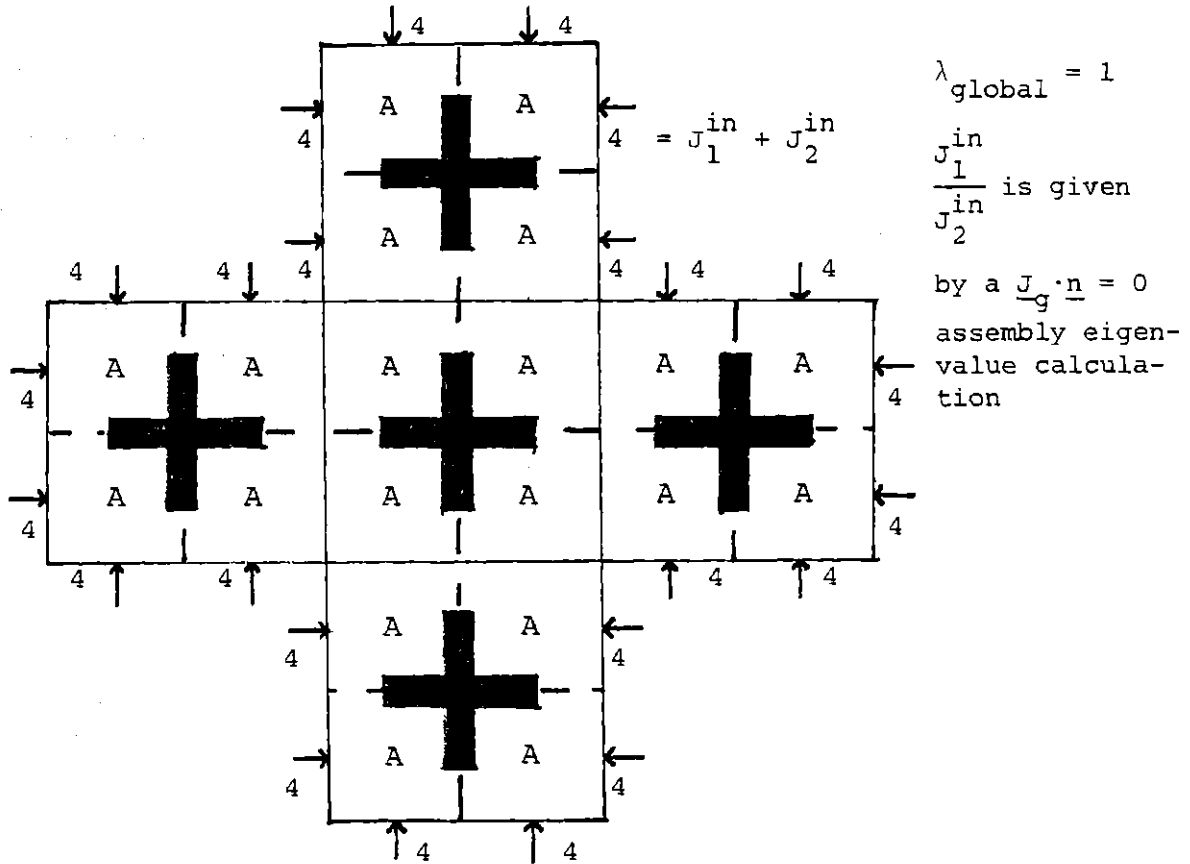
Spatial shape of J_g^{in}:

(1) For the first standard solution, it is the distribution obtained from a $\underline{J}_g \cdot \underline{n} = 0$ assembly eigenvalue calculation.

(2) For the second standard solution, it is flat.

FIGURE A.4.1   ZONE LAYOUT OF THE PRELIMINARY TEST PROBLEM
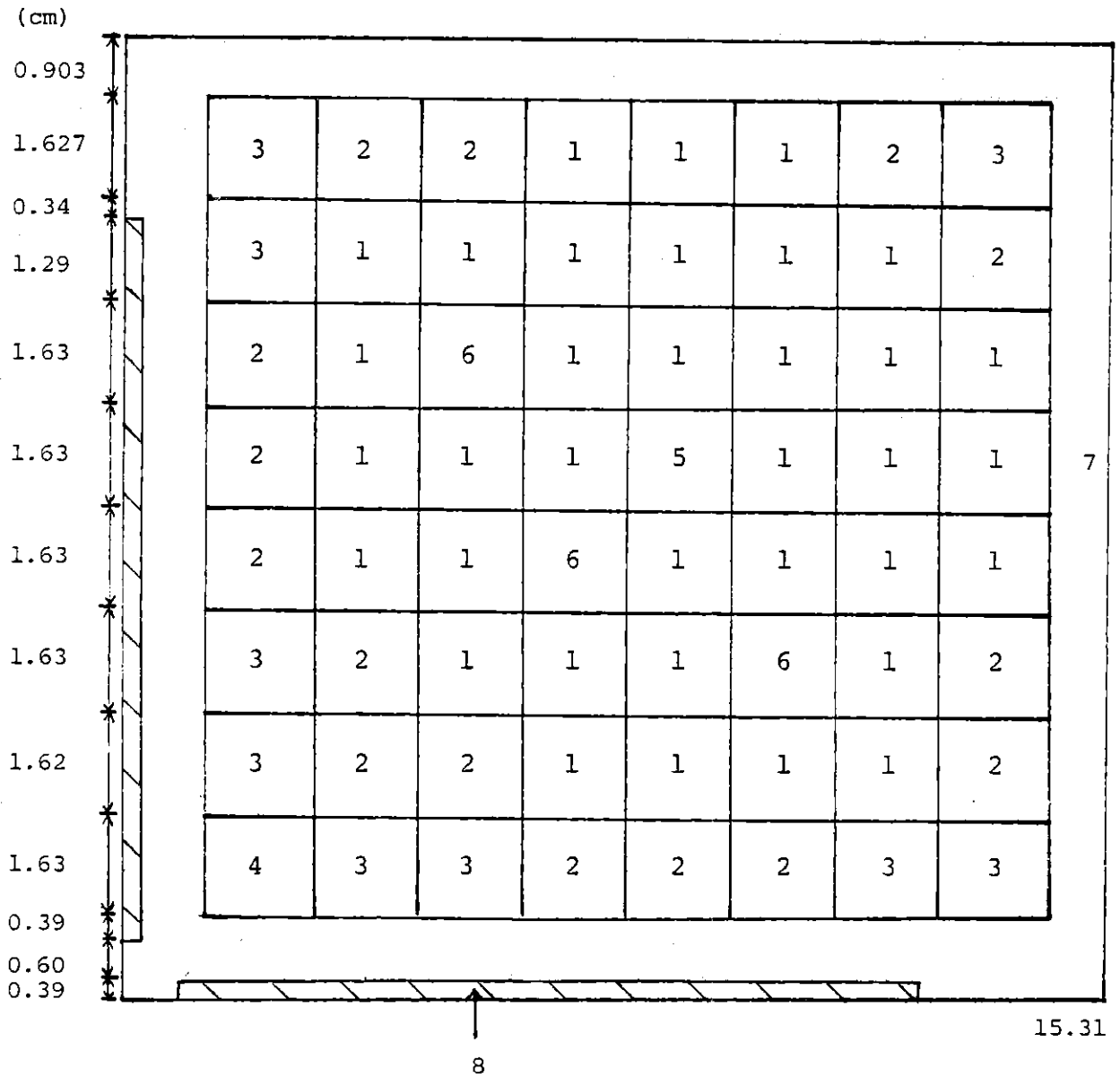
FIGURE A.4.2   ASSEMBLY DESCRIPTION FOR THE PRELIMINARY

TEST PROBLEM

Zone	Material
1	2.50 w/o fuel
2	1.90 w/o fuel
3	1.49 w/o fuel
4	1.18 w/o fuel-corner rod
5	The water rod
6	The gadolinium rods
7	Channel walls and wide and narrow gaps
8	Control rod

TABLE A.4.1 MATERIAL DESCRIPTION FOR THE PRELIMINARY TEST PROBLEM

TABLE A.4.2. HETEROGENEOUS CROSS SECTIONS FOR THE PRILIMINARY TEST PROBLEM

COMPOSITION	GROUP	DIFF. COEFF.	REMOVAL X-S	OUTSCATTER X-S	NU-FISSION X-S
1	GROUP 1	0.141060E+01	0.255200E-01	0.162170E-01	0.651540E-02
	GROUP 2	0.379930E+00	0.751790E-01	0.0	0.121890E+00
2	GROUP 1	0.139490E+01	0.257680E-01	0.166060E-01	0.559700E-02
	GROUP 2	0.378210E+00	0.637000E-01	0.0	0.971490E-01
3	GROUP 1	0.137490E+01	0.262460E-01	0.171350E-01	0.491400E-02
	GROUP 2	0.380550E+00	0.546390E-01	0.0	0.779920E-01
4	GROUP 1	0.134520E+01	0.259190E-01	0.167510E-01	0.427110E-02
	GROUP 2	0.391690E+00	0.461890E-01	0.0	0.610660E-01
5	GROUP 1	0.158160E+01	0.281970E-01	0.277330E-01	0.0
	GROUP 2	0.307530E+00	0.869100E-02	0.0	0.0
6	GROUP 1	0.139730E+01	0.290910E-01	0.162010E-01	0.589980E-02
	GROUP 2	0.271070E+00	0.444140E+00	0.0	0.268800E-01
7	GROUP 1	0.152290E+01	0.268460E-01	0.262490E-01	0.0
	GROUP 2	0.312270E+00	0.875880E-02	0.0	0.0
8	GROUP 1	0.111330E+01	0.874190E-01	0.375290E-02	0.0
	GROUP 2	0.184010E+00	0.967260E+00	0.0	0.0

$$\chi_1 = 1.0$$

$$\chi_2 = 0.0$$

$$\nu = 2.5$$

A.5   THE HOMOGENEOUS TEST PROBLEM
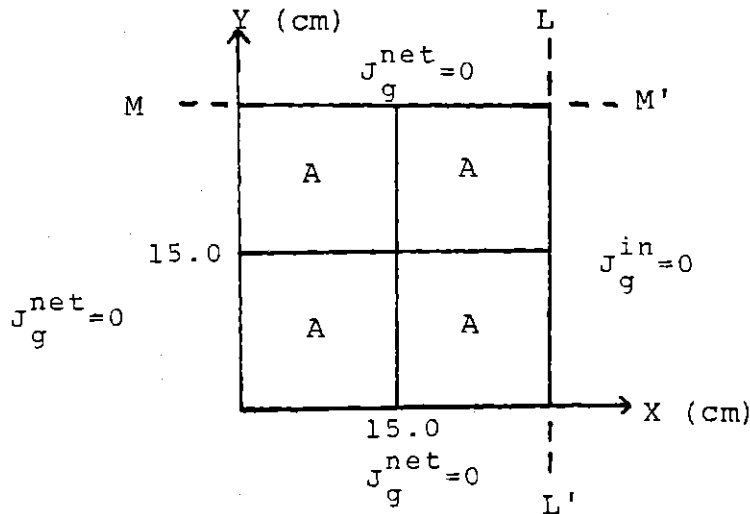
A is a homogeneous assembly.

FIGURE A.5.1   CORE LAYOUT FOR THE HOMOGENEOUS TEST PROBLEM

D_1 (cm)   1.844 D_2 (cm)   0.4284

Σ_{R_1} (cm^{-1})   0.02481 Σ_{R_2} (cm^{-1})   0.05946

Σ_{21} (cm^{-1})   0.01874 $\nu\Sigma_{f_2}$ (cm^{-1})   0.07254

$\nu\Sigma_{f_1}$ (cm^{-1})   0.004556

ν = 2.5

χ_1 = 1.0

χ_2 = 0.0

TABLE A.5.1   CROSS SECTIONS FOR THE HOMOGENEOUS TEST PROBLEM

APPENDIX B

USING CITATION TO GENERATE RESPONSE

MATRICES

B.1   USING CITATION TO GENERATE PARTIAL

CURRENT RESPONSE MATRICES

B.2   USING CITATION TO GENERATE NET CURRENT

RESPONSE MATRICES

B.1 USING CITATION TO GENERATE PARTIAL CURRENT RESPONSE MATRICES

In Chapter Three we have pointed out that the generation of the i-th column of the response matrices [R] and [R'] for a region is equivalent to solving a fixed-source problem defined by the geometry of that region with a unit incoming partial current for the subsurface and group associated with the i-th element of $[J^{in}]$ and with zero incoming partial currents for all other groups and subsurfaces. With angular and spatial approximation made for the unit incoming partial current, the problem is well-defined and can be solved by any method available. However, to be consistent with our full core reference calculations which are generated with a diffusion theory code, a multi-group diffusion theory finite-difference code "CITATION" was used to solve these fixed source problems. Unfortunately, used directly, CITATION can only solve extrapolated and reflected boundary value problems. Thus, a trick is needed to solve problems with unit incoming partial currents as boundary conditions.

In CITATION a region is divided into a regular array of small right rectangular parallelopipeds (meshes) with grid indices defined by

$$\ell, \, m, \, n \equiv \begin{cases} i = 0, \, 1, \, 2, \ldots I; \; u, \, v, \, w = x \\ j = 0, \, 1, \, 2, \ldots J; \; u, \, v, \, w = y \\ k = 0, \, 1, \, 2, \ldots K; \; u, \, v, \, w = z. \end{cases}$$

The neutron balance equations within each mesh is given by

$$(J^x_{g_{i,j,k}} - J^x_{g_{i-1,j,k}})(y_j - y_{j-1})(z_k - z_{k-1})$$

$$+ (J^y_{g_{i,j,k}} - J^y_{g_{i,j-1,k}})(x_i - x_{i-1})(z_k - z_{k-1})$$

$$+ (J_{g_{i,j,k}} - J_{g_{i,j,k-1}})(x_i - x_{i-1})(y_j - y_{j-1})$$

$$+ \Sigma_{t_{g_{i,j,k}}} \phi_{g_{i,j,k}} V_{i,j,k} = \sum_{g'=1}^{G} (\Sigma_{gg'_{i,j,k}} + \frac{\chi_g}{\lambda} \nu\Sigma_{f_{g'_{i,j,k}}}) \phi_{g'_{i,j,k}} V_{i,j,k}$$

$$+ S_{g_{i,j,k}} V_{i,j,k};$$

$$i = 1, 2, \ldots I$$

$$j = 1, 2, \ldots J \qquad\qquad (B.1)$$

$$k = 1, 2, \ldots K$$

$$g = 1, 2, \ldots G$$

where

$J^u_{g_{\ell,m,n}}$ is the face-averaged group-g net current in direction u on the mesh face (u_ℓ, v, w); $v \in [v_{m-1}, v_m]$, $w \in [W_{n-1}, w_n]$,

$\phi_{g_{i,j,k}}$ is the volume-averaged group g flux for mesh (i,j,k),

$S_{g_{i,j,k}}$ is the volume-averaged group g external source for mesh (i,j,k),

$V_{i,j,k}$ $= (x_i - x_{i-1})(y_j - y_{j-1})(z_k - z_{k-1})$ is the volume of the mesh,

G is the total number of groups,

λ is the global reactor eigenvalue which is set arbitrarily for a fixed-source problem.

In this equation, the cross section notations are stand-

ard. The net currents for the interior faces are then expressed in terms of average fluxes by Fick's law and continuity of fluxes across faces. On boundary faces, the net currents are related to the average fluxes by boundary conditions.

In order to use CITATION directly, the boundary conditions must either be net currents equal to zero or have the form

$$J^{\hat{n}}_{g_s} = \frac{1}{1/C_s + \Delta/2D_{g_s}} \phi_{g_s} \qquad (B.2)$$

where

$J^{\hat{n}}_{g_s}$ is the face-averaged group g net current in direction $\hat{n}$ at the boundary surface,

$\hat{n}$ is the outward normal of the boundary surfaces,

Δ is the $\hat{n}$-direction mesh size of meshes neighboring the boundary surface,

D_{g_s} is the group g diffusion coefficient in those meshes neighboring the boundary surfaces,

ϕ_{g_s} is the volume-averaged group g flux in those meshes neighboring the boundary surface,

C_s is a constant that can be arbitrarily specified.

The fixed-source problem which we are trying to solve has an incoming partial current equal to 1 for one group on one subsurface and zero otherwise. To show how this condition can be simulated we shall assume that the unit incoming partial current is in group g on the boundary subsurface $(x=x_0,y,z)$; $y \in [y_0,y_p]$, $z \in [z_0,z_q]$, $p \leq J$, $q \leq K$. The group-g net

currents on those mesh faces belonging to this subsurface
are given by

$$
\begin{aligned}
J^x_{g_{0,j,k}} &= J^{in}_{g_{0,j,k}} - J^{out}_{g_{0,j,k}} \\[2mm]
&= - D_{g_{1,j,k}} \left. \frac{\partial \phi_g}{\partial x} \right|_{0,j,k} \\[2mm]
&= - D_{g_{1,j,k}} \frac{\phi_{g_{1,j,k}} - \phi^s_{g_{0,j,k}}}{\dfrac{x_1 - x_0}{2}} \; ; \qquad\qquad (B.3)
\end{aligned}
$$

$$ j = 1, 2, \ldots p; \quad k = 1, 2, \ldots q $$

where

$J^{in}_{g_{0,j,k}}$ and $J^{out}_{g_{0,j,k}}$ are the face-averaged group-g partial currents on mesh face (x_0, y, z); $y \in [y_{j-1}, y_j]$, $z \in [z_{k-1}, z_k]$,

$\left. \dfrac{\partial \phi}{\partial x} \right|_{0,j,k}$ is the x-directional derivative of the face-averaged group-g flux evaluated at mesh face (x_0, y, z); $y \in [y_{j-1}, y_j]$, $z \in [z_{k-1}, z_k]$,

$\phi^s_{g_{0,j,k}}$ is the face-averaged group-g flux on mesh face (x_0, y, z); $y \in [y_{j-1}, y_j]$, $z \in [z_{k-1}, z_k]$.

The other terms in this equation are the same as those de-
fined in equation (B.1) and (B.2).

The last equality in Eq. (B-3) is a finite difference
approximation, consistent with CITATION, for the derivative.
It is consistent in the sense that CITATION also uses the
same approximation to express Fick's law. Using the diffu-

sion theory approximation, we have for these mesh faces

$$\phi^s_{g_{0,j,k}} = 2(J^{in}_{g_{0,j,k}} + J^{out}_{g_{0,j,k}}) \qquad (B.4)$$

Then

$$J^x_{g_{0,j,k}} = - D_{g_{1,j,k}} \frac{\phi_{g_{1,j,k}} - 2(J^{in}_{g_{0,j,k}} + J^{out}_{g_{0,j,k}})}{\dfrac{x_1 - x_0}{2}}$$

$$= J^{in}_{g_{0,j,k}} - J^{out}_{g_{0,j,k}} \qquad (B.5)$$

Thus, the outgoing partial currents on these mesh faces are given by

$$\qquad\qquad\qquad\qquad\qquad\qquad\qquad\qquad\qquad (B.6)$$

$$J^{out}_{g_{0,j,k}} = \frac{\dfrac{x_1 - x_0}{2} - 2D_{g_{1,j,k}}}{\dfrac{x_1 - x_0}{2} + 2D_{g_{1,j,k}}} J^{in}_{g_{0,j,k}} + \frac{D_{g_{1,j,k}}}{\dfrac{x_1 - x_0}{2} + 2D_{g_{1,j,k}}} \phi_{g_{1,j,k}}$$

and the total leakage from these mesh faces is given by

$$-J^x_{g_{0,j,k}} (y_j - y_{j-1})(z_k - z_{k-1}) = -(y_j - y_{j-1})(z_k - z_{k-1})(J^{in}_{g_{0,j,k}} - J^{out}_{g_{0,j,k}})$$

$$= \frac{-4D_{g_{1,j,k}} (y_j - y_{j-1})(z_k - z_{k-1})}{\dfrac{x_1 - x_0}{2} + 2\,D_{g_{1,j,k}}} J^{in}_{g_{0,j,k}}$$

$$+ \frac{D_{g_{1,j,k}} (y_j - y_{j-1})(z_k - z_{k-1})}{\dfrac{x_1 - x_0}{2} + 2\,D_{g_{1,j,k}}} \phi_{g_{1,j,k}} \qquad (B.7)$$

Similar equations for outgoing partial currents and leakages can be derived for the other subsurfaces and groups. Since incoming partial currents are zero for other subsurfaces and groups, only the term involving the average fluxes will be left. Substituting the leakage expressions into equation (B.1) and moving the term involving $J^{in}_{g_{0,j,k}}$ to the right-hand side, we see that the problem that we are trying to solve is equivalent to a problem with distributed sources $S_{g'_{i,j,k}}$ where

$$S_{g'_{i,j,k}} = \begin{cases} \dfrac{4\,D_{g_{1,j,k}}}{\dfrac{x_1-x_0}{2} + 2\,D_{g_{1,j,k}}} \dfrac{J^{in}_{g_{0,j,k}}}{x_1 - x_0} & ; \begin{array}{l} i=0, \\ j=1,2,\ldots p, \\ k=1,2,\ldots q, \\ g'=g, \end{array} \\ \\ 0 \quad \text{otherwise} \end{cases}$$

(B.8)

and with boundary conditions

$$J^{\hat{n}}_{g'_s} = \frac{1}{2 + \Delta/2D_{g'_s}}\,\phi_{g'_s} \quad ; \quad g'=1,2,\ldots G \qquad (B.9)$$

All terms in these equations are defined in equation (B.2). The $J^{in}_{g_{0,j,k}}$ in equation (B.8) is given by our spatial approximation and the normalization

$$\sum_{k=1}^{q} \sum_{j=1}^{p} J^{in}_{g_{0,j,k}} (y_j-y_{j-1})(z_k-z_{k-1}) = 1 \qquad (B.10)$$

Comparison of equation (B.2) and (B.9) shows that the C_s for this equivalent problem is equal to 0.5.

For problems with a unit incoming partial current on other subsurface or group, the same kind of equivalent problem can be defined and thus all the fixed-source problems needed to generate response matrices [R] and [R'] can be solved by CITATION.

Physically, every element of [R] and [R'] should be nonnegative as long as the region being examined is, in a vacuum, subcritical. However, because of the limitation of diffusion theory, some outgoing partial currents obtained using equation (B.6) may be negative, and thus some elements of [R] may be negative.

A similar derivation can be carried out for a problem with incoming partial currents not equal to zero for several subsurfaces and energy groups. The result is equivalent to a CITATION problem with $C_S = 0.5$ and distributed sources $S_{g_{i,j,k}}$ again defined by equation (B.8) (except for corner meshes where the contributions from all sides to the source term have to be summed). In Section 3.4.1, we used this technique to obtain the reference results.

B.2 USING CITATION TO GENERATE NET CURRENT RESPONSE MATRICES

In Chapter Four we have pointed out that the generation of the i-th column of the response matrices [R] and [R'] for a region is equivalent to solving a fixed-source problem defined by the geometry of that region with a unit net current (in the outward normal direction) for the subsurface

and group associated with the i-th element of [J] and with

zero net currents for all other groups and subsurfaces.

With angular and spatial approximations made for the unit

net current, the problem is well-defined and can be solved

by any standard method available. However, for the same

reason that partial current response matrices are generated

by CITATION (i.e., because we wish to use diffusion theory

as a numerical standard), net current response matrices are

generated by the same code. As mentioned in the previous

section, CITATION can only solve extrapolated and reflected

boundary value problems. Thus a trick is needed to solve

problems with unit net currents as boundary conditions.

To show how this condition can be simulated we shall

assume that the unit net current is in group-g on the

boundary subsurface $(x=x_0, y, z)$; $y \in [y_0, y_p]$, $z \in [z_0, z_q]$,

$p \leq J$, $q \leq K$. The group-g net currents on those mesh faces

belonging to this subsurface are given by the spatial approx-

imation and the normalization

$$\sum_{k=1}^{q} \sum_{j=1}^{p} J^x_{g_{0,j,k}} (y_j - y_{j-1})(z_k - z_{k-1}) = -1 \qquad (B.11)$$

In this equation there is a minus sign because the outward

normal direction is in the negative x-direction. On the

other subsurfaces and groups, the net currents are zero.

Substituting these values for the leakage terms into equa-

tion (B.1) and moving the term involving $J^x_{g_{0,j,k}}$ to the

right hand side, we see that the problem we are trying to

solve is equivalent to a problem with distributed sources $S_{g'_{i,j,k}}$ where

$$
S_{g'_{i,j,k}} = \begin{cases} \dfrac{J^x_{g_{0,j,k}}}{x_1 - x_0} \; ; & \begin{aligned} i &= 0, \\ j &= 1, 2, \ldots p, \\ k &= 1, 2, \ldots q, \\ g' &= g, \end{aligned} \\[3em] 0 \quad \text{otherwise} \end{cases} \tag{B.12}
$$

and with zero net currents for all groups and subsurfaces as boundary conditions.

After the mesh volume-averaged fluxes are determined, the group-g face-averaged fluxes on the subsurfaces ($x=x_0$, y,z) can be determined by

$$
\phi^s_{g_{0,j,k}} = \frac{x_1-x_0}{2} \; \frac{J_{g_{0,j,k}}}{D_{g_{1,j,k}}} + \phi_{g_{1,j,k}} \tag{B.13}
$$

All terms in this equation are defined in the previous section. For the face-averaged fluxes on the other subsurfaces and groups only the term involving the average fluxes will be left because the net currents for those subsurfaces and groups are zero.

From equation (B.11) we can see that $J^x_{g_{0,j,k}}$ is negative so that the equivalent problem has a negative source. If the region has an infinite multiplication factor smaller than 1, the total power in the region resulting from this negative source will be negative. Since CITATION does not allow negative total power (although negative fluxes are

allowed), we solve this fixed-source problem by changing the sign of the sources. After the solution is obtained, the sign is again changed.

For problems with a unit net current on other subsurfaces or groups, the same kind of equivalent problem can be defined and thus all the fixed-source problems needed to generate response matrices $[R]$ and $[R']$ can be solved by CITATION.

If a region has an infinite multiplication factor smaller than 1, the region in an infinite lattice with a positive source will have positive fluxes everywhere because this is a problem that is physically realizable. Because of the linearity of the neutron balance equation, the same region in an infinite lattice with a negative source will have everywhere negative fluxes. Thus, the elements of the net current response matrices for such regions will all be negative. On the other hand if a region has an infinite multiplication larger than 1, the fluxes resulting from a positive source in such a region in an infinite lattice may have both signs since there is no everywhere positive physical solution in a supercritical infinite lattice with a positive source. Thus, the elements of the net current response matrices for such regions may have both signs.

APPENDIX C

AN EFFICIENT WAY TO INVERT $[A_{i,j}]$

To obtain the response matrix [R] for a cluster (i,j), a (8*G*NSEG) x (8*G*NSEG) matrix $[A_{i,j}]$ defined following equation (3.7) must be inverted. Because of the sparseness of $[A_{i,j}]$, the problem can be simplified. First, $[A_{i,j}]$ is expressed as

$$[A_{i,j}] = \begin{bmatrix} [A_1] & [A_2] \\ [A_3] & [A_4] \end{bmatrix}$$

where $[A_\alpha]$ (α = 1, 2, 3, 4) are of the same size (i.e., (4*G*NSEG)*(4*G*NSEG)). Then the inverse of $[A_{i,j}]$ will be

$$[A_{i,j}]^{-1} = \begin{bmatrix} [B_1] & [B_2] \\ [B_3] & [B_4] \end{bmatrix}$$

where

$$[B_4] = \{[A_4] + [C_1][A_2]\}^{-1}$$
$$[B_3] = [B_4][C_1]$$
$$[B_2] = [C_2][B_4]$$
$$[B_1] = [A_1]^{-1} + [C_2][B_3]$$
$$[C_1] = -[A_3][A_1]^{-1}$$
$$[C_2] = -[A_1]^{-1}[A_2]$$

Since

$$[A_1] = \begin{bmatrix} [I] & [0] & [0] & -[R_{14}^{i+\frac{1}{2},j}] \\ [0] & [I] & [0] & [0] \\ [0] & -[R_{23}^{i,j+\frac{1}{2}}] & [I] & [0] \\ [0] & [0] & [0] & [I] \end{bmatrix}$$

its inverse $[A_1]^{-1}$ will be

$$[A_1]^{-1} = \begin{bmatrix} [I] & [0] & [0] & [R_{14}^{i+\frac{1}{2},j}] \\ [0] & [I] & [0] & [0] \\ [0] & [R_{23}^{i,j+\frac{1}{2}}] & [I] & [0] \\ [0] & [0] & [0] & [I] \end{bmatrix}$$

Then $[C_1]$ and $[C_2]$ will be

$$[C_2] = \begin{bmatrix} [R_{11}^{i+\frac{1}{2},j}] & [R_{14}^{i+\frac{1}{2},j}][R_{21}^{i+\frac{1}{2},j+\frac{1}{2}}] & [0] & [R_{14}^{i+\frac{1}{2},j}][R_{22}^{i+\frac{1}{2},j+\frac{1}{2}}] \\ [0] & [R_{11}^{i+\frac{1}{2},j+\frac{1}{2}}] & [0] & [R_{12}^{i+\frac{1}{2},j+\frac{1}{2}}] \\ [0] & [R_{23}^{i,j+\frac{1}{2}}][R_{11}^{i+\frac{1}{2},j+\frac{1}{2}}] & [R_{22}^{i,j+\frac{1}{2}}] & [R_{23}^{i,j+\frac{1}{2}}][R_{12}^{i+\frac{1}{2},j+\frac{1}{2}}] \\ [0] & [R_{21}^{i+\frac{1}{2},j+\frac{1}{2}}] & [0] & [R_{22}^{i+\frac{1}{2},j+\frac{1}{2}}] \end{bmatrix}$$

$$[C_1] = \begin{bmatrix} [R_{33}^{i,j}] & [R_{34}^{i,j}][R_{23}^{i,j+\frac{1}{2}}] & [R_{34}^{i,j}] & [R_{33}^{i,j}][R_{14}^{i+\frac{1}{2},j}] \\ [0] & [R_{33}^{i,j+\frac{1}{2}}] & [0] & [0] \\ [R_{43}^{i,j}] & [R_{44}^{i,j}][R_{23}^{i,j+\frac{1}{2}}] & [R_{44}^{i,j}] & [R_{43}^{i,j}][R_{14}^{i+\frac{1}{2},j}] \\ [0] & [0] & [0] & [R_{44}^{i+\frac{1}{2},j}] \end{bmatrix}$$

Now only $[A_4] + [C_1][A_2]$ need be inverted. If we define

$$[E] = \begin{bmatrix} [E_1] & [E_2] \\ [E_3] & [E_4] \end{bmatrix} = [A_4] + [C_1][A_2],$$

then the inverse of $[A_4] + [C_1][A_2]$ will be

$$[E]^{-1} = [F] = \begin{bmatrix} [F_1] & [F_2] \\ [F_3] & [F_4] \end{bmatrix}$$

where

$$[F_4] = \{[E_4] + [C_3][E_2]\}^{-1}$$

$$[F_3] = [F_4][C_3]$$

$$[F_2] = [C_4][F_4]$$

$$[F_1] = [E_1]^{-1} + [C_4][F_3]$$

$$[C_3] = -[E_3][E_1]^{-1}$$

$$[C_4] = -[E_1]^{-1}[E_2]$$

Because $[A_4] + [C_1][A_2]$ has a form

$$\begin{bmatrix} [X] & [X] & [X] & [X] \\ [0] & [X] & [X] & [X] \\ [X] & [X] & [X] & [X] \\ [X] & [X] & [0] & [X] \end{bmatrix}$$

where $[0]$ is a null matrix and $[X]$ represents a matrix with nonzero elements, $[E_1]$ will be of a form

$$\begin{bmatrix} [X] & [X] \\ [0] & [X] \end{bmatrix} = \begin{bmatrix} [E_{11}] & [E_{12}] \\ [0] & [E_{22}] \end{bmatrix}$$

Then

$$[E_1]^{-1} = \begin{bmatrix} [E_{11}]^{-1} & -[E_{11}]^{-1}[E_{12}][E_{22}]^{-1} \\ [0] & [E_{22}]^{-1} \end{bmatrix}$$

Now the $(8*G*NSEG) \times (8*G*NSEG)$ matrix inversion becomes two $(NSEG*G) \times (NSEG*G)$ and one $(2*NSEG*G) \times (2*NSEG*G)$ matrix inversion and some matrix multiplication. This method is used to obtain $[A_{i,j}]^{-1}$ in the code "RESPONSE". In addition the sparseness of $[C_1]$, $[C_2]$, $[A_2]$, $[A_4]$ and $[E_4]$ are fully used in the matrix addition and multiplication. Also in that code the sparseness of $[B_{i,j}]$, $[C_{i,j}]$ and $[D_{i,j}]$ which are defined following equation (3.7) are fully used to obtain $[R]$.

APPENDIX D

THE NONCONVERGENCY OF GAUSS-SEIDEL ITERATION

METHOD IN SOLVING THE 5-NODE PROBLEM USING NET

CURRENT RESPONSE MATRICES

In Chapter Three where partial current response matrices were used, the Gauss-Seidel iteration method was used to solve the 5-node local problems (Eq. (3.12)) to determine the partial currents on the surfaces of the central node. Although we cannot prove by standard mathematical methods that the iteration will converge, the physics of the situation suggests that it will in fact always converge. On the other hand, if net current response matrices are used, there is no physical reason that the same method will converge if it is used to solve the 5-node local problems (Eq. (4.2)) to determine the net currents on the surfaces of the central node. In order to understand the convergency better, a one dimensional one group local problem was analyzed.

For a slab of width L with a unit net current coming in through the face (x = L) and zero net current on the face (x = 0), the flux in the slab is given by

$$\phi(x) = \frac{\cosh \kappa x}{D\kappa \ \sinh \kappa L} \qquad (D.1)$$

where D   is the diffusion coefficient of the slab,

　　　　L   is the width of the slab,

　　　　$\phi(x)$ is the flux at x,

$$\kappa = \left(- \frac{\lambda_g^{-1} \nu \Sigma_f - \Sigma_a}{D} \right)^{1/2}$$

In this equation the cross section notation is standard, and

λ_g is the estimated global eigenvalue. Using (D.1), the net current response matrix $[R]$ can be obtained and it is

$$[R] \quad = \quad \frac{-1}{\kappa D \, \sinh \kappa L} \begin{bmatrix} \cosh \kappa L & 1 \\ 1 & \cosh \kappa L \end{bmatrix} \quad \text{(D.2)}$$

In this equation there is a minus sign because in the definition of net current response matrices (Eq. (4.1)), we use the outward normal direction as the positive direction.

The Gauss-Seidel iteration matrix of equation (4.2) is

$$[B_1] \quad = \quad \begin{bmatrix} [0] & -[D] \\ [0] & -[R]^{-1}[D] \end{bmatrix} \quad \text{(D.3)}$$

where $[B_1]$ is the Gauss-Seidel iteration matrix,

$[D]$ and $[R]$ are defined following equation (4.2). In order to be convergent the spectral radius of this iteration matrix which is determined by the spectral radius of $-[R]^{-1}[D]$ has to be smaller than 1. Before calculating the spectral radius of $-[R]^{-1}[D]$, we point out that another possible Gauss-Seidel iteration matrix, obtained by exchanging the order of the submatrix equations in equation (4.2), is given by

$$[B_2] \quad = \quad \begin{bmatrix} [0] & [R] \\ [0] & -[D]^{-1}[R] \end{bmatrix} \quad \text{(D.4)}$$

The spectral radius of this iteration matrix is determined by the spectral radius of $-[D]^{-1}[R]$. It is important to realize that although the eigenvalues of $-[D]^{-1}[R]$ and

$-[R]^{-1}[D]$ are the inverse of each other (since $-[D]^{-1}[R]$ is just the inverse of $-[R]^{-1}[D]$), their spectral radii are not the inverse of each other.

Because there is only one dimension, a local problem will involve only three nodes. For simplicity we assumed that all three nodes are geometrically and materially identical. Then $[D]$ is given by

$$[D] = \frac{-1}{\kappa D \sinh \kappa L} \begin{bmatrix} \cosh \kappa L & 0 \\ 0 & \cosh \kappa L \end{bmatrix} \qquad (D.5)$$

Because

$$[D]^{-1} = -\kappa D \sinh \kappa L \begin{bmatrix} \operatorname{sech} \kappa L & 0 \\ 0 & \operatorname{sech} \kappa L \end{bmatrix} \qquad (D.6)$$

$-[D]^{-1}[R]$ is given by

$$-[D]^{-1}[R] = - \begin{bmatrix} 1 & \operatorname{sech} \kappa L \\ \operatorname{sech} \kappa L & 1 \end{bmatrix} \qquad (D.7)$$

The eigenvalues of $-[D]^{-1}[R]$ are

$$\lambda = 1 \pm \operatorname{sech} \kappa L \qquad (D.8)$$

Because $-[R]^{-1}[D]$ is the inverse of $-[D]^{-1}[R]$, its eigenvalues are given by

$$\lambda' = (1 \pm \operatorname{sech} \kappa L)^{-1} \qquad (D.9)$$

If κ is real so that $0 \le \operatorname{sech} \kappa L \le 1$, the spectral radii of both iteration matrices will be larger than 1, and thus the use of both $[B_1]$ and $[B_2]$ will result in divergence. If κ is imaginary, equations (D.8) and (D.9) become

$$\lambda = 1 \pm \sec |\kappa| L \qquad\qquad (D.10)$$

$$\lambda' = (1 \pm \sec |\kappa| L)^{-1} \qquad\qquad (D.11)$$

Thus, the spectral radius of $-[D]^{-1}[R]$ is always larger than 1 and $[B_2]$ will always result in divergence. However, if $\sec |\kappa| L$ is larger than 2, the spectral radius of $-[R]^{-1}[D]$ will be smaller than 1 and $[B_1]$ will result in convergence.

It seems clear now that even for a one-dimensional one group problem, the Gauss-Seidel iteration method will not converge unless very restrictive conditions ($\kappa^2 < 0$, $\sec |\kappa| L > 2$) are met. For more complicated problems such as those two-dimensional two group problems we are concerned with, the conditions may well be even more stringent.

Because the value of κ^2 is modulated by the estimated global eigenvalue, there are always some nodes in the reactor with positive κ^2 and other nodes with negative κ^2. Thus, it is clear that in order to solve all fixed problems in a reactor by a single method, the Gauss-Seidel iteration method must be abandoned.

APPENDIX E

THE CONVERGENCY OF THE GLOBAL-LOCAL ITERATION

PROCESS USING NET CURRENT RESPONSE MATRICES

In Section 4.4.1 we found that for some cases the
global-local iteration process converged while for others
it did not. In order to have a better understanding of
this global-local iteration process, two simpler problems
described in Figure E.1 were analyzed. All nodes of
these problems are type A assemblies of the CISE benchmark.
The values of the albedo were chosen to make the eigenvalues
of these problems to be nearly the same as the eigenvalue
of the CISE benchmark so that the response matrices cal-
culated for that benchmark could be used directly in these
problems.

Various local methods using fixed response matrices
during the global-local iteration process (as in Section
4.4.1) were analyzed. The same methods using updated
response matrices (updated in accordance with the newest
estimate of the global eigenvalue) during the global-local
iterations were also tried. Results are shown on Table E.1
and E.2.

Case I to VII on Table E.1 indicate that fixing the
response matrices during global-local iterations may result
in nonconvergence. What happened was that the global
calculations were aborted by QUANDRY because either negative
homogenized cross sections were given by the previous local
calculation or a condition which would make one of the
iteration matrices in QUANDRY diverge resulted from the
previous local calculation.

$\phi = \alpha J$

Y (cm)

15.0

J=0

$\alpha = 48.47$

A   A   A

$\alpha = 2.0$

X (cm)

45.0

J=0

TEST PROBLEM (a)

$\alpha = 17.45$

Y (cm)

30.0

J=0

A   A   A

A   A   A

$\alpha = 2.0$

X (cm)

45.0

J=0
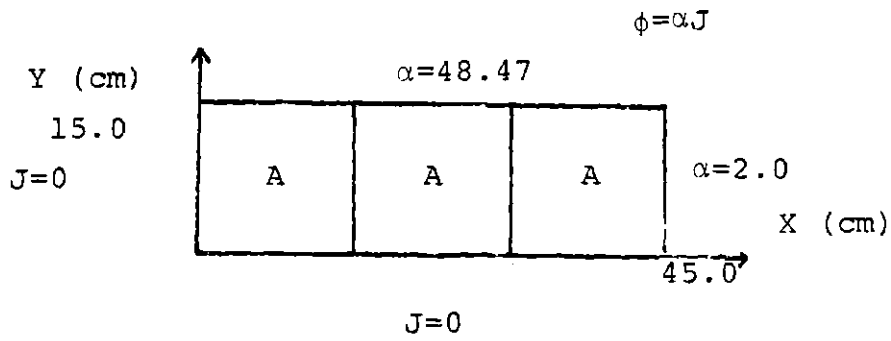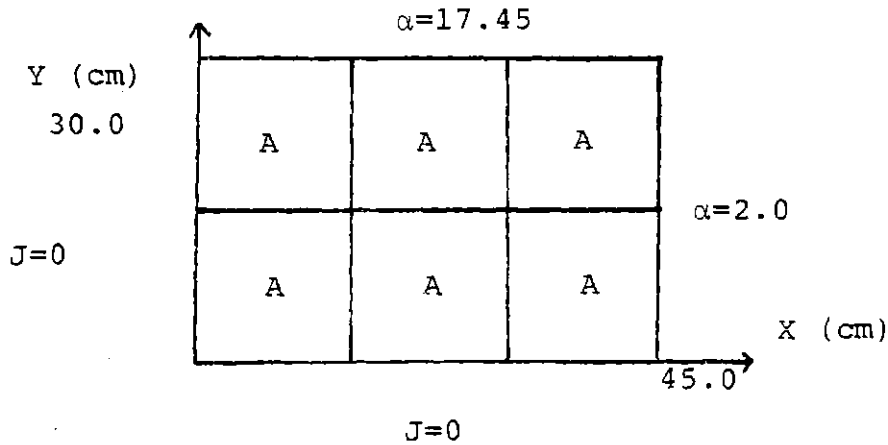
TEST PROBLEM (b)

A is the type A assembly of CISE benchmark (described in Appendix A.1).

FIGURE E.1   CORE LAYOUT FOR PROBLEMS USED TO TEST THE CONVERGENCE OF THE GLOBAL-LOCAL ITERATION PROCESS.

Case	Problem	Model for Global Calculation	Method for Local Calculation	Response Matrices used in Local Calculation	Convergency
I	a	F	N5S2	Fixed	Yes
II	b	F	N1S1	Fixed	Yes
III	b	F	N5S1	Fixed	No
IV	b	F	N5S2	Fixed	No
V	b	F	N1S1	Updated	Yes
VI	b	F	N5S1	Updated	Yes
VII	b	F	N5S2	Updated	Yes
VIII	b	CMFD	N5S2	Updated	No

TABLE E.1   CONVERGENCE OF THE GLOBAL-LOCAL ITERATIONS USING DIFFER-

ENT LOCAL METHODS FOR THE TEST PROBLEMS SHOWN IN FIGURE E.1

Case	I	II	III	IV	V	VI
Model for Global Calculation	F	CMFD	F	F	F	CMFD
Initial Estimation			ADFF	ADFF	ADFF	ADFC
Method for Local Calculation			N1S1	N5S1	N5S2	N5S2

% Errors (after first iteration)		I	II	III	IV	V	VI
	λ	0.32	3.57	0.06	0.08	−0.13	1.51
	HCS_m	2.08	2.08	0.69	0.53	0.52	1.11
	ϵ_{max}	0.26	4.15	0.28	0.47	0.63	53.06
	ϵ_{av}	0.20	1.89	0.14	0.20	0.26	12.32

No. of iterations to converge				4	3	33	Failed to converge

% Errors (after convergence)		I	II	III	IV	V	VI
	λ			0.07	0.07	−0.12	
	HCS_m			0.52	0.53	0.51	
	ϵ_{max}			0.46	0.46	0.17	
	ϵ_{av}			0.20	0.20	0.09	

TABLE E.2   THE ERRORS FOR PROBLEM (b) (SHOWN IN FIGURE E.1) USING DIFFERENT LOCAL METHODS AND UPDATED RESPONSE MATRICES

Case VIII on Table E.1 indicates that with a crude global model the global-local iterations may not converge even if updated response matrices are used in the local calculations. A detailed examination of the results of this case was made, and it showed that for such a crude model, the oscillation of the global-local iterations has a very large amplitude. It is not surprising that with such an oscillation a stage at which one of the iteration matrices in QUANDRY becomes divergent may be reached during the global-local iterations. Moreover, the global-local iteration itself is a nonlinear process which may not be convergent, especially with such a crude global model.

For Methods N1S1 and N5S1 both the converged global and local solutions should be just those obtained from solving the entire problem by the response matrix method using 1-segment response matrices and thus should be equal to each other. However, if during the global-local iterations response matrices are not updated, the converged global and local solutions should be different. This is because without updating the response matrices neither the global nor the local converged solutions (if they exist) will be the solutions obtained from solving the entire problem by the response matrix method.

For Method N5S2, because of the spatial approximation used to define each fixed-source problem for the local

calculations, the global and local calculations are solving two different problems and each will try to converge to its own solution. The results for Problem (b) and the CISE benchmark were checked, and results are shown in Table E.3 to verify these points.

Case[1]	I	II	III	IV	V
Problem	b[2]	b	b	CISE	b
Method used for local calculation	N1S1	N1S1	N5S1	N5S1	N5S2
Response matrices used for local calculation	Fixed	Updated	Updated	Fixed	Updated
Max % differences in $\overline{\phi}_g$	11.8	0.16	3.27	130.	15.3
Max % differences in J^u_g	12.3	0.15	12.6	685.	52.5
Max % differences in $\phi^u_g(u_\ell)$	15.5	0.21	3.70	142.	17.3
No. of nodes having differences > 1%	many	0	1[3]	many	many

[1] All cases use the flat transverse leakage model and start with the ADFF results as initial estimation.

[2] This is problem (b) shown in Figure E.1.

[3] This node is the one which has two surfaces with albedo boundary surfaces. The large errors come from round-off.

TABLE E.3   DIFFERENCES BETWEEN THE LOCAL AND GLOBAL CONVERGENT SOLUTIONS

APPENDIX F

NORMALIZED POWER DENSITIES

FIGURE F.1 NORMALIZED POWER DENSITIES AND ERRORS FOR THE CISE BENCHMARK USING
PARTIAL CURRENT RESPONSE MATRICES (CLUSTER HOMOGENIZATION)

REFERENCE   ---   0.1903   Y = 4
START ADFF, FLAT MODEL, N1S2, 1ST ITERATION   ---   -6.82 %
START ADFF, FLAT MODEL, N5S2, 1ST ITERATION   ---   4.17 %
START ADFF, FLAT MODEL, N5S2, 2ND ITERATION   ---   2.22 %
START ADFQ, QUADRATIC MODEL, N5S2, 1ST ITERATION ---   3.75 %

                                         0.8877   0.9266   Y = 3
                                         2.56 %   -6.34 %
                                        -1.78 %   -4.76 %
                                         0.99 %   0.41 %
                                        -1.69 %   -5.06 %

                              1.0039   1.4200   1.3781   0.4767   Y = 2
                             30.20 %   6.90 %   -15.30 %   -28.10 %
                             14.80 %   -0.21 %   -9.80 %   2.32 %
                              7.98 %   2.04 %   -4.29 %   -1.60 %
                             15.80 %   0.21 %   -10.20 %   3.77 %

                   1.0352   1.3191   1.0974   1.5209   0.5698   Y = 1
                  47.80 %   39.90 %   8.35 %   17.80 %   -30.20 %
                  28.10 %   19.90 %   2.42 %   -11.60 %   -1.59 %
                   9.54 %   8.33 %   -0.40 %   -7.82 %   -6.59 %
                  29.00 %   20.90 %   2.61 %   -12.10 %   -2.33 %

              X =   1   2   3   4   5

FIGURE F.2 NORMALIZED POWER DENSITIES AND ERRORS FOR THE CISE BENCHMARK USING
PARTIAL CURRENT RESPONSE MATRICES (ASSEMBLY HOMOGENIZATION)

REFERENCE
START REF., QUADRATIC MODEL, N5S2, 1ST ITERATION

X =	1	2	3	4	5	6	7	8	
					---	0.6493			Y = 6
						-3.01 %			
					0.6846	0.7850	0.6270		Y = 5
					0.83 %	-1.98 %	0.16 %		
				0.8820	0.7304	0.8841	0.8655		Y = 4
				5.83 %	1.31 %	-4.64 %	-6.90 %		
			0.9108	1.0824	1.2814	1.1197	1.0642	0.7515	Y = 3
			12.80 %	7.02 %	0.08 %	-5.90 %	-8.73 %	-10.50 %	
		0.8887	0.8101	1.2566	1.2195	1.4165	1.1008	0.8753	Y = 2
		20.71 %	15.80 %	8.27 %	-0.74 %	-7.70 %	-11.70 %	-14.00 %	
	0.8814	1.0362	1.2094	0.8404	1.0294	1.2581	1.3359	0.9722	Y = 1
	24.50 %	21.50 %	16.70 %	10.50 %	0.87 %	-7.31 %	-12.20 %	-14.80 %	

FIGURE F.3.I NORMALIZED POWER DENSITIES AND ERRORS FOR THE CISE BENCHMARK USING 'QUADRATIC' TRANSVERSE LEAKAGE MODEL AND NET CURRENT RESPONSE MATRICES (I)

REFERENCE
ADFQ
START ADFQ, N1S1, 1ST ITERATION
START ADFQ, N1S1, 4TH ITERATION

X =	1	2	3	4	5	6	7	8	
					---	0.6493			Y = 6
					---	-1.32 %			
					---	-2.87 %			
					---	-3.05 %			
					0.6846	0.7850	0.6270		Y = 5
					-0.13 %	-0.03 %	-0.60 %		
					-1.04 %	0.43 %	-1.66 %		
					-0.74 %	0.41 %	-1.78 %		
				0.8820	0.7304	0.8841	0.8655		Y = 4
				-3.04 %	-2.40 %	0.12 %	-0.29 %		
				-0.15 %	-1.13 %	-0.17 %	-0.79 %		
				-0.08 %	-0.72 %	-0.14 %	-0.90 %		
			0.9108	1.0824	1.2814	1.1197	1.0642	0.7515	Y = 3
			-1.66 %	1.12 %	0.99 %	-0.07 %	-0.24 %	-0.72 %	
			-0.29 %	1.39 %	0.97 %	-1.00 %	-0.85 %	-1.68 %	
			-0.34 %	1.39 %	1.02 %	-0.97 %	-0.85 %	-1.81 %	
		0.8887	0.8101	1.2566	1.2195	1.4165	1.1008	0.8753	Y = 2
		-0.84 %	-1.29 %	1.72 %	0.90 %	0.04 %	-0.28 %	-0.56 %	
		0.56 %	-0.37 %	1.68 %	0.71 %	-0.63 %	-1.18 %	-0.70 %	
		0.52 %	-0.36 %	1.64 %	0.72 %	-0.59 %	-1.15 %	-0.85 %	
	0.8814	1.0362	1.2094	0.8404	1.0294	1.2581	1.3359	0.9722	Y = 1
	-0.46 %	2.13 %	2.27 %	-0.64 %	-2.19 %	0.43 %	-0.02 %	-0.50 %	
	0.48 %	2.61 %	2.70 %	-0.16 %	-0.80 %	-0.34 %	-0.18 %	-0.48 %	
	0.38 %	2.46 %	2.59 %	-0.16 %	-0.58 %	-0.28 %	-0.14 %	-0.61 %	

FIGURE F.3.II NORMALIZED POWER DENSITIES AND ERRORS FOR THE CISE BENCHMARK USING 'QUADRATIC'
TRANSVERSE LEAKAGE MODEL AND NET CURRENT RESPONSE MATRICES (II)

Legend (4 values per cell, top to bottom):
- REFERENCE
- START ADFQ, N1S2, 1ST ITERATION
- START ADFQ, N1S2, 3RD ITERATION
- START ADFQ, N5S1, 1ST ITERATION

Data	X=1	X=2	X=3	X=4	X=5	X=6	X=7	X=8	Y
REFERENCE					---	0.6493			Y = 6
N1S2 1ST					---	-2.93 %			
N1S2 3RD					---	-3.11 %			
N5S1 1ST					---	-2.88 %			
REFERENCE					0.6846	0.7850	0.6270		Y = 5
N1S2 1ST					-1.04 %	0.41 %	-1.81 %		
N1S2 3RD					-0.76 %	0.38 %	-1.93 %		
N5S1 1ST					-0.47 %	0.76 %	-1.56 %		
REFERENCE				0.8620	0.7304	0.8841	0.8655		Y = 4
N1S2 1ST				-0.12 %	-1.12 %	-0.18 %	-0.84 %		
N1S2 3RD				-0.02 %	-0.71 %	-0.15 %	-0.96 %		
N5S1 1ST				0.32 %	-0.26 %	0.08 %	-0.69 %		
REFERENCE			0.9108	1.0824	1.2814	1.1197	1.0642	0.7515	Y = 3
N1S2 1ST			-0.25 %	1.42 %	0.99 %	-1.00 %	-0.87 %	-1.75 %	
N1S2 3RD			-0.29 %	1.44 %	1.05 %	-0.96 %	-0.88 %	-1.90 %	
N5S1 1ST			-0.41 %	1.39 %	1.06 %	-0.90 %	-0.73 %	-1.72 %	
REFERENCE		0.8887	0.8101	1.2566	1.2195	1.4165	1.1008	0.8753	Y = 2
N1S2 1ST		0.62 %	-0.32 %	1.72 %	0.73 %	-0.63 %	-1.20 %	-0.81 %	
N1S2 3RD		0.60 %	-0.30 %	1.69 %	0.75 %	-0.58 %	-1.18 %	-0.98 %	
N5S1 1ST		-0.05 %	-0.86 %	1.85 %	0.68 %	-0.62 %	-1.12 %	-0.82 %	
REFERENCE	0.8814	1.0362	1.2094	0.8404	1.0294	1.2581	1.3359	0.9722	Y = 1
N1S2 1ST	0.54 %	2.67 %	2.76 %	-0.11 %	-0.77 %	-0.33 %	-0.20 %	-0.58 %	
N1S2 3RD	0.46 %	2.54 %	2.66 %	-0.10 %	-0.56 %	-0.28 %	-0.18 %	-0.74 %	
N5S1 1ST	-0.08 %	2.04 %	2.41 %	-0.46 %	-0.61 %	-0.37 %	-0.18 %	-0.62 %	

X =   1   2   3   4   5   6   7   8

FIGURE F.3.III NORMALIZED POWER DENSITIES AND ERRORS FOR THE CISE BENCHMARK USING 'QUADRATIC' TRANSVERSE LEAKAGE MODEL AND NET CURRENT RESPONSE MATRICES (III)

REFERENCE
START ADFQ, N5S1, 3RD ITERATION
START ADFQ, N5S2, 1ST ITERATION
START ADFQ, N1S2 THEN N5S2

X =	1	2	3	4	5	6	7	8	
					0.6493 -3.23 % -1.09 % -1.48 %				Y = 6
				0.6846 -0.01 % 0.86 % -0.10 %	0.7850 0.29 % -0.36 % -1.35 %	0.6270 -1.94 % -0.81 % -1.26 %			Y = 5
			0.8820 -0.11 % 0.67 % 0.76 %	0.7304 -0.38 % 0.54 % 0.26 %	0.8841 -0.24 % -0.20 % -0.75 %	0.8655 -1.05 % -0.91 % -1.39 %			Y = 4
		0.9108 0.12 % 0.58 % 1.22 %	1.0824 1.63 % 0.17 % 0.32 %	1.2814 0.95 % 0.35 % 0.08 %	1.1197 -1.19 % 0.06 % -0.23 %	1.0642 -1.09 % 0.12 % -0.20 %	0.7515 -2.08 % -0.82 % -1.20 %		Y = 3
		0.8887 0.60 % 0.65 % 1.64 %	0.8101 0.12 % 0.05 % 0.98 %	1.2566 2.66 % 0.06 % 0.31 %	1.2195 0.72 % 0.12 % 0.03 %	1.4165 -0.94 % 0.30 % 0.17 %	1.1008 -1.45 % -0.12 % -0.29 %	0.8753 -1.14 % -0.31 % -0.60 %	Y = 2
	0.8814 0.38 % 0.47 % 1.33 %	1.0362 2.64 % -0.09 % 0.69 %	1.2094 3.02 % -0.16 % 0.45 %	0.8404 0.18 % -0.05 % 0.58 %	1.0294 -0.53 % 0.45 % 0.66 %	1.2581 -0.55 % -0.03 % -0.00 %	1.3359 -0.47 % -0.02 % -0.06 %	0.9722 -0.91 % -0.38 % -0.41 %	Y = 1

F-6

FIGURE F.4.I NORMALIZED POWER DENSITIES AND ERRORS FOR THE CISE BENCHMARK USING 'FLAT' TRANSVERSE LEAKAGE MODEL AND NET CURRENT RESPONSE MATRICES (I)

	X=1	X=2	X=3	X=4	X=5	X=6	X=7	X=8	
REFERENCE				---	0.6493				Y = 6
ADFF				---	-2.84 %				
START ADFF, N1S1, 1ST ITERATION				---	-2.97 %				
START ADFF, N1S1, 4TH ITERATION				---	-3.05 %				
START ADFF, N1S2, 1ST ITERATION				---	-3.03 %				
				0.6846	0.7850	0.6270			Y = 5
				-0.78 %	0.27 %	-1.54 %			
				-0.99 %	0.32 %	-1.68 %			
				-0.75 %	0.40 %	-1.79 %			
				-0.99 %	0.30 %	-1.83 %			
			0.8620	0.7304	0.8841	0.8655			Y = 4
			-3.46 %	-3.01 %	0.19 %	-0.28 %			
			-0.18 %	-1.05 %	-0.20 %	-0.86 %			
			-0.07 %	-0.72 %	-0.14 %	-0.91 %			
			-0.15 %	-1.03 %	-0.21 %	-0.91 %			
		0.9108	1.0824	1.2814	1.1197	1.0642	0.7515		Y = 3
		-2.81 %	1.48 %	1.70 %	-0.12 %	-0.19 %	-1.05 %		
		-0.30 %	1.43 %	1.00 %	-0.98 %	-0.86 %	-1.68 %		
		-0.32 %	1.40 %	1.01 %	-0.97 %	-0.85 %	-1.81 %		
		-0.25 %	1.47 %	1.02 %	-0.98 %	-0.88 %	-1.76 %		
		0.8887	0.8101	1.2566	1.2195	1.4165	1.1008	0.8753	Y = 2
		-1.86 %	-2.47 %	2.13 %	1.33 %	0.23 %	-0.29 %	-0.19 %	
		0.60 %	-0.39 %	1.68 %	0.72 %	-0.61 %	-1.16 %	-0.75 %	
		0.54 %	-0.35 %	1.64 %	0.72 %	-0.59 %	-1.16 %	-0.85 %	
		0.67 %	-0.33 %	1.72 %	0.75 %	-0.60 %	-1.18 %	-0.87 %	
	0.8814	1.0362	1.2094	0.8404	1.0294	1.2581	1.3359	0.9722	Y = 1
	-1.62 %	2.34 %	2.85 %	-1.44 %	-2.86 %	0.53 %	0.71 %	0.28 %	
	0.46 %	2.61 %	2.68 %	-0.22 %	-0.73 %	-0.28 %	-0.17 %	-0.52 %	
	0.41 %	2.48 %	2.59 %	-0.15 %	-0.57 %	-0.29 %	-0.16 %	-0.62 %	
	0.53 %	2.68 %	2.74 %	-0.18 %	-0.70 %	-0.28 %	-0.19 %	-0.64 %	

X =   1   2   3   4   5   6   7   8

FIGURE F.4.II NORMALIZED POWER DENSITIES AND ERRORS FOR THE CISE BENCHMARK USING 'FLAT'
TRANSVERSE LEAKAGE MODEL AND NET CURRENT RESPONSE MATRICES (II)

	X=1	X=2	X=3	X=4	X=5	X=6	X=7	X=8	
REFERENCE				---	0.6493				Y = 6
START ADFF, N1S2, 4TH ITERATION				---	-3.11 %				
START ADFF, N5S1, 1ST ITERATION				---	-2.77 %				
START ADFF, N5S1, 4TH ITERATION				---	-2.92 %				
START ADFF, N5S2, 1ST ITERATION				---	-1.48 %				
				0.6846	0.7850	0.6270			Y = 5
				-0.76 %	0.37 %	-1.94 %			
				-0.41 %	0.68 %	-1.57 %			
				-0.45 %	0.53 %	-1.71 %			
				0.37 %	-1.29 %	-1.14 %			
			0.8820	0.7304	0.8841	0.8655			Y = 4
			-0.03 %	-0.71 %	-0.15 %	-0.97 %			
			0.51 %	0.11 %	0.09 %	-0.76 %			
			0.20 %	-0.26 %	-0.04 %	-0.88 %			
			0.72 %	0.42 %	-0.58 %	-1.35 %			
		0.9108	1.0824	1.2814	1.1197	1.0642	0.7515		Y = 3
		-0.27 %	1.45 %	1.04 %	-0.97 %	-0.88 %	-1.90 %		
		-0.37 %	1.44 %	1.13 %	-0.87 %	-0.77 %	-1.75 %		
		-0.28 %	1.44 %	1.06 %	-0.94 %	-0.86 %	-1.84 %		
		0.99 %	0.49 %	0.37 %	-0.08 %	-0.29 %	-1.06 %		
		0.8887	0.8101	1.2566	1.2195	1.4165	1.1008	0.8753	Y = 2
		0.62 %	-0.29 %	1.69 %	0.75 %	-0.59 %	-1.19 %	-0.98 %	
		0.23 %	-0.97 %	1.48 %	0.70 %	-0.57 %	-1.14 %	-0.83 %	
		0.47 %	-0.59 %	1.59 %	0.71 %	-0.61 %	-1.19 %	-0.90 %	
		1.12 %	0.50 %	0.50 %	0.27 %	0.25 %	-0.32 %	-0.69 %	
	0.8814	1.0362	1.2094	0.8404	1.0294	1.2581	1.3359	0.9722	Y = 1
	0.49 %	2.56 %	2.67 %	-0.10 %	-0.54 %	-0.28 %	-0.19 %	-0.75 %	
	-0.02 %	2.07 %	2.22 %	-0.64 %	-0.46 %	-0.30 %	-0.16 %	-0.62 %	
	0.25 %	2.35 %	2.48 %	-0.32 %	-0.52 %	-0.32 %	-0.21 %	-0.68 %	
	0.88 %	0.31 %	0.24 %	0.20 %	0.66 %	-0.01 %	-0.03 %	-0.38 %	

X =   1   2   3   4   5   6   7   8

FIGURE F.5 NORMALIZED POWER DENSITIES AND ERRORS FOR THE CISE BENCHMARK USING 'CMFD' GLOBAL MODEL AND NET CURRENT RESPONSE MATRICES

REFERENCE
ADFC
START ADFC, N5S2, 1ST ITERATION
START REF., N5S2, 1ST ITERATION

X =	1	2	3	4	5	6	7	8	
				---	0.6493				Y = 6
				---	2.27 %				
				---	-1.74 %				
				---	-2.54 %				
				0.6846	0.7850	0.6270			Y = 5
				-5.24 %	15.33 %	5.51 %			
				-7.15 %	-0.27 %	5.13 %			
				0.02 %	-0.89 %	-2.52 %			
			0.8820	0.7304	0.8841	0.8655			Y = 4
			-19.06 %	-15.03 %	5.94 %	11.15 %			
			-3.42 %	-6.13 %	-3.31 %	1.39 %			
			0.48 %	0.29 %	-0.36 %	-1.49 %			
		0.9108	1.0824	1.2814	1.1197	1.0642	0.7515		Y = 3
		-24.27 %	-10.12 %	4.03 %	9.35 %	23.82 %	8.60 %		
		-3.63 %	-2.22 %	-3.33 %	-0.01 %	-0.34 %	-7.94 %		
		0.59 %	-0.19 %	-0.04 %	0.03 %	0.15 %	-1.04 %		
	0.8887	0.8101	1.2566	1.2195	1.4165	1.1008	0.8753		Y = 2
	-34.28 %	-29.74 %	-7.09 %	-1.40 %	14.56 %	18.36 %	18.05 %		
	-3.91 %	0.58 %	0.42 %	-1.15 %	1.77 %	2.63 %	3.57 %		
	0.80 %	0.77 %	0.36 %	-0.04 %	0.44 %	0.10 %	-0.21 %		
0.8814	1.0362	1.2094	0.8404	1.0294	1.2581	1.3359	0.9722		Y = 1
-37.58 %	-29.68 %	-19.11 %	-25.78 %	-13.22 %	8.31 %	24.97 %	20.20 %		
-3.24 %	-2.69 %	3.89 %	3.20 %	-1.35 %	1.49 %	3.30 %	8.01 %		
0.79 %	0.18 %	0.47 %	0.75 %	0.74 %	0.24 %	0.21 %	-0.31 %		

FIGURE F.6.I NORMALIZED POWER DENSITIES AND ERRORS FOR THE CISE BENCHMARK USING 'QUADRATIC'
TRANSVERSE LEAKAGE MODEL AND NET CURRENT RESPONSE MATRICES GENERATED FROM
PARTIAL CURRENT RESPONSE MATRICES (I)

REFERENCE
START ADFQ, N1S1, 1ST ITERATION
START ADFQ, N1S1, 5TH ITERATION

X =	1	2	3	4	5	6	7	8	
				---	0.6493				Y = 6
				---	-2.47 %				
				---	-2.57 %				
				0.6846	0.7850	0.6270			Y = 5
				1.68 %	-1.11 %	-2.68 %			
				0.23 %	-1.07 %	-2.54 %			
			0.8820	0.7304	0.8841	0.8655			Y = 4
			5.47 %	1.50 %	-3.10 %	-6.57 %			
			5.49 %	1.39 %	-2.94 %	-6.43 %			
		0.9108	1.0824	1.2814	1.1197	1.0642	0.7515		Y = 3
		11.75 %	7.45 %	0.51 %	-6.40 %	-9.55 %	-11.33 %		
		9.74 %	6.30 %	0.37 %	-5.76 %	-8.69 %	-9.12 %		
	0.8887	0.8101	1.2566	1.2195	1.4165	1.1008	0.8753		Y = 2
	19.50 %	14.62 %	8.83 %	0.20 %	-7.49 %	-11.83 %	-13.86 %		
	17.47 %	12.77 %	8.03 %	0.02 %	-6.56 %	-10.53 %	-11.35 %		
0.8814	1.0362	1.2094	0.8404	1.0294	1.2581	1.3359	0.9722		Y = 1
23.03 %	21.43 %	17.18 %	10.36 %	1.27 %	-6.73 %	-12.47 %	-15.23 %		
19.88 %	18.59 %	15.15 %	9.60 %	1.01 %	-6.06 %	-11.01 %	-12.30 %		

FIGURE F.6.II NORMALIZED POWER DENSITIES AND ERRORS FOR THE CISE BENCHMARK USING 'QUADRATIC'
TRANSVERSE LEAKAGE MODEL AND NET CURRENT RESPONSE MATRICES GENERATED FROM
PARTIAL CURRENT RESPONSE MATRICES (II)

REFERENCE ---
START ADFQ, N1S2, 1ST ITERATION ---
START ADFQ, N1S2, 5TH ITERATION ---
START ADFQ, N5S2, 1ST ITERATION ---

X =	1	2	3	4	5	6	7	8	
					0.6493 -3.85 % -4.13 % -7.30 %				Y = 6
					0.6846 0.75 % -0.04 % -5.00 %	0.7850 -0.69 % -0.76 % -9.35 %	0.6270 -0.92 % -0.31 % -5.28 %		Y = 5
				0.8820 3.38 % 3.62 % 4.27 %	0.7304 0.26 % 0.33 % -1.07 %	0.8841 -2.79 % -2.92 % -6.57 %	0.8655 -4.89 % -4.72 % -9.04 %		Y = 4
			0.9108 7.80 % 6.92 % 11.93 %	1.0824 6.15 % 5.62 % 7.44 %	1.2814 1.14 % 1.22 % 1.85 %	1.1197 -4.32 % -4.16 % -4.36 %	1.0642 -5.99 % -5.46 % -9.51 %	0.7515 -8.80 % -8.06 % -11.37 %	Y = 3
		0.8887 13.27 % 12.63 % 18.93 %	0.8101 9.62 % 8.88 % 14.16 %	1.2566 6.99 % 6.56 % 8.61 %	1.2195 0.43 % 0.40 % 1.82 %	1.4165 -5.43 % -5.18 % -4.30 %	1.1008 -8.37 % -7.77 % -9.61 %	0.8753 -10.87 % -10.16 % -14.73 %	Y = 2
	0.8814 15.68 % 14.52 % 22.32 %	1.0362 15.86 % 14.74 % 19.60 %	1.2094 12.86 % 12.17 % 15.26 %	0.8404 6.84 % 6.61 % 10.30 %	1.0294 0.14 % 0.06 % 2.82 %	1.2581 -4.70 % -4.58 % -3.79 %	1.3359 -8.46 % -7.74 % -8.80 %	0.9722 -11.36 % -10.44 % -12.56 %	Y = 1

F-11

FIGURE F.7 NORMALIZED POWER DENSITIES AND ERRORS FOR THE CISE BENCHMARK USING 'FLAT' TRANSVERSE LEAKAGE MODEL AND NET CURRENT RESPONSE MATRICES GENERATED FROM PARTIAL CURRENT RESPONSE MATRICES

Row legend (5 lines per cell, top to bottom):
- REFERENCE
- START ADFF, N1S1, 1ST ITERATION
- START ADFF, N1S1, 5TH ITERATION
- START ADFF, N5S1, 1ST ITERATION
- START ADFF, N5S2, 1ST ITERATION

X =	1	2	3	4	5	6	7	8	
				---	0.6493				Y = 6
				---	-2.59 %				
				---	-2.55 %				
				---	-6.38 %				
				---	-6.39 %				
				0.6846	0.7850	0.6270			Y = 5
				1.69 %	-1.22 %	-2.71 %			
				0.36 %	-0.92 %	-2.43 %			
				-4.57 %	-4.09 %	-6.46 %			
				-4.06 %	-7.15 %	-4.23 %			
			0.8820	0.7304	0.8841	0.8655			Y = 4
			5.38 %	1.51 %	-3.14 %	-6.60 %			
			5.30 %	1.44 %	-2.88 %	-6.32 %			
			4.36 %	-1.11 %	-4.41 %	-8.12 %			
			3.91 %	1.11 %	-5.81 %	-7.55 %			
		0.9108	1.0824	1.2814	1.1197	1.0642	0.7515		Y = 3
		11.70 %	7.49 %	0.53 %	-6.39 %	-9.51 %	-11.24 %		
		9.51 %	6.18 %	0.47 %	-5.73 %	-8.66 %	-9.07 %		
		13.22 %	8.46 %	1.13 %	-6.38 %	-9.97 %	-12.80 %		
		11.27 %	6.98 %	1.45 %	-4.30 %	-8.46 %	-10.30 %		
	0.8887	0.8101	1.2566	1.2195	1.4165	1.1008	0.8753		Y = 2
	19.53 %	14.53 %	8.83 %	0.24 %	-7.48 %	-11.81 %	13.91 %		
	17.27 %	12.63 %	7.98 %	0.06 %	-6.51 %	-10.49 %	-11.30 %		
	21.97 %	15.99 %	9.71 %	1.16 %	-6.84 %	-11.94 %	-15.33 %		
	17.76 %	13.22 %	7.97 %	1.29 %	-4.60 %	-9.18 %	-13.27 %		
0.8814	1.0362	1.2094	0.8404	1.0294	1.2581	1.3359	0.9722		Y = 1
23.05 %	21.43 %	17.13 %	10.22 %	1.32 %	-6.65 %	-12.42 %	-15.21 %		
19.55 %	18.38 %	15.08 %	9.51 %	0.94 %	-6.05 %	-10.88 %	-12.18 %		
25.52 %	23.29 %	18.12 %	10.81 %	2.36 %	-6.00 %	-12.01 %	-14.31 %		
20.81 %	18.20 %	14.07 %	9.30 %	2.24 %	-4.14 %	-8.60 %	-11.42 %		

FIGURE F.8.I NORMALIZED POWER DENSITIES AND ERRORS FOR THE HAFAS BENCHMARK USING 'QUADRATIC'
TRANSVERSE LEAKAGE MODEL AND NET CURRENT RESPONSE MATRICES (I)

Row	X=1	X=2	X=3	X=4	X=5	X=6	X=7	X=8	X=9	Y
REFERENCE						---	1.0885	0.6886	0.3936	Y = 7
ADFQ						---	1.31 %	1.54 %	1.86 %	
START ADFQ, N1S1, 1ST ITERATION						---	0.15 %	-0.59 %	-1.24 %	
START ADFQ, N1S2, 1ST ITERATION						---	0.13 %	-0.61 %	-1.29 %	
						1.4634	1.1996	0.9887	0.5091	Y = 6
						0.55 %	1.38 %	0.62 %	1.43 %	
						0.17 %	0.59 %	0.61 %	-0.00 %	
						0.16 %	0.58 %	0.59 %	-0.10 %	
					0.9642	1.2596	1.3550	0.9697	0.6332	Y = 5
					-2.52 %	1.38 %	0.97 %	0.93 %	1.14 %	
					-1.12 %	1.31 %	1.27 %	0.75 %	-0.12 %	
					-1.12 %	1.31 %	1.26 %	0.73 %	-0.21 %	
				1.1174	0.8669	1.2401	1.0813	0.9988	0.5632	Y = 4
				-5.29 %	-2.13 %	0.75 %	1.60 %	0.14 %	1.49 %	
				-1.97 %	-0.44 %	1.22 %	1.27 %	0.04 %	0.10 %	
				-1.96 %	-0.43 %	1.21 %	1.26 %	0.02 %	0.05 %	
			1.6583	1.5325	1.3736	0.7878	0.7339	0.7761	0.5737	Y = 3
			-0.79 %	0.48 %	0.64 %	-4.65 %	-1.93 %	0.75 %	1.03 %	
			-1.23 %	0.71 %	1.13 %	-1.08 %	-1.19 %	0.78 %	0.70 %	
			-1.22 %	0.73 %	1.14 %	-1.08 %	-1.19 %	0.77 %	0.69 %	
		1.7191	1.5115	1.7175	1.2374	0.8282	0.6215	0.8096	0.4973	Y = 2
		-0.29 %	-0.10 %	0.08 %	1.47 %	-4.17 %	-0.51 %	0.54 %	1.55 %	
		-1.63 %	-1.37 %	0.37 %	1.22 %	-1.29 %	-0.66 %	0.46 %	0.49 %	
		-1.61 %	-1.35 %	0.39 %	1.24 %	-1.28 %	-0.66 %	0.46 %	0.50 %	
	1.4962	1.2997	1.3517	1.0752	0.9239	0.9993	1.0152	0.7833	0.5503	Y = 1
	-0.41 %	0.00 %	-1.35 %	-4.44 %	-0.89 %	1.18 %	1.10 %	0.49 %	0.92 %	
	-1.28 %	-1.35 %	-1.45 %	-1.78 %	-0.95 %	2.07 %	1.66 %	-0.46 %	-0.96 %	
	-1.26 %	-1.34 %	-1.43 %	-1.77 %	-0.94 %	2.08 %	1.67 %	-0.46 %	-0.95 %	

X = 1   2   3   4   5   6   7   8   9

FIGURE F.8.II NORMALIZED POWER DENSITIES AND ERRORS FOR THE HAFAS BENCHMARK USING 'QUADRATIC'
TRANSVERSE LEAKAGE MODEL AND NET CURRENT RESPONSE MATRICES (II)

REFERENCE
START ADFQ, N5S1, 1ST ITERATION
START ADFQ, N5S2, 1ST ITERATION

Y	X=1	X=2	X=3	X=4	X=5	X=6	X=7	X=8	X=9
7						---	1.0885	0.6886	0.3936
						---	-4.00 %	-5.31 %	-6.32 %
						---	7.38 %	7.10 %	7.17 %
6						1.4634	1.1996	0.9887	0.5091
						-1.68 %	-2.84 %	-3.73 %	-4.83 %
						7.06 %	7.40 %	6.84 %	7.12 %
5					0.9642	1.2596	1.3550	0.9697	0.6332
					13.16 %	1.35 %	-1.47 %	-2.89 %	-4.52 %
					2.24 %	7.54 %	8.12 %	7.02 %	6.51 %
4				1.1174	0.8669	1.2401	1.0813	0.9988	0.5632
				10.75 %	25.59 %	9.32 %	1.02 %	-2.73 %	-3.89 %
				-4.43 %	-5.81 %	-5.00 %	9.67 %	5.89 %	5.69 %
3			1.6583	1.5325	1.3736	0.7878	0.7339	0.7761	0.5737
			-3.21 %	0.82 %	8.39 %	20.84 %	5.07 %	-2.26 %	-2.78 %
			-4.67 %	-4.58 %	-6.48 %	-6.48 %	2.02 %	3.57 %	3.40 %
2		1.7191	1.5115	1.7175	1.2374	0.8282	0.6215	0.8096	0.4973
		-5.60 %	-4.65 %	-1.99 %	1.49 %	4.55 %	0.12 %	-2.00 %	-2.82 %
		-4.37 %	-4.26 %	-4.78 %	-4.45 %	-3.71 %	-3.13 %	1.01 %	1.56 %
1	1.4962	1.2997	1.3517	1.0752	0.9239	0.9993	1.0152	0.7833	0.5503
	-5.88 %	-5.67 %	-5.07 %	-3.99 %	-2.30 %	-0.26 %	-0.61 %	-3.59 %	-5.64 %
	-4.28 %	-4.26 %	-4.58 %	-4.29 %	-4.09 %	-3.46 %	-1.93 %	-0.07 %	0.06 %

X =   1   2   3   4   5   6   7   8   9

FIGURE F.8.III NORMALIZED POWER DENSITIES AND ERRORS FOR THE HAFAS BENCHMARK USING 'QUADRATIC' TRANSVERSE LEAKAGE MODEL AND NET CURRENT RESPONSE MATRICES (III)

Legend (four values per cell, in order):
- REFERENCE
- START REF., N5S2, 1ST ITERATION
- START REF., N5S1, 1ST ITERATION
- START ADFQ, N1S2 THEN N5S2

	X = 1	2	3	4	5	6	7	8	9	
						---	1.0885	0.6886	0.3936	Y = 7
						---	0.24 %	-0.03 %	0.03 %	
						---	-5.41 %	-6.66 %	-7.66 %	
						---	-0.15 %	-0.25 %	0.01 %	
						1.4634	1.1996	0.9887	0.5091	Y = 6
						0.17 %	0.27 %	-0.04 %	0.10 %	
						-2.92 %	-4.05 %	-4.86 %	-5.84 %	
						-0.76 %	-0.33 %	-0.32 %	-0.01 %	
					0.9642	1.2596	1.3550	0.9697	0.6332	Y = 5
					0.37 %	0.46 %	0.06 %	0.24 %	-0.06 %	
					11.22 %	0.43 %	-2.16 %	-3.43 %	-4.89 %	
					-0.19 %	-0.65 %	-0.79 %	-0.00 %	-0.17 %	
				1.1174	0.8669	1.2401	1.0813	0.9988	0.5632	Y = 4
				-0.06 %	-0.45 %	-0.54 %	0.49 %	0.12 %	0.11 %	
				7.59 %	23.31 %	8.20 %	1.14 %	-1.89 %	-2.93 %	
				0.03 %	1.30 %	0.76 %	-0.60 %	-0.30 %	-0.02 %	
			1.6583	1.5325	1.3736	0.7878	0.7339	0.7761	0.5737	Y = 3
			-0.18 %	-0.11 %	-0.96 %	-0.40 %	0.52 %	0.23 %	-0.28 %	
			-6.37 %	-1.96 %	6.36 %	21.74 %	11.71 %	2.00 %	-0.34 %	
			-0.03 %	-0.15 %	0.78 %	0.59 %	-0.61 %	0.23 %	-0.36 %	
		1.7191	1.5115	1.7175	1.2374	0.8282	0.6215	0.8096	0.4973	Y = 2
		0.14 %	0.27 %	-0.37 %	-0.26 %	0.05 %	0.47 %	-0.04 %	-0.09 %	
		-9.17 %	-7.95 %	-4.74 %	-0.03 %	9.34 %	20.96 %	4.87 %	0.80 %	
		0.70 %	0.68 %	-0.19 %	-0.41 %	-0.61 %	-0.67 %	0.05 %	-0.15 %	
	1.4962	1.2997	1.3517	1.0752	0.9239	0.9993	1.0152	0.7833	0.5503	Y = 1
	0.22 %	0.27 %	-0.06 %	0.13 %	-0.18 %	-0.24 %	-0.22 %	0.27 %	0.09 %	
	-9.64 %	-9.32 %	-8.46 %	-6.75 %	-2.82 %	3.23 %	5.95 %	3.27 %	0.74 %	
	0.94 %	0.89 %	0.48 %	0.42 %	-0.43 %	-0.63 %	-0.63 %	0.10 %	0.39 %	

FIGURE F.9.I NORMALIZED POWER DENSITIES AND ERRORS FOR THE LSHBWR BENCHMARK USING 'QUADRATIC'
TRANSVERSE LEAKAGE MODEL AND NET CURRENT RESPONSE MATRICES (I)

```
REFERENCE                         ---   1.4395   1.0378   0.5283                               Y = 4
ADFQ                              ---   1.92 %  -0.64 %   2.03 %
START ADFQ, N1S1, 1ST ITERATION ---   1.17 %   0.76 %   0.06 %
START ADFQ, N1S2, 1ST ITERATION ---   1.17 %   0.75 %   0.06 %

                              1.4255   1.4424   1.2212   0.6741                               Y = 3
                             -0.83 %  -0.57 %  -0.66 %   2.86 %
                             -0.46 %  -0.17 %   1.82 %   0.65 %
                             -0.46 %  -0.17 %   1.82 %   0.65 %

                    1.6944   1.5376   1.4774   0.9563   0.4499   0.3884   0.1945              Y = 2
                    0.27 %  -0.23 %   0.18 %  -8.85 %   8.05 %   3.09 %   5.81 %
                   -0.10 %  -0.12 %  -0.09 %  -1.51 %  -0.67 %   1.60 %   1.13 %
                   -0.10 %  -0.12 %  -0.09 %  -1.51 %  -0.67 %   1.60 %   1.13 %

          1.8779   1.7798   1.5992   1.5012   0.9178   0.4275   0.4123   0.2399              Y = 1
          0.47 %   0.38 %  -0.13 %   0.17 %  -9.07 %   9.61 %   4.83 %   6.34 %
          0.04 %  -0.02 %  -0.08 %  -0.49 %  -2.70 %  -2.85 %   2.16 %   3.42 %
          0.04 %  -0.02 %  -0.08 %  -0.49 %  -2.70 %  -2.85 %   2.16 %   3.42 %


    X =   1        2        3        4        5        6        7        8
```

FIGURE F.9.II NORMALIZED POWER DENSITIES AND ERRORS FOR THE LSHBWR BENCHMARK USING 'QUADRATIC' TRANSVERSE LEAKAGE MODEL AND NET CURRENT RESPONSE MATRICES (II)

Label	X=1	X=2	X=3	X=4	X=5	X=6	X=7	X=8	
REFERENCE ---				1.4395	1.0378	0.5283			Y = 4
START AOFQ, N5S1, 1ST ITERATION ---				-1.29 %	-1.01 %	0.70 %			
START AOFQ, N5S2, 1ST ITERATION ---				4.49 %	2.90 %	1.97 %			
START AOFQ, N1S2 THEN N5S2 ---				-0.15 %	-1.34 %	-1.17 %			
START AOFQ, N1S2, 6TH ITERATION ---				0.50 %	-0.03 %	-0.19 %			
			1.4255	1.4424	1.2212	0.6741			Y = 3
			-3.93 %	-2.56 %	2.30 %	6.96 %			
			5.10 %	3.76 %	2.13 %	3.23 %			
			-0.08 %	-0.39 %	-0.74 %	0.42 %			
			-1.05 %	-0.62 %	1.83 %	1.22 %			
		1.6944	1.5376	1.4774	0.9563	0.4499	0.3884	0.1945	Y = 2
		-5.24 %	-4.28 %	-2.46 %	4.82 %	35.83 %	12.62 %	11.62 %	
		5.74 %	5.29 %	3.53 %	-1.79 %	-32.81 %	-38.75 %	-31.88 %	
		-0.25 %	-0.15 %	-0.13 %	0.75 %	5.42 %	-0.67 %	-1.23 %	
		-1.08 %	-0.85 %	-0.37 %	0.75 %	2.49 %	2.16 %	1.65 %	
	1.8779	1.7798	1.5992	1.5012	0.9178	0.4275	0.4123	0.2399	Y = 1
	-5.89 %	-5.54 %	-4.61 %	-3.26 %	0.48 %	10.18 %	15.30 %	14.55 %	
	6.23 %	5.94 %	5.31 %	3.51 %	-1.63 %	-20.00 %	-33.20 %	-35.31 %	
	-0.31 %	-0.30 %	-0.19 %	0.01 %	1.17 %	3.56 %	-0.34 %	-1.75 %	
	-1.16 %	-1.09 %	-0.86 %	-0.71 %	0.32 %	1.33 %	3.25 %	4.09 %	

X =   1   2   3   4   5   6   7   8